Univerza v Ljubljani
Universitas Labacensis

University of Ljubljana
Faculty of Electrical Engineering

Tomaž Vrtovec

AUTOMATIC ANALYSIS OF THREE-DIMENSIONAL SPINE IMAGES

PhD thesis

Supervisor: Prof. Dr. Franjo Pernuš

Ljubljana, 2007

Univerza v Ljubljani
Universitas Labacensis

Univerza v Ljubljani
Fakulteta za elektrotehniko

Tomaž Vrtovec

AVTOMATSKA ANALIZA TRIDIMENZIONALNIH SLIK HRBTENICE

Doktorska disertacija

Mentor: prof. dr. Franjo Pernuš

Ljubljana, 2007

The juice was worth the squeeze.

◆

Sok je bil vreden stiska.

Contents

Statement

I undersigned Tomaž Vrtovec hereby state that I have prepared the PhD thesis independently under the supervision of Prof. Dr. Franjo Pernuš. Contribution from other collaborators is entirely quoted in acknowledgments or/and at individual chapters.

Ljubljana, June 26th 2007

Tomaž Vrtovec, B.Sc.

Izjava

Podpisani Tomaž Vrtovec izjavljam, da sem doktorsko disertacijo izdelal samostojno pod mentorstvom prof. dr. Franja Pernuša. Izkazano pomoč drugih sodelavcev sem v celoti navedel v zahvali in/ali pri posameznih poglavjih.

Ljubljana, 26. junij 2007

Tomaž Vrtovec, univ.dipl.inž.el.

I have made this longer, because I have not had the time to make it shorter.

Blaise Pascal, 1623 - 1662
(Provincial Letters: Letter XVI, 1657)

Abbreviations

1D	one dimension, one-dimensional
2D	two dimensions, two-dimensional
3D	three dimensions, three-dimensional
6D	six dimensions, six-dimensional
CA	curvature angle
CAD	computer-aided diagnosis
CPR	curved planar reformation
CT	computed tomography
EDO	edge distance optimization
GC	geometric curvature
MIP	maximum intensity projection
MR	magnetic resonance
LL	lumbar lordosis
LSF	least squares fitting
LTS	least trimmed squares
pixel	picture element
SNR	signal-to-noise ratio
TJ	thoracolumbar junction
TK	thoracic kyphosis
voxel	volume element

There are no facts, only interpretations.

Friedrich W. Nietzsche, 1844 - 1900
(Notebooks, 1887)

Abstract

Medical images are of extreme importance for diagnosing and understanding of normal and pathological conditions of the human body. To some extent, the quality of image-assisted medical examinations depends on the acquisition of images, interpretation of the information present in images and on the research activity and clinical environment that stimulate image formation and its application.

In the past decades, advances in medical imaging technology and computerized medical image processing led to the development of new three-dimensional (3D) image acquisition techniques that have become important clinical tools in modern diagnostic radiology and medical health care. Although two-dimensional (2D) images, especially radiographic (X-ray) images, are still widely present in clinical examination due to relatively low acquisition price and wide area of application, they are slowly being replaced by 3D images. The continuous increase in the number of acquired cross-sections, reduction in cross-sectional thickness and relatively short acquisition time led to the expansion of 3D imaging techniques. Among the most important 3D techniques are computed tomography (CT) and magnetic resonance (MR) imaging, which provide qualitative data of the imaged structures. However, characteristic features of these techniques and variable positioning of the patient during image acquisition still represent a major source of variability that causes errors in the interpretation of image information. On the other hand, human capability of discovering and diagnosing diseases by proper interpretation of medical images is limited due to our non-systematic search patterns. Moreover, the presence of noise may conceal the natural anatomical background, such as actual geometrical relationship between anatomical structures, which may further hamper mental reconstruction of the 3D image information. Errors in interpretation may also be caused by similar characteristics of normal and pathological conditions and by the natural biological variability in human anatomy. Image

interpretation therefore depends to a great extent on adequate presentation and measurement of the information about anatomical structures or physiological processes. As the information of interest is often associated with characteristic features of the selected structure or process, it is crucial to use specially designed image processing techniques for visualization and quantitative evaluation. Techniques for visualization and quantitative evaluation of medical images are therefore extremely valuable in the development of image-assisted diagnosis, planning of surgical interventions and assessment of medical treatment outcomes.

This thesis concentrates on the design, development and validation of automated techniques that aim to improve the visualization of 3D spine images, and techniques for an improved quantitative evaluation of the most important parameters of the spine in 3D, such as the spinal curvature and vertebral rotation. The fields of visualization and quantitative evaluation of spine images are closely related, as knowledge of spine parameters may provide a more effective spine visualization, and, on the other hand, proper spine visualization may allow a more effective measurement of spine parameters.

Dejstev ni, so samo interpretacije.

FRIEDRICH W. NIETZSCHE, 1844 - 1900
(Zvezki, 1887)

Povzetek

Informacijska vsebina medicinskih slik je ključnega pomena za odkrivanje in razumevanje normalnih in bolezenskih stanj človeškega organizma. Kakovost slikovno podprtih medicinskih preiskav je v veliki meri odvisna od tehnike zajema slik, interpretacije informacijske vsebine slik ter od raziskovalnega oziroma medicinskega okolja, ki spodbuja zajemanje slik in njihovo uporabo.

Napredek na področju medicinskih slikovnih tehnik ter na področju računalniške obdelave medicinskih slik je v zadnjih desetletjih privedel do razvoja novih tridimenzionalnih (3D) tehnik zajema slik, ki so nepogrešljive v sodobni zdravstveni oskrbi. 3D slike so pričele nadomeščati dvodimenzionalne (2D) slike, predvsem rentgenske, ki pa so še vedno močno prisotne pri medicinskih preiskavah zaradi nizke cene zajema ter širokega področja uporabe. Neprestano povečevanje števila slikovnih rezin v enem zajemu, zmanjševanje debeline slikovnih rezin ter časa, potrebnega za zajem slike (tabela 1.1, str. 20), je namreč povzročilo razmah uporabe 3D slikovnih tehnik (Sakas, 2002). Med najpomembnejšimi 3D slikovnimi tehnikami sta predvsem računalniška tomografija (CT) in magnetna resonanca (MR), ki dajeta kakovostne podatke o slikanih anatomskih strukturah. Spremenljive lastnosti uporabljenih tehnik kot tudi spremenljiva lega pacienta med postopkom zajema pa so še vedno vir napak pri interpretaciji informacijske vsebine slik. Po drugi strani smo ljudje pri interpretaciji medicinskih slik v smislu sposobnosti odkrivanja in diagnosticiranja obolenj omejeni zaradi naših nesistematičnih iskalnih vzorcev, poleg tega pa prisotnost šuma v slikah lahko povzroči prikrivanje naravnega anatomskega ozadja, kot so na primer dejanski geometrijski odnosi med anatomskimi strukturami, kar lahko ovira miselno rekonstrukcijo slikovne informacije v 3D. Nenazadnje pa lahko

napake pri interpretaciji povzročijo tudi podobne značilnosti nekaterih normalnih in bolezenskih stanj ter naravna biološka variabilnost človeške anatomije in fiziologije. Interpretacija slik je torej močno odvisna od načina predstavitve ter merjenja informacije o anatomskih strukturah ali o fizioloških procesih. Ker je informacija o določeni strukturi ali procesu pogosto povezana s karakterističnimi lastnostmi te strukture ali procesa, je uporaba specifičnih tehnik prikazovanja ter kvantitativnega vrednotenja medicinskih slik ključnega pomena za razvoj slikovno podprte medicinske diagnostike, načrtovanje terapevtskih posegov ter vrednotenje učinkov zdravljenja.

Poškodbe in degeneracijska obolenja hrbtenice predstavljajo področje v medicini, kjer trenutni načini zdravljenja kljub doseganju pričakovanih kliničnih rezultatov še niso povsem primerni (Toyone in dr., 2005). Bolečine v hrbtenici se ponavadi zdravijo s kombinacijo sredstev proti bolečinam ter fizioterapije, v primeru akutnih obolenj ali travmatičnih poškodb hrbtenice pa se ponavadi opravi kirurški poseg. Kljub temu pa so rezultati zdravljenja pri velikem številu pacientov nezadovoljivi. S trenutnim znanjem o fizičnih ter biomehaničnih lastnostih hrbtenice je namreč nemogoče natančno napovedati rezultate zdravljenja, poleg tega pa je odkrivanje, prikazovanje ter kvantitativno vrednotenje obolenj hrbtenice oteženo zaradi kompleksnosti in členjene sestave hrbtenice. Po drugi strani pa sodobne tehnike zajema slik omogočajo kakovosten vpogled v celotno anatomijo hrbtenice. Tehnika CT je primerna za opazovanje hrbteničnih kosti, medtem ko tehnika MR omogoča vpogled v mehka tkiva in je torej primerna za opazovanje medvretenčnih ploščic[1], hrbtenjače[2] ter korenin živcev[3,4], ki izhajajo iz hrbtenjače. Razvoj sodobnih tehnik prikazovanja ter kvantitativnega vrednotenja lahko torej pripomore k natančnejši medicinski diagnozi ter načrtovanju učinkovitejših strategij zdravljenja hrbteničnih obolenj.

V doktorski disertaciji smo načrtovali, razvili ter vrednotili izvirne avtomatske (samodejne) postopke za izboljšanje prikazovanja 3D medicinskih slik hrbtenice ter avtomatske postopke za kvantitativno vrednotenje nekaterih najpomembnejših parametrov hrbtenice v 3D, kot sta ukrivljenost hrbtenice ter rotacija vretenc. Področji prikazovanja ter kvantitativnega vrednotenja sta v primeru slik hrbtenice tesno povezani, saj poznavanje najpomembnejših parametrov hrbtenice omogoča učinkovitejše prikazovanje hrbtenice kot anatomske strukture, po drugi strani pa ustrezno prikazovanje hrbtenice omogoča pravilnejše kvantitativno vrednotenje parametrov hrbtenice.

[1] medvretenčna ploščica: ploščica med telesoma sosednjih vretenc, ki sestoji iz vezivne hrustančevine in notranjega pulpoznega jedra; intervertebralni diskus (slika 1.4, str. 28)

[2] hrbtenjača: del centralnega živčevja iz centralne sive in periferne bele možganovine, ki leži v hrbteničnem kanalu; hrbtni mozeg

[3] sprednja korenina spinalnega živca: motorični del spinalnega živca, ki izstopa iz sprednjega stebra hrbtnega mozga in se ob medvretenčni odprtini združi z zadajšnjo korenino v spinalni živec

[4] zadajšnja korenina spinalnega živca: senzorični del spinalnega živca, ki vstopa v zadajšnji del hrbtnega mozga

P.1 Prikazovanje in kvantitativno vrednotenje slik

Proces nastajanja slike lahko pojmujemo kot preslikavo določenih lastnosti slikanega objekta v prostorsko domeno slike, ki je osnova za prikazovanje slikanega objekta in njegovih lastnosti, za nadaljnje kvantitativno vrednotenje strukture ali funkcije slikanega objekta ter nenazadnje za pravilno interpretacijo informacije o slikanem objektu. Osnovni namen prikazovanja slik je učinkovita izraba informacijske vsebine v slikah, od katere je odvisno nadaljnje kvantitativno vrednotenje ter interpretacija slik. Na področju razvoja tehnik za prikazovanje medicinskih slik je najpomembnejše izluščevanje klinično pomenljive informacije, kar omogoča razvoj natančne ter neinvazivne medicinske diagnostike ter zdravljenja.

P.1.1 Prikazovanje medicinskih slik

Prostorsko prikazovanje slik je definirano kot preslikava slikovne informacije iz 3D prostorske domene slike na 2D napravo za prikazovanje (Rubin in dr., 1996, Robb, 2000, Udupa, 2000). Tehnike prikazovanja so naslednje:

- 2D prikazovanje slik združuje tiste tehnike prikazovanja, kjer so na osnovi 3D slike določeni tisti 2D prerezi, ki najugodneje prikazujejo izbrane značilnosti slik:
  - Originalni prerezi prikazujejo originalne slikovne elemente vzolž primarnih ravnin rekonstrukcije. Pri CT so te ravnine ponavadi orientirane prečno, medtem ko so pri MR orientirane vzporedno z izbrano vzbujevalno ravnino (slika 1.1a, str. 23).
  - Večravninski prerezi prikazujejo originalne slikovne elemente vzdolž ravnin, ki so pravokotne na primarno ravnino rekonstrukcije. Glede na orientacijo teh ravnin ločimo prečne[5], stranske[6] in čelne[7] prereze (slika 1.1b, str. 23).
  - Poševni prerezi prikazujejo originalne slikovne elemente vzdolž ravnin, ki oklepajo poljuben kot s primarno ravnino rekonstrukcije (slika 1.1c, str. 23).
  - Ukrivljeni prerezi (CPR; *ang.* curved planar reformation) prikazujejo originalne slikovne elemente vzdolž poljubnih ukrivljenih ploskev, ki so raztegnjene in prikazane kot ravnine (slika 1.1d, str. 23).
- 3D prikazovanje slik združuje tiste tehnike prikazovanja, kjer so na osnovi 3D slike določene tiste 2D projekcije, ki najugodneje prikazujejo izbrane 3D strukture v sliki:

[5]prečni prerez: prerez, ki pod pravim kotom prečka vzdolžno os telesa, organa ali strukture; transverzalni, aksialni prerez (slika 1.3, str. 26)

[6]stranski prerez: prerez, ki poteka vzporedno z ravnino, ki deli telo, organ ali strukturo na leve in desne dele; lateralni, sagitalni prerez (slika 1.3, str. 26)

[7]čelni prerez: prerez, ki poteka vzporedno z ravnino, ki deli telo, organ ali strukturo na anteriorne in posteriorne dele; frontalni, koronalni prerez (slika 1.3, str. 26)

- Projekcije maksimalne intenzitete (MIP; *ang.* maximum intensity projection) prikazujejo največje intenzitete originalnih slikovnih elementov vzdolž vzporednih projekcijskih žarkov, ki so pravokotni na poljubno orientirano ravnino projekcije (slika 1.2a, str. 24).
- Upodabljanje površine je prikazovanje površine strukture v sliki s kombinacijo projekcije geometrijskih primitivov (točka, daljica, trikotnik, poligon) in modelov prikazovanja (barvni model, model senčenja). Površino strukture je potrebo predhodno razgraditi, notranjost strukture pa med prikazovanjem ni vidna (slika 1.2b, str. 24).
- Upodabljanje prostornine je neposredno prikazovanje strukture v sliki s kombinacijo projekcije potekov slikovne intenzitete vzdolž projekcijskih žarkov ter modelov prikazovanja (barvni model, model senčenja, model prosojnosti). Razgradnja površine strukture ni potrebna, notranjost strukture pa je med prikazovanjem vidna (slika 1.2c, str. 24).

Uveljavljene tehnike 2D prikazovanja anatomskih struktur temeljijo na ravninskih (večravninskih in poševnih) prerezih 3D slik. Z ravninskimi prerezi pa ne moremo vedno slediti ukrivljenim anatomskim strukturam ali anatomskim strukturam cevaste oblike (npr. hrbtenica, žile, črevesje), zato je prikazovanje teh struktur velikokrat nezadovoljivo, saj vsi pomembni deli struktur niso hkrati vidni v enem samem ravninskem prerezu. Posledica tega je lahko nezadostna kakovost diagnostične informacije o opazovanih ukrivljenih strukturah. Rešitev tega problema je uporaba tehnike prikazovanja z ukrivljenimi prerezi, ki so pravokotni ali tangentni na krivuljo vzdolž strukture. Koordinatni sistem, ki ga določa 3D slika, je tako preslikan v koordinatni sistem, ki ga določa opazovana 3D anatomska struktura. Ročno orisovanje krivulje, ki sledi ukrivljeni anatomski strukturi, je najenostavnejši način prikazovanja ukrivljenih prerezov. Tak pristop pa je časovno zamuden ter težaven zaradi kompleksne navigacije v 3D prostoru.

Ukrivljeni prerezi se kot tehnika prikazovanja uporabljajo na področju angiografije[8] za prikazovanje žil ter za vrednotenje bolezenskih znakov na žilah (He in dr., 2001, Kanitsar in dr., 2002, 2003, Maddah in dr., 2003, Ochi in dr., 1999, Raman in dr., 2002, 2003, Saroul in dr., 2003), na področju pankreatografije[9] za prikazovanje in vrednotenje bolezni trebušne slinavke (Gong in Xu, 2004, Prokesch in dr., 2002a, 2002b), za prikazovanje možganov (Leonardi in dr., 1991) ter na področjih bronhoskopije[10] (Law in Heng, 2000, Perchet in dr., 2004) in kolonoskopije[11] (Ge in dr., 1999, Samara in dr., 1999, Wan in dr., 2002). Natančno določanje krivulje oziroma sredinskega poteka opazovane cevaste strukture (Aylward in Bullitt, 2002, Bitter in dr., 2000) je bistvenega pomena pri vseh pristopih prikazovanja z ukrivljenimi prerezi. Prikazovanje ukrivl-

[8] angiografija: rentgenski prikaz ožilja z vbrizganjem kontrastnega sredstva za diagnostične namene

[9] pankreatografija: rentgenski prikaz izvodil trebušne slinavke z vbrizganjem kontrastnega sredstva

[10] bronhoskopija: pregled sapnika in bronhialnega vejevja z bronhoskopom, to je optično napravo za opazovanje notranjosti sapnika

[11] kolonoskopija: vizualni pregled celotnega črevesja s koloskopom, to je podaljšanim upogljivim endoskopom; koloskopija

jenih prerezov sicer omogočajo tudi namenski računalniški programi ter programski paketi proizvajalcev CT in MR skenerjev, vendar pa to zahteva ročno orisovanje krivulje, ki sledi ukrivljeni anatomski strukturi. Čeprav MR skenerji omogočajo poljubno orientacijo vzbujevalne ravnine in torej lahko posnemanjo prikazovanje s poševnimi prerezi, je tako prikazovanje še vedno odvisno od operaterja, ki orientacijo ravnine nastavi, ter od lege pacienta v skenerju. Poleg tega obstaja tudi možnost pridobivanja ukrivljenih prerezov neposredno iz MR skenerja (Börnert, 2003, Börnert in Schäffter, 1996, Jochimsen in Norris, 2002), vendar pa kakovost tako pridobljenih slik, ki so sicer ukrivljene le v eni dimenziji (1D), ni zadovoljiva zaradi nizke prostorske ločljivosti ter prisotnosti artefaktov intenzitetne modulacije. Razvoj avtomatskih tehnik za prikazovanje slik z ukrivljenimi prerezi lahko torej pomembno prispeva k interpretaciji 3D informacije v medicinskih slikah.

P.1.2 Kvantitativno vrednotenje medicinskih slik

Kvantitativno vrednotenje slik je izražanje slikovne informacije izbranih merljivih lastnosti slik z numeričnimi vrednostmi, ki so opremljene z ustreznimi merskimi enotami (Bankman in dr., 2000, Brown in McNitt-Gray, 2000). Značilni primeri so računanje razdalje med točkami ter ploščine ali prostornine območja v sliki. Pri obdelavi medicinskih slik kvantitativno vrednotenje obsega merjenje geometrijskih lastnosti izbranih anatomskih struktur (npr. premer krvne žile) ali lastnosti, ki so iz teh geometrijskih lastnosti izpeljane (npr. pretok krvi skozi žilo). Pomembna področja uporabe vključujejo morfometrijo[12], računalniško podprto diagnostiko (CAD, *ang.* computer-aided diagnosis), načrtovanje ter analizo rezultatov zdravljenja, slikovno podprte kirurške posege ter posnemanje strukture in funkcije normalnih in patoloških tkiv. Postopki za kvantitativno vrednotenje so najbolj uporabni takrat, kadar so popolnoma avtomatski oziroma zahtevajo čim manj ročnega poseganja. Poleg računalniških algoritmov pa so pomembne tudi tehnike za preverjanje točnosti ter zanesljivosti teh algoritmov, saj je potrebno pokazati njihovo klinično vrednost in možnost uporabe. Algoritem je zato potrebno preizkusiti na resničnih slikah, rezultate pa primerjati z referenčnimi meritvami iste lastnosti, ki jih v istih slikah opravijo strokovnjaki ali posamezniki z ustreznimi izkušnjami na izbranem področju, ali z drugimi referenčnimi meritvami. Zanesljivost delovanja avtomatskega postopka mora biti primerljiva ali večja od referenčnih meritev, kar je potrebno potrditi z ustreznimi eksperimenti ter statistično analizo rezultatov. Kvantitativno vrednotenje je bistvenega pomena za objektivno primerjanje merjenih lastnosti med pacienti. Nenazadnje je pa pomembno upoštevati tudi ustreznost dobljenih rezultatov v medicinskem okolju.

[12] morfometrija: merjenje organizma in njegovih delov

P.2 Prikazovanje in kvantitativno vrednotenje slik hrbtenice

P.2.1 Prikazovanje slik hrbtenice

Pri pregledovanju 3D slike hrbtenice s tehnikami prikazovanja na osnovi ravninskih prerezov lahko hrbtenica seka stranske ali čelne ravnine, medtem ko prečna ravnina ni vedno postavljena na isto višino vretenčnih teles[13] ali medvretenčnih ploščic. Vsi pomembni strukturni deli hrbtenice torej ne morejo biti prikazani hkrati v enem samem prerezu, kar je prisotno že pri prikazovanju normalne hrbtenice zaradi njene naravne ukrivljenosti v obliki črke "S", bolj pa je poudarjeno v primeru bolezenske ukrivljenosti hrbtenice, na primer pri skoliozi[14] ali povečani kifozi[15] oziroma lordozi[16].

Doslej je bilo predstavljenih že veliko načinov prikazovanja CT slik hrbtenice, katerih namen je bil izboljšati kvantitativno ter kvalitativno vrednotenje deformacij hrbtenice. Z uporabo stransko orientiranih poševnih prerezov so Rabassa in dr. (1993) pokazali, da se je prikazovanje medvretenčnih sklepov[17] izboljšalo, medtem ko so prečno orientirani poševni prerezi omogočali opazovanje ravnin, vzporednih z medvretenčnimi ploščicami. Čeprav je bilo prikazovanje omejeno na poševne prereze, so avtorji priporočili, da bi le-ti v določenih kliničnih primerih lahko nadomestili uveljavljene večravninske CT prereze, na primer pri vrednotenju stenoze[18] medvretenčne odprtine[19] ali pri določanju mesta poškodbe hrbtenice. Poševne prereze v vratnem predelu hrbtenice, ki so bili pravokotni na daljšo os leve in desne medvretenčne odprtine, so uporabljali tudi Roberts in dr. (2003a). Z njihovo pomočjo so izboljšali doslednost ter ponovljivost pri interpretaciji stenoze medvretenčne odprtine med različnimi opazovalci ter priporočili uporabo poševnih prerezov v rutinskem vrednotenju tega obolenja (slika 1.5a, str. 29). Rothman in dr. (1984) so pokazali, da so ukrivljeni prerezi, ki so jih pridobili z ročnim povezovanjem točk v krivuljo, zelo uporabni pri določanju dejanskih anatomskih odnosov med strukturami vratnega predela hrbtenice. V posameznem ukrivljenem prerezu so lahko namreč hkrati opazovali hrbtenjačo, korenine živcev, ki izhajajo iz hrbtenjače, ter medvretenčne sklepe. Newton in dr. (2002) so izboljšali prepoznavo ter interpretacijo kongenitalnih[20] deformacij hrbtenice s pomočjo ukrivljenih prerezov, določenih z ročnim orisovanjem hrbtenice v večravninskih prerezih. Prednost ukrivljenih v primerjavi z večravninskimi prerezi je bila najbolj izrazita pri hrbtenicah z znatno stransko ali čelno ukrivljenostjo (slika 1.5b, str. 29). Menten in dr. (2005)

[13] telo vretenca: masivni del vretenca, ki nosi težo in iz njega izhajajo odrastki (slika 1.4, str. 28)

[14] skolioza: nefiziološka ukrivljenost hrbtenice vstran zaradi mišičnih ali kostnih okvar

[15] kifoza: ukrivljenost hrbtenice navzad (slika 1.6, str. 30)

[16] lordoza: ukrivljenost hrbtenice v sprednji smeri (slika 1.6, str. 30)

[17] medvretenčni sklep: sklep, sestavljen iz zgornjih in spodnjih sklepnih odrastkov vretenca, ki tvorijo stik s sosednjim vretencem (slika 1.4, str. 28)

[18] hrbtenična stenoza: zožitev hrbteničnega kanala z okvaro živčevja zaradi degenerativnih sprememb na hrbtenici

[19] medvretenčna odprtina: parna stranska odprtina med vretencema za prehod spinalnega živca; intervertebralni foramen (slika 1.4, str. 28)

[20] kongenitalen: tisti, ki obstaja že ob rojstvu (deden ali nastal zaradi škodljivih vplivov v nosečnosti)

so predstavili posebno metodo prikazovanja slik hrbtenice, ki ravno tako temelji na tehniki prikazovanja z ukrivljenimi prerezi. Posebnost je v tem, da so bili ukrivljeni prerezi določeni preko krivulj, ki v slikah prečnih CT prerezov približno sledijo robu hrbteničnega kanala[21]. Strukture na prednjem ter zadnjem delu hrbtenice so bile na ta način prikazane hkrati, s čimer se je izboljšalo vrednotenje kongenitalnih deformacij hrbtenice. Ročno določanje točk oziroma krivulj, ki določajo potek ukrivljenih prerezov, je skupna lastnost vseh predstavljenih načinov prikazovanja. S polavtomatsko metodo so Kaminsky in dr. (2004) razgrajevali hrbtenico v ukrivljenih prerezih ter se tako izognili težavam z orientacijo v standardih večravninskih prerezih. Preslikava je bila določena s 3D zlepki[22], ki so opisovali centralno krivuljo hrbtenice. Krivuljo so določili ročno v stranskih in čelnih prerezih ali pa avtomatsko z iskanjem največjega premera navideznih krogel, postavljenih v telesa vretenc ali vzdolž hrbteničnega kanala.

V zadnjih letih je MR postala uveljavljena tehnika zajema slik hrbtenice, saj omogoča pridobivanje 3D slik tako mehkih tkiv kot tudi določenih kostnih struktur hrbtenice z ustrezno nastavitvijo parametrov slikanja (Brown in Semelka, 1999, Grenier in dr., 2005, 2006). Namenske večkanalne tuljave za slikanje hrbtenice pa še dodatno izboljšajo ločljivost ter razmerje signal-šum v slikah (SNR, *ang.* signal-to-noise ratio). V prikazovanju hrbteničnih nepravilnosti, poškodb ter obolenj MR velikokrat prekaša druge slikovne tehnike, kot sta na primer CT tehnika ali precej invazivna mielografija[23]. Poleg tega pa je MR še posebej primerna za longitudinalne raziskave ter analize rezultatov zdravljenja, saj pacient ni izpostavljen ionizacijskemu sevanju.

Uporaba različnih tehnik prikazovanja se je tudi na področju obdelave MR slik hrbtenice izkazala kot učinkovita. Apicella in Mirowitz (1995) sta poročala, da se večravninski MR prerezi lahko uporabijo za kompenzacijo navidezne asimetrije 3D anatomskih struktur, ki jo povzroči spremenljiva lega pacienta med postopkom zajema, ter da se tak način prikazovanja lahko uporabi pri različnih anatomskih strukturah. V primeru slik hrbtenice bi se lahko uporabili za izboljšanje prikazovanja hrbteničnega kanala ali medvretenčnih odprtin. Da bi se izognili napakam pri merjenju rotacije vretenc, so Birchall in dr. (1997) ter Adam in Askin (2006) na podlagi stranskih in čelnih prerezov ročno določili poševne prereze, ki so potekali vzporedno z zgornjo ali spodnjo vretenčno ploščico[24] oziroma vzporedno z vretenčnimi ploščicami skozi središče telesa vsakega vretenca. Liljenqvist in dr. (2002) so se osredotočili na morfologijo[25] vretenca, ki je zelo pomembna pri vstavljanju vijakov v pedikle vretenca[26] kot dela kirurškega posega pri zdravljenju skolioze (Kuklo in dr., 2005a). Merjenje dolžine, širine ter kota pedikla je potekalo v ročno določenih poševnih MR prerezih, ki so potekali pravokotno na telesa vretenc.

[21] hrbtenični kanal: kanal, ki ga oklepajo telesa in loki vretenc ter vsebuje hrbtenjačo in njene ovojnice; vretenčni kanal (slika 1.4, str. 28)

[22] zlepek: matematična funkcija, določena s odsekoma zveznimi polinomi

[23] mielografija: rentgenska preiskava prostora hrbtnega mozga s kontrastnim sredstvom

[24] vretenčna ploščica: tanek sloj hrustanca med površino telesa vretenca ter medvretenčno ploščico na zgornjem ali spodnjem delu telesa vretenca

[25] morfologija: veda o zgradbi normalnih ali patološko spremenjenih celic, tkiv, organov ali organizmov

[26] pedikel vretenca: ožji del vretenčnega loka, ki izhaja iz telesa vretenca (slika 1.4, str. 28)

P.2.2 Kvantitativno vrednotenje slik hrbtenice

Kvantitativno vrednotenje parametrov hrbtenice lahko pomembno prispeva k načrtovanju kirurških posegov (Aronsson in dr., 1996, Duke in dr., 2005, Herring in dr., 1998, Tamura in dr., 2005), analizi rezultatov kirurških posegov (Kuklo in dr., 2005b, Lee in dr., 2004, Petit in dr., 2004), spremljanju poteka zdravljenja hrbteničnih obolenj (Asazuma in dr., 2004, Stokes in Aronsson, 2001) ter pri določanju referenčnih vrednosti normalnih ter bolezenskih stanj (Cyteval in dr., 2002, Sevastik in dr., 1995). Med najpomembnejšimi parametri vrednotenja hrbtenice so ukrivljenost hrbtenice, dolžina hrbtenične krivulje, Cobbov kot, položaj središčnih točk teles vretenc ter prečni, stranski in čelni kot rotacije vretenc (Stokes, 1994) (slika 1.7, str. 31). Pri vrednotenju skoliotičnih deformacij pa sta v ospredju predvsem dva parametra, in sicer ukrivljenost hrbtenice ter rotacija vretenc. Ker vzroki za nastanek ter razvoj skolioze, tako kongenitalne kot idiopatične[27], še vedno niso povsem znani, je poleg ugotavljanja primernosti obstoječih slikovnih tehnik (Cassar-Pullicino in Eisenstein, 2002, Do in dr., 2001, Schmitz in dr., 2001, Wright, 2000) pomemben tudi razvoj sistemov za razvrščanje skoliotičnih deformacij (Ajemba in dr., 2005, King in dr., 1983, Lenke in dr., 2001, Poncet in dr., 2001, Ramirez in dr., 2006). Nenazadnje je pa pomembno tudi dokazati klinično vrednost takih sistemov razvrščanja (Arlet in dr., 2003, Coonrad in dr., 1998, Edgar, 2002, Ogon in dr., 2002, Richards in dr., 2003).

Metode vrednotenja ukrivljenosti hrbtenice so bile najprej razvite za uporabo v čelno orientiranih rentgenskih slikah, saj le-te prikazujejo najpomembnejši del deformacije v primeru skolioze. Ena najstarejših metod merjenja ukrivljenosti, ki je sicer še vedno v uporabi, je Fergusonova metoda (Ferguson, 1930). Stopnja deformacije je določena s kotom med premicama, ki povezujeta središče apikalnega vretenca[28] s središčema vretenc na konceh deformacije[29] (slika 1.8a, str. 33). Greenspanov indeks (Greenspan in dr., 1978) omogoča merjenje ukrivljenosti posameznih vretenc in je zato uporaben za merjenje kratkih segmentov ter relativno šibkih hrbteničnih krivulj. Središči vretenc na konceh deformacije določata hrbtenično premico, na katero se pravokotno določijo dodatne premice skozi središča vretenc na krivulji hrbtenice (slika 1.8b, str. 33). Razmerje vsote dolžin teh premic proti dolžini hrbtenične premice predstavlja merilo (indeks) za deformacijo, ki zavzame pri normalni hrbtenici vrednost nič. Najbolj uveljavljena metoda za vrednotenje ukrivljenosti hrbtenice v čelnih rentgenskih slikah je Cobbova metoda (Cobb, 1948). Stopnjo deformacije določa Cobbov kot, izmerjen med premicama, ki potekata vzporedno z zgornjo vretenčno ploščico na zgornjem koncu deformacije ter vzporedno s spodnjo vretenčno ploščico na spodnjem koncu deformacije (slika 1.8c, str. 33). Hrbtenične krivulje, ki imajo Cobbov kot večji od 10 stopinj, se pojmujejo kot skoliotične. Kljub temu, da so široko v uporabi, vse predstavljene metode temeljijo na ročnem določanju vretenc ter drugih lastnosti hrbtenice, kar se kaže v njihovi relativno visoki variabilnosti ter

[27] idiopatičen: tisti, ki nastane zaradi neznanega vzroka ali neodvisno od drugih bolezni

[28] apikalno vretence: vretence, ki se nahaja v konici (središču) deformacije hrbtenice

[29] vretenci na konceh deformacije: vretenci, ki sta najbolj nagnjeni proti konkavnemu delu deformacije hrbtenice

nezanesljivosti (Beekman in Hall, 1979, Carman in dr., 1990, Deacon in dr., 1984, Diab in dr., 1995, Morrissy in dr., 1990, Shea in dr., 1998, Stokes in dr., 1993, Wills in dr., 2007, Zmurko in dr., 2003). Po drugi strani pa so bile predstavljene številne študije, kjer so ukrivljenost hrbtenice zaradi njenega zveznega poteka skušali opisati z različnimi matematičnimi funkcijami, kot so npr. sinusne funkcije (Drerup in Hierholzer, 1996), zlepki (Kaminsky in dr., 2004, Verdonck in dr., 1998, Yang in dr., 2007), polinomske funkcije (Patwardhan in dr., 1996, Peng in dr., 2005), ter tudi s statističnimi metodami, kot je npr. kriging interpolacija[30] (Poncet in dr., 1999).

Zanesljivost ter natančnost merjenja Cobbovega kota ter sistemov za razvrščanje skoliotičnih deformacij so poskušali izboljšati s pomočjo računalniških algoritmov (Chockalingam in dr., 2002, Goh in dr., 2000a, Stokes in Aronsson, 2006). Vendar pa je največji vzrok za nenatančnost metode ta, da se relativno zapletena 3D deformacija hrbtenice vrednoti z relativno enostavno meritvijo v enem 2D prerezu, in sicer v čelni rentgenski sliki. Cheung in dr. (2002) so poskušali izboljšati meritve z ugotavljanjem poteka sredinske krivulje hrbtenice na podlagi kombiniranja čelne in stransko orientirane rentgenske slike. Poleg rentgenskih slik so ukrivljenost hrbtenice skušali vrednotiti tudi v slikah, pridobljenih z drugimi slikovnimi tehnikami, na primer v stereoradiografskih[31] slikah ter stereofotografijah[32] hrbta (Asamoah in dr., 2000, Bendels in dr., 2005, Bergeron in dr., 2005, Drerup in Hierholzer, 1994, Gille in dr., 2007, Liljenqvist in dr., 1998, Stokes in dr., 1988, Tredwell in dr., 1999, Zubairi, 2002), v stereoradiografskih slikah prsnega koša (Aykroyd in Mardia, 2003, Boisvert in dr., 2006, Jaremko in dr., 2001) ali v moiréovih[33] ter drugih topografskih slikah hrbta (Kim in dr., 2001, Knott in dr., 2006), ter celo z različnimi neinvazivnimi primomočki, kot je na primer elektrogoniometer[34] (Campbell-Kyureghyan in dr., 2005) ali skoliometer[35] (Amendt in dr., 1990). Vrednotenje ukrivljenosti hrbtenice je bilo seveda opravljeno tudi v prečnih CT prerezih slik hrbtenice (Adam in dr., 2005, Verdonck in dr., 1998), ki omogočajo kakovostne prikaze 3D geometrije hrbtenice. Slikanje celotne dolžine hrbtenice s CT tehniko pa predstavlja precej invaziven pristop zaradi izpostavljanja relativno visoki količini ionizacijskega sevanja (Brant-Zawadzki, 2002). Pristop, ki temelji na CT slikanju, torej ne pride v poštev v primerih, kjer se zahteva večkratni zajem slik (npr. pri spremljanju poteka deformacije ali zdravljenja). Ker pri tehniki MR ionizacijskega sevanja ni, lahko le-ta predstavlja alternativo pri določanju hrbtenične krivulje (Wessberg in dr., 2006).

Vrednotenje rotacij vretenc je bilo največkrat omejeno na prečne rotacije, to je rotacije vretenca okoli vzdolžne osi hrbtenice. To je v veliki meri tudi vzrok, da je sinonim za prečno rotacijo

[30] kriging interpolacija: skupina geostatističnih metod za prostorsko linearno interpolacijo vrednosti naključnega polja

[31] stereoradiografija: tehnika zajemanja parov rentgenskih slik, preko katerih se lahko rekonstruira lastnosti objektov v 3D

[32] stereofotografija: tehinka zajemanja fotografij mreže, ki je projicirana na opazovani objekt pod različnimi koti, kar omogoča opazovanje globine objekta

[33] moiréove topografske slike: slike opisujejo obliko 3D objekta na podlagi progastih svetlobnih vzorcev; svetlobo, ki je projicirana na objekt, opazujemo s posebno kamero, svetlostna intenziteta progastih vzorcev pa določa ekvidistančna področja oddaljenosti od kamere

[34] elektrogoniometer: naprava za zvezno merjenje kotov v sklepih med okončinami

[35] skoliometer: naprava za merjenje kota asimetrije trupa

velikokrat kar izraz “rotacija”. Glede na razpoložljivost tehnologije za zajemanje slik so se razvili različni pristopi k merjenju prečne rotacije v čelnih, stranskih in prečnih ravninskih prerezih. Določanje prečne rotacije v čelnih rentgenskih slikah je med prvimi predstavil Cobb (1948). Metoda je temeljila na določanju položaja trnastega odrastka vretenca[36], ki ponavadi leži na sredini telesa vretenca. Z naraščajočo rotacijo pa se trnasti odrastek prične sukati proti konkavni strani hrbtenične krivulje. Na podlagi delitve telesa vretenca na šest enakih odsekov je bila stopnja prečne rotacije določena z odsekom, ki je vseboval trnasti odrastek (slika 1.9a, str. 35). Podobnega principa se poslužuje metoda, ki sta jo predstavila Nash in Moe (1969), saj temelji na določanju položaja pediklov vretenca. Pedikli, ki ponavadi ležijo na zunanji strani telesa vretenca, se namreč z naraščajočo rotacijo pričnejo premikati proti konveksni strani hrbtenične krivulje (slika 1.9b, str. 35).

Predstavljeni metodi sta spodbudili nastanek številnih študij, ki so poskušale vpeljati različne geometrijske principe za kar najbolj natančen opis anatomskih lastnosti vretenc v čelnih rentgenskih slikah ter različne polavtomatske računalniške pristope za izboljšanje natančnosti meritev prečne rotacije vretenc (Benson in dr., 1976, Chi in dr., 2006, Coetsier in dr., 1977, Deacon in dr., 1984, Drerup, 1984, 1985, 1992, Mehta, 1973, Perdriolle in Vidal, 1985, Stokes in dr., 1986). Analiza natančnosti raznovrstnih pristopov (Drerup in Hierholzer, 1992a, 1992b, Ho in dr., 1993, Omeroğlu in dr., 1996, Russell in dr., 1990, Skalli in dr., 1995, Weiss, 1995) je pokazala, da je vrednotenje prečne rotacije v čelnih rentgenskih slikah nezanesljivo. Razlog za to je največkrat v tem, da rentgenske projekcije ne dajejo zadovoljive ali dovolj kakovostne informacije o opazovanih anatomskih strukturah.

Kljub temu, da stranske rentgenske slike niso primerne za merjenje prečnih rotacij vretenc, se lahko v njih meri stranska rotacija vretenc, to je rotacija okrog osi, ki poteka od leve do desne strani telesa. Na podlagi stranske rotacije se lahko določijo maskimalne vrednosti kifoze in lordoze, naklon križnega predela hrbtenice ter razlike v naklonu med sosednjimi vretenci. Največkrat se je uporabila kar Cobbova metoda (Bernhardt in Bridwell, 1989, Côté in dr., 1997, Korovessis in dr., 1998, Stagnara in dr., 1982) (slika 1.10a, str. 36). Zaradi že omenjenih pomanjkljivosti tega postopka pa so bili predlagani alternativni pristopi. Določanje Cobbovega kota v stereoradiografskih slikah so na primer predstavili De Smet in dr. (1980), Stokes (1989), Dumas in dr. (2004) ter Poncet in dr. (2001). Harrison in dr. (2000) so merili rotacijo na podlagi premic, ki so bile ročno določene tangentno na zadnjo stran izbranih teles vretenc (slika 1.10b, str. 36). V delu Goh in dr. (2000a) je merilo za stransko rotacijo predstavljal povprečni polmer ukrivljenosti dveh krožnih lokov, ki sta potekala skozi ročno določene točke na vogalih vretenčnih teles (slika 1.10c, str. 36). Pinel-Giroux in dr. (2006) so sestavili krivuljo hrbtenice iz štirih krožnih lokov, tangentnih na središča izbranih teles vretenc. Izmerjena rotacija je bila določena s kotom med premicami, ki so povezovale središča krožnih lokov s središči vretenčnih teles, ter referenčno vodoravno premico (slika 1.10d, str. 36). Podoben pristop so predstavili Janik

[36]trnasti odrastek vretenca: odrastek, ki štrli iz loka vretenca navzad in je pripenjališče nekaterim hrbtnim mišicam; spinozni procesus vretenca (slika 1.4, str. 28)

in dr. (1998) za ledveno lordozo ter Harrison in dr. (1998, 2002, 2004) za prsno kifozo, kjer so kote določali s pomočjo elips, ki so se kar najbolje prilegale točkam v vogalih vretenčnih teles (slika 1.10e, str. 36). Prince in dr. (2007) so vrednotili stransko rotacijo vretenc z indeksom kifoze, ki je bil določen kot razmerje med največjo razdaljo hrbtenice do referenčne čelne ravnine ter dolžino premice, ki je povezovala merjeni točki na hrbtenici.

Najbolj intuitiven način merjenja prečne rotacije vretenc je vrednotenje v prečnih prerezih (Heithoff in Herzog, 1991), vendar je to postalo mogoče šele z razvojem 3D slikovnih tehnik. Izkazalo se je, da je mogoče prečno rotacijo vretenc najbolj natančno določiti v CT slikah (Krismer in dr., 1996, Kuklo in dr., 2005b). Prvi poskus merjenja rotacije v prečnih CT prerezih sta predstavila Aaro in Dahlborn (1981). Prečna rotacija je bila določena s kotom med premico, ki je potekala skozi stičišče obeh plošč vretenčnega loka[37,38] in skozi središče telesa vretenca, ter referenčno stransko ravnino (slika 1.11a, str. 38). Na podoben način so prečno rotacijo definirali Ho in dr. (1993). Kot, ki sta ga določali premici skozi stičišče vsake plošče vretenčnega loka s pediklom in skozi stičišče obeh plošč vretenčnega loka, je bil najprej razpolovljen z dodatno premico. Prečna rotacija je bila nato določena s kotom med to premico ter med referenčno stransko ravnino (slika 1.11b, str. 38). Še bolj kompleksna je metoda, ki temelji na ročnem določanju petih značilnih točk anatomije vretenca (Krismer in dr., 1996), in sicer točk v središču telesa vretenca, na koncu trnastega odrastka vretenca, v središču hrbteničnega kanala med obema ploščama vretenčnega loka ter točk na najbolj posteriorni in anteriorni[39] strani hrbteničnega kanala. Tako izbrane točke so tvorile premice, ki so glede na referenčno stransko krivuljo določale različne kote prečne rotacije (slika 1.11c, str. 38). Göçen in dr. (1999) so rotacijo definirali s kotom med premico, ki je potekala skozi najbolj posteriorni točki obeh pediklov vretenca, ter referenčno stransko ravnino CT slike (slika 1.11d, str. 38).

Kljub zelo natančno podanim metodam vrednotenja prečne rotacije so opisane študije zanemarjale dejstvo, da so lahko vretenca zaradi deformacije hrbtenice rotirana tudi v stranski in čelni smeri, kar lahko povzroči napako pri meritvah v obliki "navidezne" prečne rotacije. Skalli in dr. (1995) so primerjali vrednosti, izmerjene v 3D, z vrednostmi, izmerjenimi v 2D, ter ugotovili, da je merjenje prečne rotacije vretenc v prečnih prerezih lahko nenatančno, še posebej v primeru izrazitih stranskih ali čelnih rotacij vretenc. Krismer in dr. (1996) so poročali, da lahko napake pri merjenju nastopijo tudi v primeru popolnoma simetričnih vretenc ter tudi pri nadomeščanju prečnih prerezov s poševnimi prerezi. Yazici in dr. (2001) so primerjali meritve v prečnih CT prerezih z meritvami v čelnih rentgenskih slikah, pridobljenih pri stoječem in ležečem položaju pacienta. Ugotovili so, da lega pacienta vpliva na meritve tako v prečnih kot tudi v čelnih prerezih, kar je seveda lahko pojmovano kot dodatna rotacija v 3D.

Predlagane računalniško podprte metode za vrednotenje prečne rotacije vretenc v CT slikah

[37] plošča vretenčnega loka: zadajšnji del vretenčnega loka, iz katerega navzad izhaja trnasti odrastek vretenca; lamina arkusa vretenca (slika 1.4, str. 28)

[38] vretenčni lok: koščeni lok na zadajšnji strani vretenca; arkus vretenca

[39] anterioren: tisti, ki je v telesu pred čim ali v sprednjem delu organa; sprednji, ventralen

so zaradi precejšnjega ročnega poseganja zgolj polavtomatske. Metoda, ki so jo predstavili Rogers in dr. (2005), je temeljila na ročnem določanju za meritve najprimernejšega prečnega prereza ter središčne točke rotacije na anteriornem robu hrbteničnega kanala. Rotacija glede na izbrani drugi prerez je bila nato določena z iskanjem največje korelacije slikovnih intenzitet v obeh prerezih (slika 1.12a, str. 40). Kouwenhoven in dr. (2006) so določali prečno rotacijo v slikah normalnih hrbtenic s pomočjo ročno določenih prečnih prerezov skozi središča teles vretenc. Rotacija je bila določena s kotom med premico, ki je povezovala središče hrbteničnega kanala s težiščem vretenca, določenega s postopkom razgradnje na osnovi rasti področja, ter med premico, ki je povezovala središče hrbteničnega kanala s prsnico na višini vretenca T5[40] (slika 1.12b, str. 40). Adam in Askin (2006) sta pravilne vrednosti rotacije v 3D poskušala določiti z uporabo poševnih prerezov, v katerih sta določala naklon premice, ki je razpolavljala telo vretenca. Naklon premice je bil določen z iskanjem največje korelacije slikovnih intenzitet v razpolovljenih območjih vretenčnega telesa (slika 1.12c, str. 40).

Vrednotenje prečne rotacije vretenc v MR slikah so predstavili Birchall in dr. (1997), ki so za merjenje uporabili tehniko, ki sta jo predlagala Aaro in Dahlborn (1981) za CT slike (slika 1.13a, str. 41). Podobno so Birchall in dr. (2005) določali rotacije v MR slikah z metodo po Hoju in dr. (1993), ki je bila prav tako razvita za CT slike. Metode, ki so jih predstavili Haughton in dr. (2002) ter Rogers in dr. (2002), so temeljile na ročnem določanju prečnega MR prereza ter ročnem določanju središča rotacije ter krožnih področij, ki so zaobjemala vretence. Prečna rotacija vretenca glede na neko drugo vretence je bila izračunana na podlagi iskanja največje korelacije med krožnimi področji obeh vretenc (sliki 1.13b, str. 41 in 1.13c, str. 41). Metodo, ki je temeljila na simetriji vretenca v prečnih MR prerezih, sta predstavila Booth in Clausi (2001). Zasuk vsakega prereza okoli hrbtenjače, ki je torej predstavljala središče rotacije, je bil določen z iskanjem najmanjše povprečne kvadratne razlike slikovnih intenzitet v področjih, ki jih je z razpolavljanjem prereza določala navpična premica skozi hrbtenjačo. Reisman in dr. (2006) so določali stranske rotacije medvretenčnih ploščic v stranskih MR prerezih, in sicer na podlagi iskanja podobnosti področij slike nad in pod vsako medvretenčno ploščico.

Vrednotenje ukrivljenosti hrbtenice ter rotacije vretenc ima pomembno vlogo pri različnih postopkih obdelave slik ter medicinskih raziskavah (Doi in dr., 1997). Zaradi tega je sestavni del različnih raziskav v povezavi s hrbtenico, na primer pri merjenju ravnotežja telesa (Berthonnaud in dr., 2005b, Glassman in dr., 2005b, 2005a, Mac-Thiong in dr., 2003), na področju biomehanične analize hrbtenice (Cholewicki in dr., 1996, Huysmans in dr., 2004, Oda in dr., 2002, Orchowski in dr., 2000, Stokes, 1997, Teo in dr., 2007, Wever in dr., 1999), morfometrije vretenc in hrbtenice (Goh in dr., 2000b, Liljenqvist in dr., 2000, Masharawi in dr., 2004, Nojiri in dr., 2005, Parent in dr., 2002, Porter, 2000, Roberts in dr., 2003b, Smyth in dr., 1997, Tan in dr., 2002, 2004), pri združevanju rentgenskih, CT in MR slik hrbtenice (Chen in Wang, 2004, Hu in Haynor, 2004, Hu in dr., 2005, Panigrahy in dr., 2000), rekonstrukciji slik

[40] hrbtenico sestavlja sedem vratnih vretenc (od C1 do C7), dvanajst prsnih vretenc (od T1 do T12), pet ledvenih vretenc (od L1 do L5), križnica ali sakralni predel ter trtične kosti (slika 1.6, str. 30)

hrbtenice (Benameur in dr., 2005a, 2005b, Bifulco in dr., 2002, Chen in Wang, 2004, Gille in dr., 2007, Huynh in dr., 1997, Novosad in dr., 2004, Perdriolle in dr., 2001) ter pri razgradnji vretenc in hrbtenice (Carballido-Gamio in dr., 2004, Ghebreab in Smeulders, 2004, Herring in Dawant, 2001, Hoad in Martel, 2002, Hoad in dr., 2001, Muggleton in Allen, 1997, Peng in dr., 2005, Yao in dr., 2006, Zamora in dr., 2003, Zheng in dr., 2004).

P.3 Motivacija

Kljub vsem omenjenim težavam in omejitvam sodobne slikovne tehnike omogočajo natančnejšo diagnostiko ter načrtovanje učinkovitejših strategij zdravljenja hrbteničnih obolenj. Naraščajoče število medicinskih slik ter kliničnih informacij spodbuja razvoj metod za računalniško podprto diagnostiko (CAD) (Giger, 2002). Povečanje učinkovitosti v interpretaciji teh podatkov, zmanjšanje variabilnosti in napak zaradi ročnega vrednotenja ter premik od interpretacije proti kvantitativnemu vrednotenju predstavljajo najpomembnejše razloge za razvoj CAD sistemov (Doi in dr., 1997). Računalniško podprto prikazovanje ter kvantitativno vrednotenje 3D slik hrbtenice predstavljata torej velik izziv na področju analize in obdelave medicinskih slik.

P.4 Izvirni prispevki k znanosti

Izvirni prispevki te doktorske disertacije združujejo načrtovanje, razvoj ter vrednotenje avtomatskih tehnik za izboljšanje prikazovanja 3D slik hrbtenice na podlagi določanja ukrivljenih prerezov ter avtomatskih tehnik za izboljšanje kvantitativnega vrednotenja najpomembnejših parametrov hrbtenice v 3D, in sicer ukrivljenosti hrbtenice ter rotacije vretenc.

P.4.1 Definicija hrbtenici lastnega koordinatnega sistema

POGLAVJE 2: Avtomatsko prikazovanje 3D slik hrbtenice z ukrivljenimi prerezi

POGLAVJE 3: Avtomatsko določanje ukrivljenih prerezov v MR slikah hrbtenice

Uveljavljene tehnike 2D prikazovanja hrbtenice temeljijo na večravninskih prerezih 3D slik. Večravninski prerezi so ponavadi predstavljeni v kartezičnem koordinatnem sistemu (x, y, z), v katerem je vsaka koordinatna os usmerjena vzdolž ali pravokotno na ravnino zajema slike. Z izbiranjem vrednosti na koordinatnih oseh x, y in z lahko prikazujemo pripadajoče stranske, čelne in prečne ravninske prereze v koordinatnem sistemu slike. Orientacija koordinatnega sistema je torej odvisna od lege pacienta med zajemom slike ter popolnoma neodvisna od hrbtenice kot opazovane anatomske strukture. Za rešitev tega problema predlagamo hrbtenici lasten koordinatni sistem (u, v, w), ki je neodvisen od lege pacienta med zajemom slike. Koordinatne osi

hrbtenici lastnega sistema so usmerjene skladno z anatomijo hrbtenice ter tako hkrati opisujejo geometrijske in klinično pomenljive lastnosti hrbtenice. Koordinatna os *u* je usmerjena v smeri prečnih odrastkov vretenca, koordinatna os *v* v smeri trnastih odrastkov vretenca, koordinatna os *w* pa v smeri vzdolžne osi hrbtenice.

P.4.2 Razvoj postopka za avtomatsko prikazovanje CT slik hrbtenice z ukrivljenimi prerezi

POGLAVJE 2: Avtomatsko prikazovanje 3D slik hrbtenice z ukrivljenimi prerezi

V tem poglavju je predstavljena avtomatska metoda za prikazovanje CT slik hrbtenice z ukrivljenimi prerezi. Postopek temelji na preslikavi slike iz karteziˇcnega koordinatnega sistema v hrbtenici lasten koordinatni sistem (poglavje P.4.1). Preslikava med koordinatnima sistemoma je določena na osnovi krivulje, ki poteka skozi središča teles vretenc, ter na rotaciji vretenc okoli te krivulje. Pri določanju poteka hrbtenične krivulje smo se oprli na anatomsko lastnost hrbtenice, da so telesa vretenc lokalno največje kostne strukture v hrbtenici ter da jih je mogoče v CT slikah uspešno razgraditi. Rotacija vretenc okoli hrbtenične krivulje pa je določena na podlagi simetrije anatomske strukture vretenca v prerezih, ki so pravokotni na hrbtenično krivuljo. Slednje omogoča, da je rotacija vretenc dejansko določena v 3D. Hrbtenična krivulja ter rotacija vretenc okoli krivulje sta modelirani s polinomskimi funkcijami. Parametre, ki določajo polinomske funkcije, smo poiskali z optimizacijskimi postopki. Predlagano metodo smo kvalitativno ter kvantitativno vrednotili v petih CT slikah hrbtenice. Rezultati so pokazali, da je metoda učinkovita v primeru normalnih kot tudi bolezenskih hrbteničnih krivulj, ter da so rezultati metode skladni z ročno določenimi vrednostmi za hrbtenično krivuljo in rotacijo vretenc.

P.4.3 Razvoj postopka za avtomatsko prikazovanje MR slik hrbtenice z ukrivljenimi prerezi

POGLAVJE 3: Avtomatsko določanje ukrivljenih prerezov v MR slikah hrbtenice

V tem poglavju je predstavljena avtomatska metoda za prikazovanje MR slik hrbtenice z ukrivljenimi prerezi. Metoda temelji na preslikavi slike iz karteziˇcnega koordinatnega sistema v hrbtenici lasten koordinatni sistem (poglavje P.4.1). Preslikava med koordinatnima sistemoma je določena na osnovi krivulje, ki poteka skozi središča teles vretenc, ter na rotaciji vretenc okoli te krivulje. Hrbtenična krivulja ter rotacija vretenc okoli krivulje sta modelirani s polinomskimi funkcijami. Parametri polinomskih funkcij so določeni z robustno regresijo začetnih ocen položajev središč vretenčnih teles ter prečnih rotacij vretenc. Začetne vrednosti smo določili z optimizacijski postopki, ki temeljijo na simetriji anatomske strukture vretenca ter homogenosti

slikovnih intenzitet na področju telesa vretenca in medvretenčnih ploščic v prečnih prerezih MR slik. Predlagano metodo smo kvalitativno in kvantitativno vrednotili v 21 T_1- in T_2-uteženih MR slikah. Rezultati so pokazali, da metoda učinkovito opisuje anatomijo hrbtenice.

P.4.4 Razvoj postopka za kvantitativno vrednotenje ukrivljenosti hrbtenice v 3D

POGLAVJE 4: Kvantitativna analiza ukrivljenosti hrbtenice v 3D: Uporaba v CT slikah normalne hrbtenice

V tem poglavju je predstavljen postopek za kvantitativno vrednotenje ukrivljenosti hrbtenice v 3D. Obstoječe metode za vrednotenje ukrivljenosti hrbtenice so preveč zapletene za klinično uporabo, poleg tega pa deformacijo hrbtenice opisujejo le v 2D, medtem ko lahko s 3D opisovanjem pridobimo bolj celovito oceno o 3D ukrivljenosti hrbtenice. Ukrivljenosti hrbtenice smo vrednotili z geometrijsko ukrivljenostjo (GC, *ang.* geometric curvature) ter kotom ukrivljenosti (CA, *ang.* curvature angle) v 30 CT slikah normalne hrbtenice, in sicer na podlagi 3D hrbteničnih krivulj skozi središča teles vretenc, določenih s pomočjo dveh različnih metod. Prva metoda temelji na iskanju krivulje skozi ročno določena središča vretenčnih teles s postopkom najmanjših kvadratov. Pri drugi metodi pa se središča vretenčnih teles avtomatsko določijo s pomočjo optimizacijskega postopka, ki temelji na računalniško podprti analizi slik. V obeh primerih je normalna hrbtenična krivulja opisana s 3D polinomskimi funkcijami četrte stopnje. Bistvena prednost vrednotenja ukrivljenosti hrbtenice z GC in CA je v tem, da so meritve neodvisne od orientacije in velikosti hrbtenice ter tako omogočajo objektivno primerjavo med različnimi hrbteničnimi krivuljami. Poleg tega smo iz porazdelitve vrednosti GC in CA določili tudi položaje največje prsne kifoze (TK, *ang.* thoracic kyphosis), prsno-ledvenega spoja (TJ, *ang.* thoracolumbar junction) ter največje ledvene lordoze (LL, *ang.* lumbar lordosis).

P.4.5 Razvoj postopka za avtomatsko določanje položaja in rotacije vretenc v CT in MR slikah hrbtenice

POGLAVJE 5: Določanje 3D položaja in rotacije ledvenih vretenc v CT slikah z avtoporavnavo na osnovi simetrije

POGLAVJE 6: Določanje položaja in rotacije vretenc v 3D neodvisno od tehnike slikanja

V teh dveh poglavjih je predstavljena avtomatska metoda za določanje položaja ter rotacije vretenc v CT in MR slikah hrbtenice. Uveljavljene tehnike za določanje rotacije vretenc namreč nezadovoljivo izkoriščajo 3D slikovno informacijo, zaradi česar lahko nastopijo napake pri merjenju prečne rotacije, ki jih povzroči rotacija vretenc v stranski in čelni smeri. Poleg tega se meritve ponavadi opravljajo v ravninskih prerezih ter potrebujejo veliko ročnega poseganja.

Predlagani pristop k avtomatskemu določanju položaja ter rotacije vretenc v 3D ne potrebuje predhodnega določanja za meritve najustreznejših prerezov ali znanja v obliki statističnih modelov. Različne dele opazovanega vretenca smo zaobjeli z maskami v obliki eliptičnih valjev v 3D. Položaj ter rotacija mask v 3D sta določena s šestimi parametri toge preslikave, in sicer s središčem rotacije (x, y, z) ter koti rotacije (α, β, γ). Na osnovi razpolavljanja mask z njihovimi sredinskimi prečnimi, stranskimi ter čelnimi ravninami smo vrednotili naravno simetrijo telesa vretenca, hrbtenice ter hrbteničnega kanala, in sicer z robustno togo avto-poravnavo na tak način pridobljenih zrcalnih delov mask. V prvem eksperimentu smo metodo kvantitativno vrednotili na 50 ledvenih vretencih iz CT slik normalne ter skoliotične hrbtenice. V drugem eksperimentu smo metodo vrednotili na 52 vretencih, in sicer na 26 iz CT ter 26 iz MR slik hrbtenice. Rezultati so pokazali, da lahko s predlagano avto-poravnavo simetričnih delov vretenca uspešno določimo 3D položaj ter 3D rotacijo vretenc tako v CT kot tudi v MR slikah hrbtenice.

And now, the end is near,
and so I face the final curtain.
My friend, I'll say it clear,
I'll state my case, of which I'm certain.

Frank Sinatra, 1915 – 1998
(My Way, 1968)

CHAPTER 1

Introduction and Summary

Medical images are of extreme importance for diagnosing and understanding of normal and pathological conditions of the human body. To some extent, the quality of image-assisted medical examinations depends on the acquisition of images, interpretation of the information present in images and on the research activity and clinical environment that stimulate image formation and its application.

In the past decades, advances in medical imaging technology and computerized medical image processing led to the development of new three-dimensional (3D) image acquisition techniques that have become important clinical tools in modern diagnostic radiology and medical health care. Although two-dimensional (2D) images, especially radiographic (X-ray) images, are still widely present in clinical examination due to relatively low acquisition price and wide area of application, they are slowly being replaced by 3D images. The continuous increase in the number of acquired cross-sections, reduction in cross-sectional thickness and relatively short acquisition time (table 1.1, p. 20) led to the expansion of 3D imaging techniques (Sakas, 2002). Among the most important 3D techniques are computed tomography (CT) and magnetic resonance (MR) imaging, which provide qualitative data of the imaged structures. However, characteristic features of these techniques and variable positioning of the patient during image acquisition still represent a major source of variability that causes errors in the interpretation of image information. On the other hand, human capability of discovering and diagnosing diseases by proper interpretation of medical images is limited due to our non-systematic search patterns.

Moreover, the presence of noise may conceal the natural anatomical background, such as actual geometrical relationship between anatomical structures, which may further hamper mental reconstruction of the 3D image information. Errors in interpretation may also be caused by similar characteristics of normal and pathological conditions and by the natural biological variability of human anatomy. Image interpretation therefore depends to a great extent on adequate presentation and measurement of the information about anatomical structures or physiological processes. As the information of interest is often associated with characteristic features of the selected structure or process, it is crucial to use specially designed image processing techniques for visualization and quantitative evaluation. Techniques for visualization and quantitative evaluation of medical images are therefore extremely valuable in the development of image-assisted diagnosis, planning of surgical interventions and assessment of medical treatment outcomes.

Table 1.1. The evolution of the CT imaging technique.

Tabela 1.1. Razvoj CT slikovne tehnike.

Year	Innovation	Cross-sections per examination	Cross-sectional thickness [mm]	Time per cross-section [s]
1972	Prototype CT	1	10	240
1981	Clinical CT	20	5	15
1986	Dynamic CT	50	1	8
1989	Spiral CT	300	1	1
1997	Multislice (4) spiral CT	1000	1	0.5
2001	Multislice (16) spiral CT	1000	0.5	0.5
2004	Multislice (64) spiral CT	2000	0.4	0.33

Although current approaches to the treatment of spinal injuries and degenerative spinal disorders reach clinical expectations, the treatment methods are still not entirely adequate (Toyone et al., 2005). Most patients who experience spine-related pain or disability (e.g. low back pain, leg pain) are commonly treated with a combination of pain-relieving drugs and physical therapy, while surgical interventions are the preferred treatment in the case of acute disorders or traumatic spine injuries. However, the results of the treatment are unsatisfactory (e.g. persistent pain, disability) for a relatively large number of patients. The fact that current understanding of physical and biomechanical properties of the spine is inadequate to predict the exact outcomes of various treatment strategies greatly affects the management of spinal disorders. Moreover, the identification, visualization and quantitative evaluation of many spinal diseases by routine examinations is difficult because the spine is a complex and articulated anatomical structure. On the other hand, qualitative insight into the spine anatomy is possible by state-of-the-art im-

age acquisition techniques. The CT imaging technique is appropriate for observing the bones and other dense structures of the spine, while the MR imaging technique allows examination of soft tissues, such as intervertebral discs[1], spinal cord[2] and nerve roots[3,4]. Further development of spine visualization and quantitative evaluation techniques may therefore improve medical diagnosis and the design of more effective strategies for the treatment of spinal disorders.

This thesis concentrates on the design, development and validation of automated techniques that aim to improve the visualization of 3D spine images, and techniques for an improved quantitative evaluation of the most important parameters of the spine in 3D, such as the spinal curvature and vertebral rotation. The fields of visualization and quantitative evaluation of spine images are closely related, as knowledge of spine parameters may provide a more effective spine visualization, and, on the other hand, proper spine visualization may allow a more effective measurement of spine parameters.

1.1 Visualization and quantitative evaluation of images

Image formation is defined as the process of mapping selected properties of the imaged object into the image space. The image space represents the basis for visualization of the object and its properties, and may be further used for quantitative evaluation of its structure or function and interpretation of the information it contains. As quantitative evaluation and interpretation of images depend on the quality of the information of interest, the main purpose of image visualization is effective information extraction. In the field of medical image visualization, the extraction of clinically relevant information is therefore of significant importance for the development of accurate and non-invasive techniques for medical diagnosis and treatment.

1.1.1 Visualization of medical images

Volumetric image visualization is defined as the transformation of image information from a 3D image space onto a 2D display device (Robb, 2000, Rubin et al., 1996, Udupa, 2000):

- 2D image visualization is comprised of techniques that optimally display the selected property of the 3D image in 2D cross-sections:

[1] intervertebral disc: a disc between two adjacent vertebral bodies that consists of outer cartilage fibers and inner pulpous nucleus; intervertebral fibrocartilage (figure 1.4, p. 28)

[2] spinal cord: an extension of the central nervous system that consists of nerve cell bodies in the central region and neuronal white matter in peripheral regions, and is protected by the bony spinal canal

[3] anterior nerve root: the efferent motor root of a spinal nerve, which exits the frontal column of the medulla and joins the posterior nerve root at the intervertebral foramen to form a spinal nerve; ventral nerve root

[4] posterior nerve root: the afferent sensory root of a spinal nerve, which enters into the posterior part of the spinal cord; dorsal nerve root

- Original cross-sections display the primarily reconstructed images, composed of original picture elements (pixels) in image reconstruction planes. In CT imaging, the image planes are usually transversely oriented, while in MR imaging they are usually oriented parallel to the excited slab (figure 1.1a, p. 23).
- Multiplanar reformations (multiplanar cross-sections) display the originally reconstructed pixels along any arbitrary user-defined orientation that is orthogonal to image reconstruction planes. Depending on the orientation, axial[5], sagittal[6] and coronal[7] reformations can be obtained (figures 1.1b, p. 23 and 1.3, p. 26).
- Oblique reformations (oblique cross-sections) display the originally reconstructed pixels along any arbitrary user-defined plane that is inclined against the image reconstruction plane (figure 1.1c, p. 23).
- Curved planar reformations (CPRs, curved cross-sections) display the originally reconstructed pixels along any user-defined curved surface that is flattened in order to appear as a plane (figure 1.1d, p. 23).

• 3D image visualization is comprised of techniques that optimally display the selected structure in the 3D image in 2D projections:

- Maximum intensity projections (MIPs) display the brightest volume element (voxel) intensities along parallel projection lines that are orthogonal to any arbitrary user-defined projection plane (figure 1.2a, p. 24).
- Surface renderings display the surface of a structure by combining the projections of geometrical primitives (point, line, triangle, polygon) and visualization models (color effects, shading effects). The interior of the structure is not displayed, however, the structure needs to be pre-segmented (figure 1.2b, p. 24).
- Volume renderings display the whole structure by combining the projections of voxel intensities along parallel projection lines and visualization models (color effects, shading effects, transparency effects). The interior of the structure is displayed, while the segmentation of the structure is not required (figure 1.2c, p. 24).

The established techniques for 2D visualization of anatomical structures are based on planar (multiplanar and oblique) cross-sections that are obtained from 3D images of the structures. However, planar cross-sections do not always follow curved or tubular anatomical structures

[5] axial cross-section: a cross-section that is orthogonal to the longitudinal axis of the body, organ or a structure; transverse cross-section (figure 1.3, p. 26)

[6] sagittal cross-section: a cross-section that is parallel to the plane that splits the body, organ or a structure into left and right parts; lateral cross-section (figure 1.3, p. 26)

[7] coronal cross-section: a cross-section that is parallel to the plane that splits the body, organ or a structure into anterior and posterior parts; frontal cross-section (figure 1.3, p. 26)

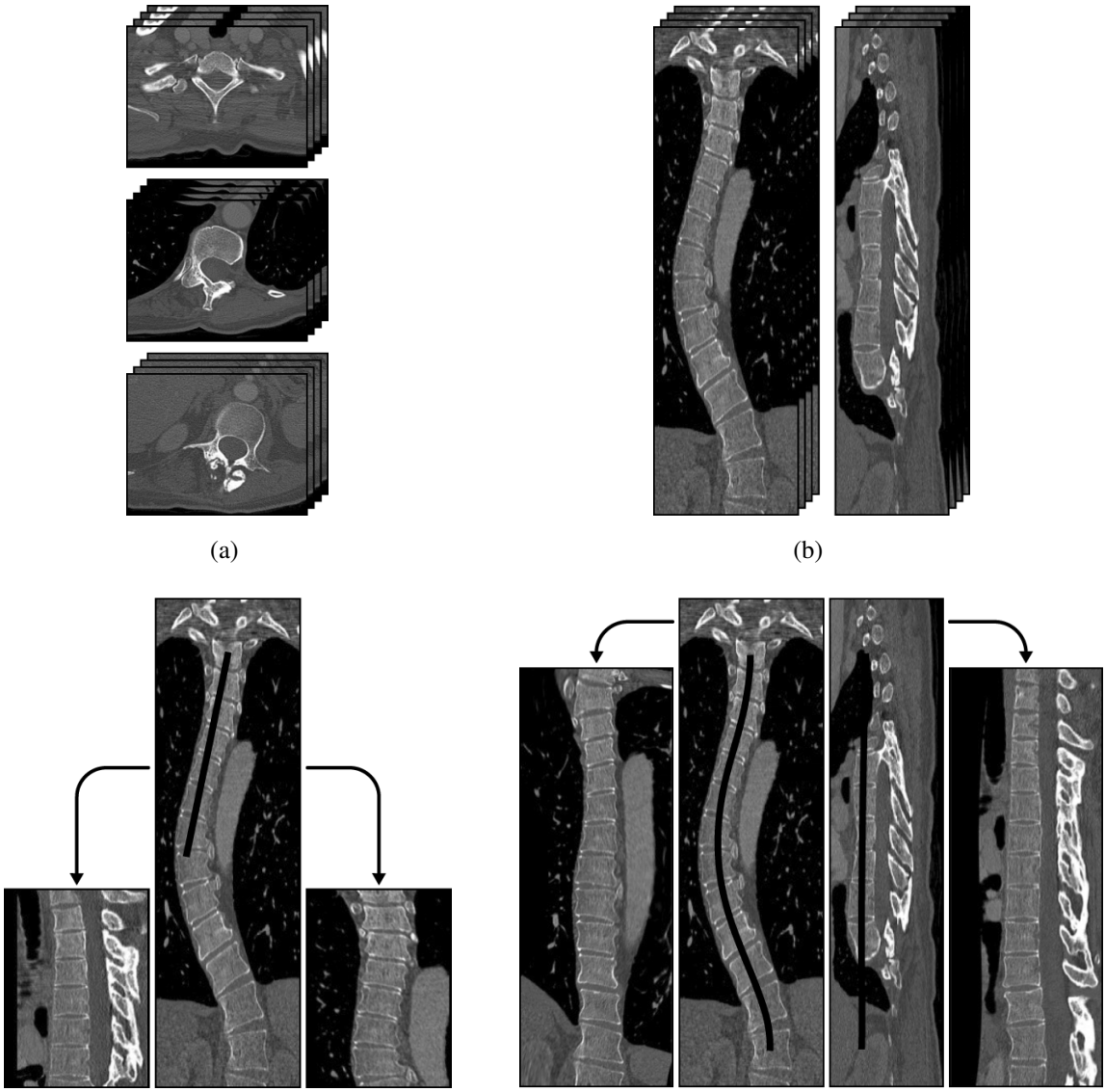

Figure 1.1. Examples of 2D volumetric visualization for a CT spine image. (a) Transversely oriented cross-sections. (b) Sagittal and coronal (multiplanar) cross-sections. (c) Oblique cross-sections. (d) Curved cross-sections.

Slika 1.1. Primeri 2D prostorskega prikazovanja CT slike hrbtenice. (a) Prečni prerezi. (b) Stranski ter čelni (večravninski) prerezi. (c) Poševni prerezi. (d) Ukrivljeni prerezi.

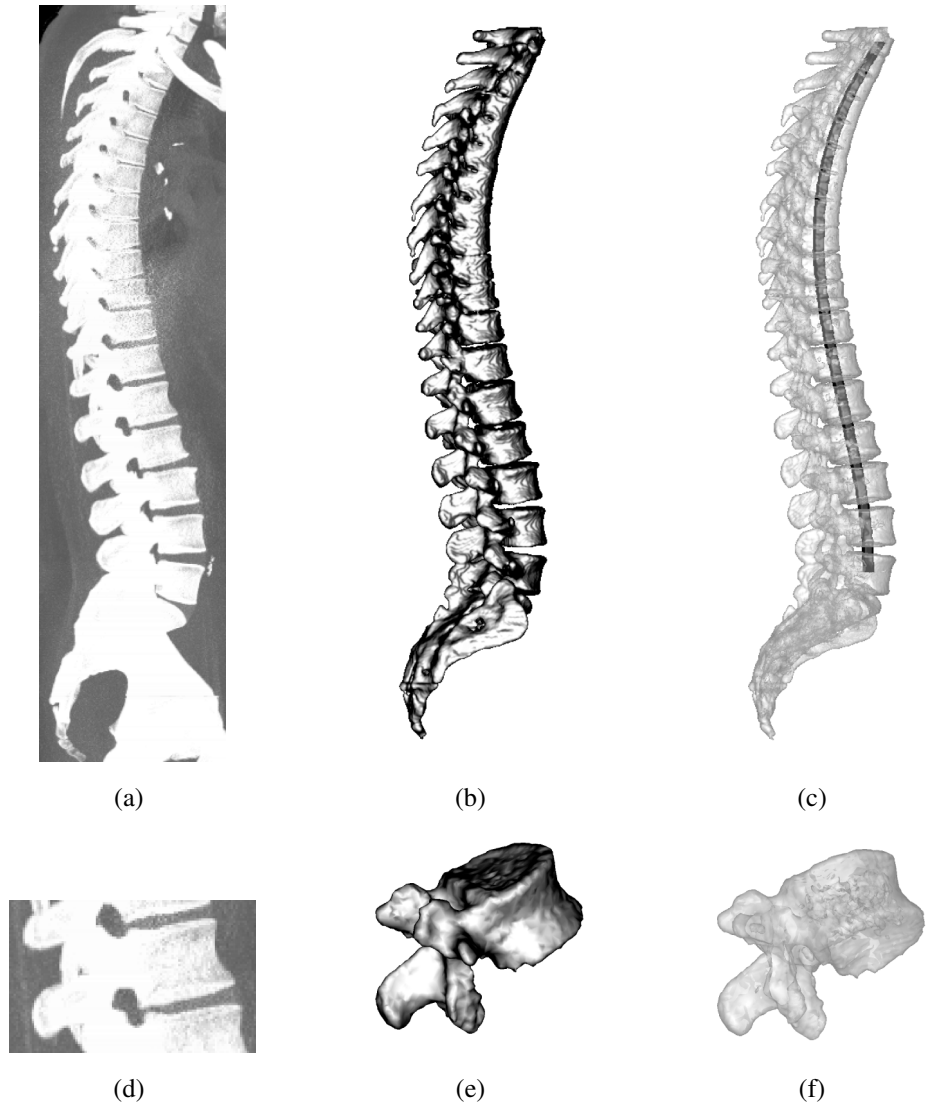

(a) (b) (c)

(d) (e) (f)

Figure 1.2. Examples of 3D volumetric visualization for a CT spine image and a single vertebra. (a),(d) Lateral MIP. (b),(e) Surface rendering. (c),(f) Volume rendering.

Slika 1.2. Primeri 3D prostorskega prikazovanja CT slike hrbtenice ter vretenca. (a),(d) Stranska projekcija maskimalne intenzitete (MIP). (b),(e) Upodabljanje površine. (c),(f) Upodabljanje prostornine.

(e.g. spine, arteries, colon). As all of the important parts of the structure are not simultaneously visible in a single planar cross-section, the visualization of such structures is often unsatisfying, which may seriously affect the quality of the diagnostic information of the observed curved structures. The use of CPR visualization technique, which generates cross-sections that are orthogonal or tangent to the curve along the structure, represents a solution to this problem. The standard coordinate system, which is determined by the 3D image, is transformed to a coordinate system that is determined by the observed 3D anatomical structure. Manual determination of the curve that follows the structure represents the easiest way to obtain curved cross-sections. However, manual curve determination is a difficult and time consuming task as it requires complex 3D spatial navigation.

As a visualization technique, CPRs are used in the field of angiography[8] to display and evaluate blood vessels (He et al., 2001, Kanitsar et al., 2002, 2003, Maddah et al., 2003, Ochi et al., 1999, Raman et al., 2002, 2003, Saroul et al., 2003), in the field of pancreatography[9] to display and evaluate pancreatic diseases (Gong and Xu, 2004, Prokesch et al., 2002a,b), for brain visualization (Leonardi et al., 1991), in the field of bronchoscopy[10] (Law and Heng, 2000, Perchet et al., 2004) and in the field of colonoscopy[11] (Ge et al., 1999, Samara et al., 1999, Wan et al., 2002). In all of the CPR visualization approaches, the determination of the curve that determines the central course of the visualized tubular structure is of utmost importance (Aylward and Bullitt, 2002, Bitter et al., 2000). Dedicated commercial software or software provided by CT and MR scanner manufacturers already allows generation of curved cross-sections, however, this requires manual determination of the curve that follows the anatomical structure. Although MR scanners allow arbitrary orientation of the image plane and can therefore simulate the generation of oblique cross-sections, such visualization is greatly influenced by the scanner operator that determines the orientation of the image plane and by the position of the patient in the scanner. Curved cross-sections can be also acquired directly from the MR scanner (Börnert, 2003, Börnert and Schäffter, 1996, Jochimsen and Norris, 2002), however, the quality of the obtained images in not adequate due to low spatial resolution of images, presence of intensity modulation artefacts and the fact that the images can be curved only in one dimension (1D). The development of automated CPR visualization techniques may therefore represent a valuable support in the interpretation of 3D medical image information.

[8] angiography: radiographic visualization of blood vessels after injection of a radiocontrast material into the blood

[9] pancreatography: radiographic visualization of the pancreatic ducts after injection of a radiocontrast material into the collecting system

[10] bronchoscopy: visual examination of the bronchi through a bronchoscope, a slender tubular instrument for inspection of the interior of the bronchi

[11] colonoscopy: visual examination of the colon with a colonoscope, a long flexible endoscope; coloscopy

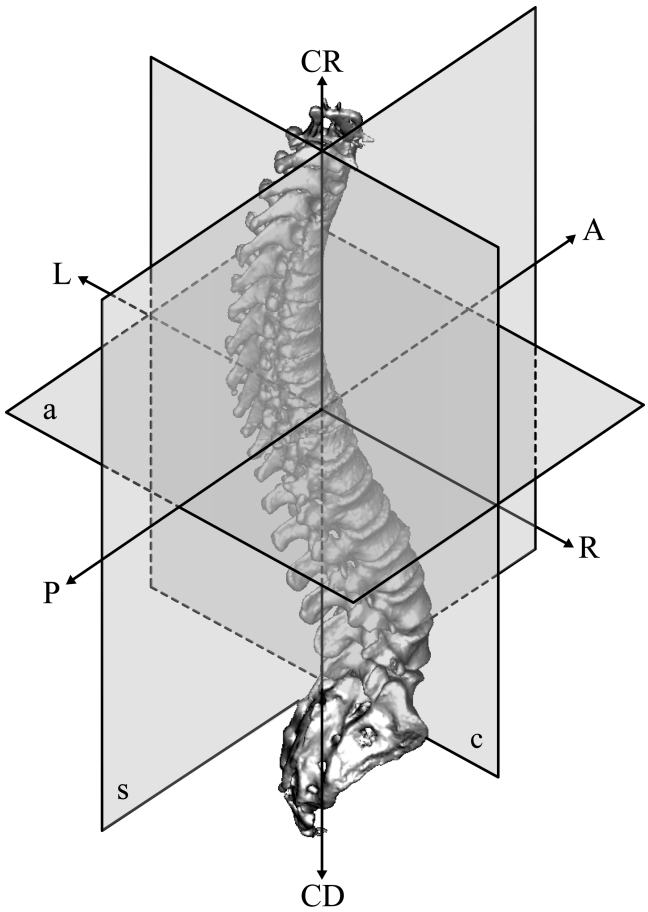

Figure 1.3. Spine orientation. Labels: A - anterior, P - posterior, L - left, R - right, CR - cranial, CD - caudal, a - axial cross-section, s - sagittal cross-section, c - coronal cross-section.

Slika 1.3. Orientacija hrbtenice. Oznake: A - spredaj, P - zadaj, L - levo, R - desno, CR - zgoraj, CD - spodaj, a - prečni prerez, s - stranski prerez, c - čelni prerez.

1.1.2 Quantitative evaluation of medical images

Quantitative evaluation of images is defined as the expression of selected measurable image properties with numerical values that are equipped with proper measurement units (Bankman et al., 2000, Brown and McNitt-Gray, 2000). Typical examples include the computation of length, area or volume in the image. In the case of medical images, quantitative evaluation represents the measurement of geometrical properties of selected anatomical structures (e.g. the diameter of a blood vessel) or properties that derive from the geometrical properties (e.g. blood flow through a vessel). Important fields of application include morphometry[12], computer-aided diagnosis (CAD), treatment planning, analysis of the treatment outcomes, image-guided surgical interventions and simulation of the structure and function of normal and

[12]morphometry: measurement of the form of organisms and their parts

pathological tissues. Quantitative evaluation techniques are most valuable when they are completely automated or require minimal manual intervention. However, to recognize the medical significance and potential use of (semi)automated techniques, methods for the verification of the accuracy and reliability of such techniques have to be provided. Quantitative evaluation techniques therefore need to be tested on real images and the results compared to reference measurements of the same property, performed in the same images by experts or adequately experienced individuals, or to other reference "gold standard" measurements. The reliability of the automated techniques has to be superior or at least comparable to the reliability of reference measurements, which can be confirmed by properly designed experiments and corresponding statistical tests. Quantitative evaluation is essential for objective comparison of the measured properties among patients. Nevertheless, it is extremely important to consider the relevance of the obtained results in clinical practice.

1.2 Visualization and quantitative evaluation of spine images

1.2.1 Visualization of spine images

When visualizing 3D spine images with planar cross-sections, the spine may intersect with sagittal and coronal planes, while the axial plane may not always be located at the same level of the vertebral bodies[13] or intervertebral discs. The important structural parts of the spine may therefore not be displayed simultaneously in any single cross-section. This is already the case when visualizing a normal spine due to its natural "S"-shaped curvature, and is even more present in pathological spinal curvatures, for example in case of scoliosis[14] or increased kyphosis[15] and lordosis[16].

Many approaches that aim to improve quantitative and qualitative evaluation of spinal deformities by an effective visualization of CT spine images have already been proposed. By generating oblique sagittal cross-sections, Rabassa et al. (1993) showed that visualization of vertebral facet joints[17] improved, while oblique axial cross-sections allowed views that were parallel to intervertebral discs. Although the visualization was limited to oblique cross-sections, the authors concluded that in certain clinical situations, such as in evaluation of neural foraminal[18] steno-

[13] vertebral body: the largest part of a vertebra from which originate the vertebral processes (figure 1.4, p. 28)

[14] scoliosis: complex non-physiological deformity of the spine in the lateral direction due to muscular or bone anomalies

[15] kyphosis: deformity of the spine in the posterior direction (figure 1.6, p. 30)

[16] lordosis: deformity of the spine in the anterior direction (figure 1.6, p. 30)

[17] vertebral facet joint: the vertebral joint between the superior articular process of one vertebra and the inferior articular process of the adjacent vertebra (figure 1.4, p. 28)

[18] intervertebral foramen: the two apertures between every pair of vertebrae for the passage of spinal nerves and blood vessels (figure 1.4, p. 28)

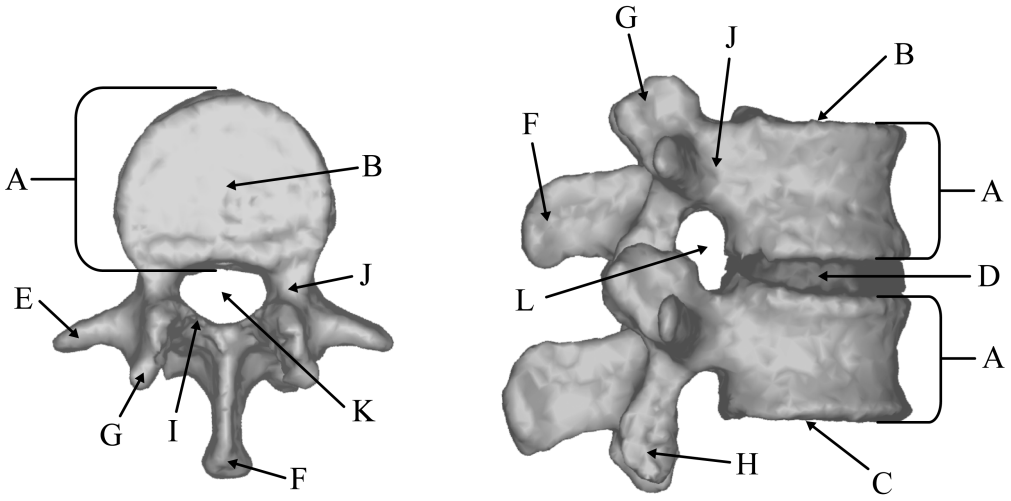

(a) (b)

Figure 1.4. Vertebral anatomy. (a) Axial view from the top. (b) Sagittal view from the right. Labels: A - vertebral body, B - superior end-plate, C - inferior end-plate, D - intervertebral disc, E - transverse process, F - spinous process, G - superior articular process, H - inferior articular process, I - lamina of the vertebral arch, J - pedicle, K - spinal canal, L - intervertebral foramen.

Slika 1.4. Anatomija vretenca. (a) Čelni pogled z vrha. (b) Stranski pogled z desne. Oznake: A - telo vretenca, B - zgornja ploščica, C - spodnja ploščica, D - medvretenčna ploščica, E - prečni odrastek, F - trnasti odrastek, G - zgornji sklepni odrastek, H - spodnji sklepni odrastek, I - plošča vretenčnega loka, J - pedikel, K - hrbtenični kanal, L - medvretenčna odprtina.

sis[19] or localization of spinal injuries, the reformatted images could supplement the original CT images. Oblique cross-sections that were orthogonal to the long axis of both left and right neural foraminae of the cervical spine region were also generated by Roberts et al. (2003a). They improved the consistency in the interpretation of the neural foraminal stenosis between observers and suggested that oblique cross-sections should be considered in routine evaluation (figure 1.5a, p. 29). Rothman et al. (1984) demonstrated that curved cross-sections, obtained by connecting manually selected points into a continuous curve, were useful in evaluation of anatomical relationships in the coronal spine region. After reformation, structures such as nerve roots, vertebral facet joints and spinal cord could be observed in a single cross-section. Congenital[20] spinal deformities were examined by Newton et al. (2002), who manually outlined the boundaries of the spine in multiplanar cross-sections and created curved cross-sections that improved the identification and interpretation of abnormalities. The benefit of curved cross-

[19] spinal stenosis: the narrowing of the spinal canal and compression of the nerves due to spine degeneration

[20] congenital: a medical condition that is present at birth (genetic or due to exposure to harmful substances during pregnancy)

[21] spinal canal: the canal formed by the vertebral bodies and vertebral arches that contains the spinal cord; vertebral canal (figure 1.4, p. 28)

Source: Roberts et al. (2003a, p. 168)

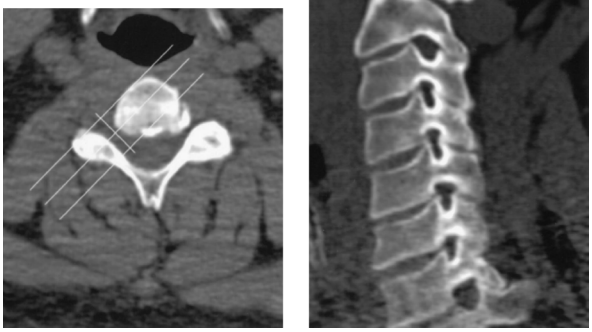

Source: Newton et al. (2002, p. 846)

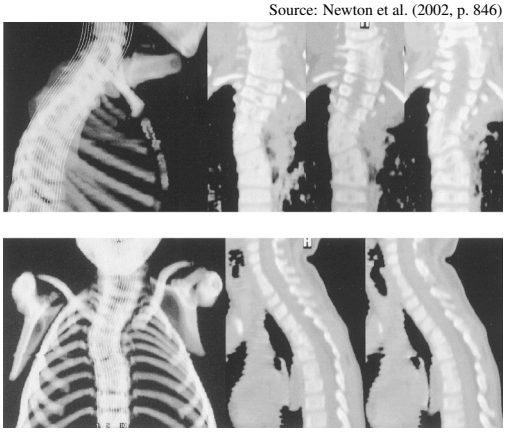

(a) (b)

Figure 1.5. Examples of oblique and curved planar reformation of CT spine images. (a) Oblique reformation after Roberts et al. (2003a). (b) CPR after Newton et al. (2002).

Slika 1.5. Primeri prikazovanja CT slik hrbtenice s poševnimi in ukrivljenimi prerezi. (a) Poševni prerezi po Robertsu in dr. (2003a). (b) Ukrivljeni prerezi po Newtonu in dr. (2002).

sections was, in comparison with multiplanar or oblique cross-sections, most valuable in the case of significant sagittal or coronal curvature of the spine (figure 1.5b, p. 29). Menten et al. (2005) presented a curved planospheric reformation method that was based on reconstruction from a cylindrical plane, defined around the approximate boundary of the spinal canal[21] within an axial CT cross-section. As a result, the anterior[22] and posterior[23] elements of the spine were displayed simultaneously in the same plane, which improved the evaluation of congenital spinal deformities.

Manual determination of points or curves that determined the curved cross-sections was required in all of the abovementioned studies. A semi-automated method was presented by Kaminsky et al. (2004), who segmented the spine on reformatted CT images in order to overcome the problems of orientation in the standard multiplanar reformation. The transformation axis was determined by a 3D spline[24], obtained either manually by delineating centerlines in sagittal and coronal cross-sections or automatically by dropping spheres of maximum possible radius through the vertebral bodies or spinal canal.

Over the past years, MR has become a more dominant modality in spine imaging, providing high-quality 3D images of soft tissues and bone structures of the spine by a correct selection of

[22] anterior: located in front of another structure or at the frontal part of an organ; ventral

[23] posterior: located behind another structure or at the rear part of an organ; dorsal

[24] spline: a mathematical function defined piecewise by polynomials

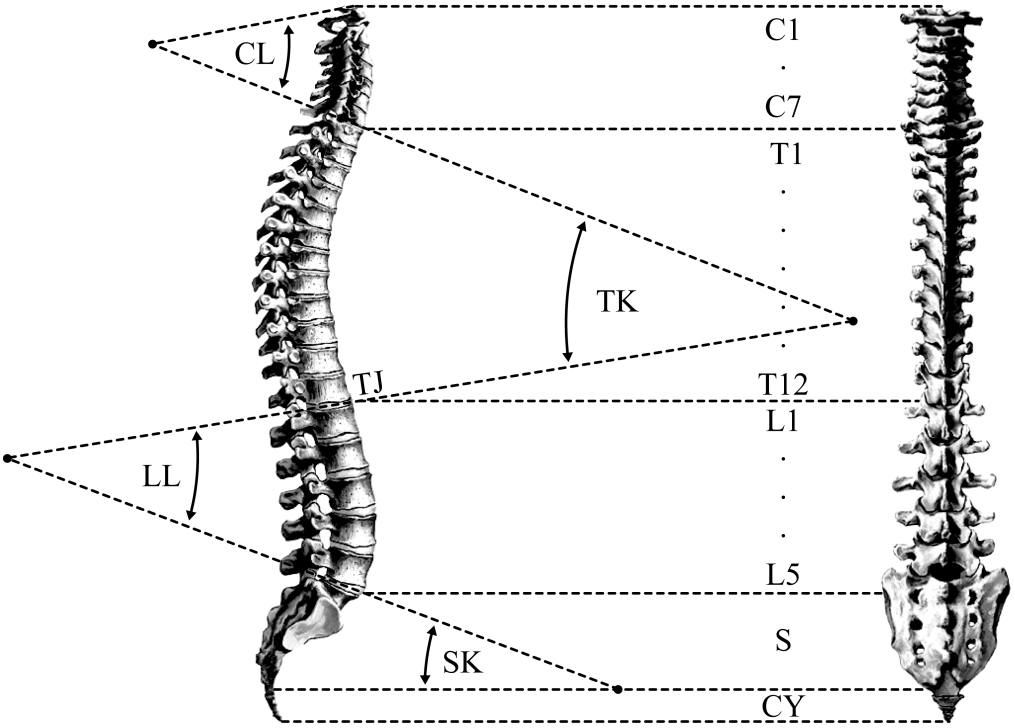

Figure 1.6. Spine anatomy. Labels: C1…C7 - cervical vertebrae, T1…T12 - thoracic vertebrae, L1…L5 - lumbar vertebrae, S - sacrum, CY - coccyx (tailbone), CL - cervical lordosis, TK - thoracic kyphosis, TJ - thoracolumbar junction, LL - lumbar lordosis, SK - sacral kyphosis.

Slika 1.6. Anatomija hrbtenice. Oznake: C1…C7 - vratna vretenca, T1…T12 - prsna vretenca, L1…L5 - ledvena vretenca, S - križnica, CY - trtica, CL - vratna lordoza, TK - prsna kifoza, TJ - prsno-ledveni spoj, LL - ledvena lordoza, SK - križna kifoza.

imaging parameters (Brown and Semelka, 1999, Grenier et al., 2005, 2006). The poor resolution of early MR scanners has been improved by dedicated multichannel spine coils with better signal-to-noise ratio (SNR). Visualization of spinal abnormalities, injuries and diseases is often superior in MR imaging than in other imaging methods, such as CT or the relatively invasive myelography[25]. Moreover, as the patient is not exposed to ionizing radiation, MR is considered to be the modality of choice for follow-up examinations and longitudinal studies.

Image reformation has already been identified as a valuable visualization technique in MR imaging of the spine. Apicella and Mirowitz (1995) reported that multiplanar cross-sections could compensate for the apparent asymmetry of 3D anatomical structures, caused by improper patient positioning or patient motion during image acquisition, and that reformatting can be applied to different anatomical structures. In the case of spine images, they can be used to

[25]myelography: a radiographic examination of the spinal cord by injecting a radiocontrast material

improve the visualization of the spinal canal and intervertebral foraminae. In order to avoid measurement errors, Birchall et al. (1997) and Adam and Askin (2006) computed the vertebral rotation from the position of landmarks that were manually placed in each oblique axial cross-section, defined in sagittal and coronal MR cross-sections through the superior and inferior vertebral end-plates[26], or parallel to the end-plates through the centers of each vertebral body. Liljenqvist et al. (2002) focused their study on vertebral morphology[27], which is of significant importance in the placement of pedicle[28] screws as a part of the surgical intervention for the treatment of scoliosis (Kuklo et al., 2005a). The pedicle width, length and angle were measured in manually determined oblique MR cross-sections that were perpendicular to the vertebral bodies.

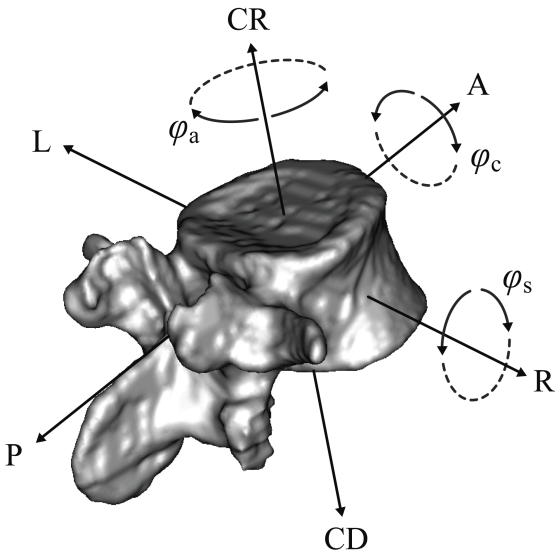

Figure 1.7. Vertebral rotation. Labels: A - anterior, P - posterior, L - left, R - right, CR - cranial, CD - caudal, φ_a - axial rotation, φ_s - sagittal rotation, φ_c - coronal rotation.

Slika 1.7. Rotacija vretenca. Oznake: A - spredaj, P - zadaj, L - levo, R - desno, CR - zgoraj, CD - spodaj, φ_a - prečna rotacija, φ_s - stranska rotacija, φ_c - čelna rotacija.

1.2.2 Quantitative evaluation of spine images

Quantitative evaluation of spine parameters is important in planning of surgical procedures (Aronsson et al., 1996, Duke et al., 2005, Herring et al., 1998, Tamura et al., 2005), analysis of surgical results (Kuklo et al., 2005b, Lee et al., 2004, Petit et al., 2004), monitoring of the

[26]vertebral end-plate: a thin layer of cartilage between the surface of a vertebra and the intervertebral disc on the superior and inferior part of the vertebral body (figure 1.4, p. 28)

[27]morphology: the study of the structure of normal or pathological cells, tissues, organs and organisms

[28]vertebral pedicle: the segment between the transverse process and the vertebral body (figure 1.4, p. 28)

progression and treatment of spinal deformities (Asazuma et al., 2004, Stokes and Aronsson, 2001), and for the determination of reference values in normal and pathological conditions (Cyteval et al., 2002, Sevastik et al., 1995). Among the most significant spine parameters are the spinal curvature, the length of the spinal axis, the Cobb angle, the location of the centers of vertebral bodies, and vertebral axial, sagittal and coronal rotation angles (Stokes, 1994) (figure 1.7, p. 31). However, the spinal curvature and vertebral rotation are the most important in the evaluation of scoliotic deformations. As the origin and cause for the progression of both congenital and idiopathic[29] scoliosis are still relatively unknown, it is not only important to assess the adequacy of the existing imaging techniques (Cassar-Pullicino and Eisenstein, 2002, Do et al., 2001, Schmitz et al., 2001, Wright, 2000), but also to develop classification systems for scoliotic deformities (Ajemba et al., 2005, King et al., 1983, Lenke et al., 2001, Poncet et al., 2001, Ramirez et al., 2006). Nevertheless, such classification systems have to be tested in order to prove their clinical value (Arlet et al., 2003, Coonrad et al., 1998, Edgar, 2002, Ogon et al., 2002, Richards et al., 2003).

As coronal cross-sections display the most significant part of a scoliotic deformity, the methods for evaluation of spinal curvature were first developed for coronal radiographic images. One of the earliest methods, which is still in use nowadays, is the Ferguson method (Ferguson, 1930). The grade of a deformity is determined by the angle between two straight lines that connect the centers of end vertebrae[30] with the center of the apical[31] vertebra (figure 1.8a, p. 33). The Greenspan index (Greenspan et al., 1978) allows to measure the deformity at each individual vertebra and is therefore valuable in measuring short-segment or small spinal curvatures. The centers of the end vertebrae are connected to form a spinal line, orthogonally to which additional lines are drawn from the center of each vertebra in the spinal curve (figure 1.8b, p. 33). The sum of the lengths of these additional lines is then divided by the length of the spinal line. The obtained value represents the measure (index) of the deformity, which for a normal spine is equal to zero. The most commonly used method for the evaluation of spinal curvature on coronal radiographs is the Cobb method (Cobb, 1948). The Cobb angle is measured between two lines that are tangent to the superior end-plate of the superior end vertebra and to the inferior end-plate of the inferior end vertebra (figure 1.8c, p. 33). Curvatures that result in a Cobb angle greater than 10 degrees are diagnosed as scoliotic. Although the aforementioned methods are still widely in use, they are based on manual identification of the vertebrae and other properties of the spine. As a result, the variability and unreliability of the methods is relatively high (Beekman and Hall, 1979, Carman et al., 1990, Deacon et al., 1984, Diab et al., 1995, Morrissy et al., 1990, Shea et al., 1998, Stokes et al., 1993, Wills et al., 2007, Zmurko et al., 2003). On the other hand, the spinal curvature was due to its continuous course described by various mathematical functions, such as sinusoids (Drerup and Hierholzer,

[29] idiopathic: a medical condition that arises spontaneously or from an unknown cause

[30] end vertebrae: the superior (cranial) and inferior (caudal) vertebra without substantial rotation but with maximal tilt towards the concavity of the curve above and below its apex

[31] apical vertebra: the vertebra located in the apex of the deformity

1996), splines (Kaminsky et al., 2004, Verdonck et al., 1998, Yang et al., 2007), polynomials (Patwardhan et al., 1996, Peng et al., 2005), and also statistical techniques, such as kriging[32] (Poncet et al., 1999).

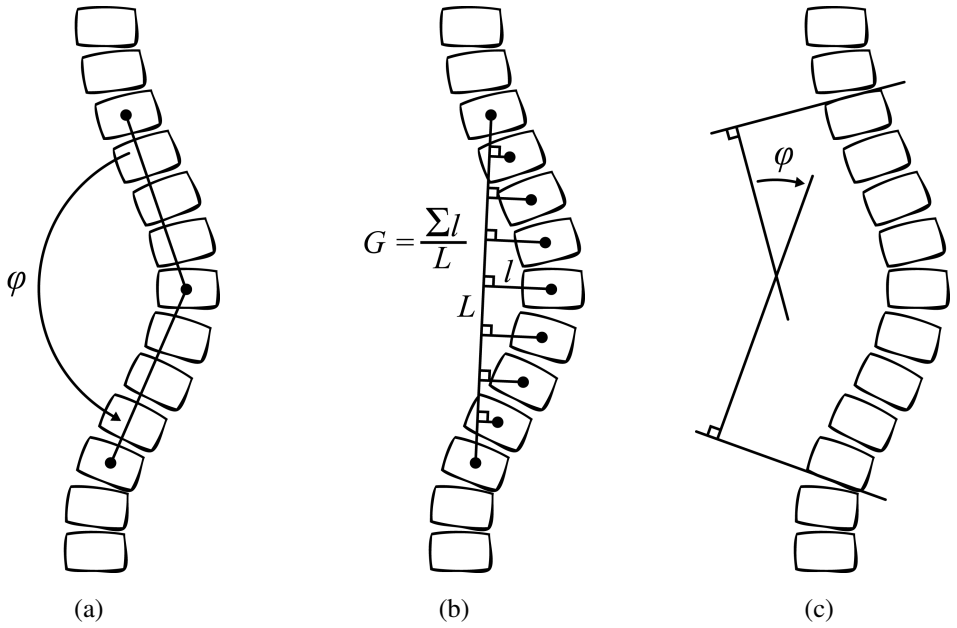

Figure 1.8. Measurement of spinal curvature in frontal radiographic images. (a) Method of Ferguson (1930). (b) Method of Greenspan et al. (1978). (c) Method of Cobb (1948).

Slika 1.8. Določanje ukrivljenosti hrbtenice v čelnih rentgenskih slikah. (a) Metoda po Fergusonu (1930). (b) Metoda po Greenspanu in dr. (1978). (c) Metoda po Cobbu (1948).

Approaches that were supported by computer alogrithms tried to improve the reliability and accuracy of the Cobb angle measurement and classification of scoliotic deformities (Chockalingam et al., 2002, Goh et al., 2000a, Stokes and Aronsson, 2006). However, the inaccuracy of the Cobb method originates from the fact that a relatively complex 3D spinal deformity is evaluated by a relatively simple measurement in a single 2D cross-section, i.e. in a coronal radiographic image. Cheung et al. (2002) proposed to improve the measurements by combining coronal and sagittal radiographs for the estimation of the spinal centerline. The spinal curvature was also estimated in images, acquired by other imaging techniques, for example in stereoradiographic[33] images and stereophotographies[34] of the back (Asamoah et al., 2000,

[32]kriging: a group of geostatistical techniques to interpolate the value of a random field at an unobserved location from observations of the random field at nearby locations

[33]stereoradiography: the method of acquiring radiographs from two slightly different positions that allows reconstruction of the properties of an object in 3D

[34]stereophotography: an imaging technique, where images of a grid projected to the observed object are acquired at different angles, allowing the observation of the depth of the object; rasterstereography

Bendels et al., 2005, Bergeron et al., 2005, Drerup and Hierholzer, 1994, Gille et al., 2007, Liljenqvist et al., 1998, Stokes et al., 1988, Tredwell et al., 1999, Zubairi, 2002), stereoradiographic images of the chest (Aykroyd and Mardia, 2003, Boisvert et al., 2006, Jaremko et al., 2001), or moiré[35] and other topographic images of the back (Kim et al., 2001, Knott et al., 2006), and even by various non-invasive instruments, such as the electrogoniometer[36] (Campbell-Kyureghyan et al., 2005) or scoliometer[37] (Amendt et al., 1990). The evaluation of spinal curvature was also performed in coronal cross-sections that were obtained from CT spine images (Adam et al., 2005, Verdonck et al., 1998), which provide qualitative views of the 3D spine geometry. However, for acquiring whole-length spine images, CT imaging is considered to be an invasive approach due to exposure of a patient to a relatively high dose of ionizing radiation (Brant-Zawadzki, 2002). Therefore, CT imaging is not recommended when multiple image acquisition is required (e.g. in monitoring of the progression of the deformity or treatment). The MR technique was, as a non-radiating alternative for imaging of spinal curvature, studied by Wessberg et al. (2006).

The evaluation of vertebral rotation was mostly limited to axial rotation, i.e. the rotation of the vertebrae around the longitudinal spinal axis. As a consequence, axial rotation is often referred to as "rotation". Depending on the image acquisition technology, various approaches to the measurement of axial vertebral rotation were developed for coronal, sagittal and axial cross-sections. One of the earliest methods for coronal radiographic images was presented by Cobb (1948). The method was based on the determination of the position of the vertebral spinous process[38], which is normally located in the middle of the vertebral body. With increasing rotation, the spinous process rotates towards the concave side of the spine curve. The grade of axial vertebral rotation was determined by dividing the vertebral body into six equal segments and identifying the segment that contained the spinous process (figure 1.9a, p. 35). A similar method was proposed by Nash and Moe (1969), where the rotation is quantified on the basis of the position of the vertebral pedicles. The pedicles are normally located in the outer parts of the vertebral body, however, with increasing rotation, they move towards the convex side of the spine curve (figure 1.9b, p. 35).

The abovementioned methods stimulated the development of various methods that attempted to improve the description of vertebral anatomy in coronal radiographs by introducing different geometrical principles and various semi-automated computer techniques that attempted to improve the accuracy of axial vertebral rotation measurement (Benson et al., 1976, Chi et al., 2006, Coetsier et al., 1977, Deacon et al., 1984, Drerup, 1984, 1985, 1992, Mehta, 1973, Perdriolle and Vidal, 1985, Stokes et al., 1986). The analysis of the performance of the pro-

[35] moiré topographic images: light is projected on the object and observed by a special camera; the shape of a 3D object is described with interference optical patterns, the intensity of which determines areas that are equidistant from the camera

[36] electrogoniometer: an instrument that measures the axis and range of motion of a joint

[37] scoliometer: a tool for measuring the angle of trunk asymmetry; inclinometer

[38] vertebral spinous process: the vertebral process that is directed backward and downward from the junction of the vertebral laminae and serves for the attachment of muscles and ligaments (figure 1.4, p. 28)

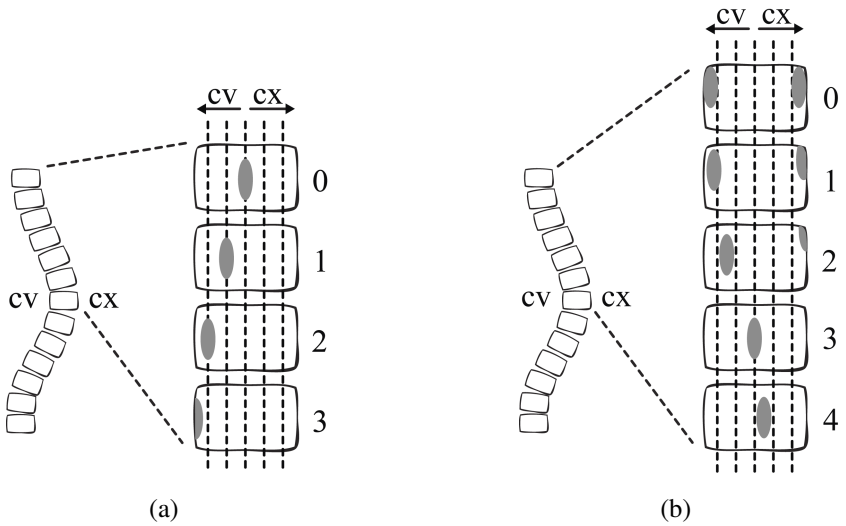

Figure 1.9. Measurement of axial vertebral rotation in coronal radiographic images. Labels: cv - concave side of the spine curve, cx - convex side of the spine curve. (a) Method of Cobb (1948). Grade of vertebral rotation: 0 - normal, 1 - mild, 2 - moderate, 3 - severe. (b) Method of Nash and Moe (1969). Grade of vertebral rotation: 0 - normal, 1 - mild, 2 - moderate, 3 - severe, 4 - marked.

Slika 1.9. Določanje prečne rotacije vretenc v čelnih rentgenskih slikah. Oznake: cv - konkavna stran hrbtenične krivulje, cx - konveksna stran hrbtenične krivulje. (a) Metoda po Cobbu (1948). Stopnja rotacije vretenca: 0 - normalna, 1 - blaga, 2 - zmerna, 3 - močna. (b) Metoda po Nashu in Moeju (1969). Stopnja rotacije vretenca: 0 - normalna, 1 - blaga, 2 - zmerna, 3 - močna, 4 - izrazita.

posed techniques (Drerup and Hierholzer, 1992a,b, Ho et al., 1993, Omeroğlu et al., 1996, Russell et al., 1990, Skalli et al., 1995, Weiss, 1995) proved that the evaluation of axial vertebral rotation in coronal radiographic images is unreliable, which is mostly because the radiographic projections do not provide sufficient or qualitative enough information of the observed anatomical structures.

Although sagittal radiographic images are not adequate for the measurement of axial vertebral rotation, they can be used to measure sagittal vertebral rotation, i.e. the rotation of the vertebrae around the latitudinal spinal axis, which is the axis from the left to the right part of the body. By measuring sagittal vertebral rotation, maximal values of kyphosis and lordosis, inclination of the sacral spine region and segmental vertebral inclinations can be obtained. The measurements were first performed by the Cobb method (Bernhardt and Bridwell, 1989, Côté et al., 1997, Korovessis et al., 1998, Stagnara et al., 1982) (figure 1.10a, p. 36), however, alternative approaches were proposed due to the already described problems. In the works of De Smet et al. (1980), Stokes (1989), Dumas et al. (2004) and Poncet et al. (2001), the Cobb angle was measured in stereoradiographic images. Harrison et al. (2000) determined the sagittal rotation as

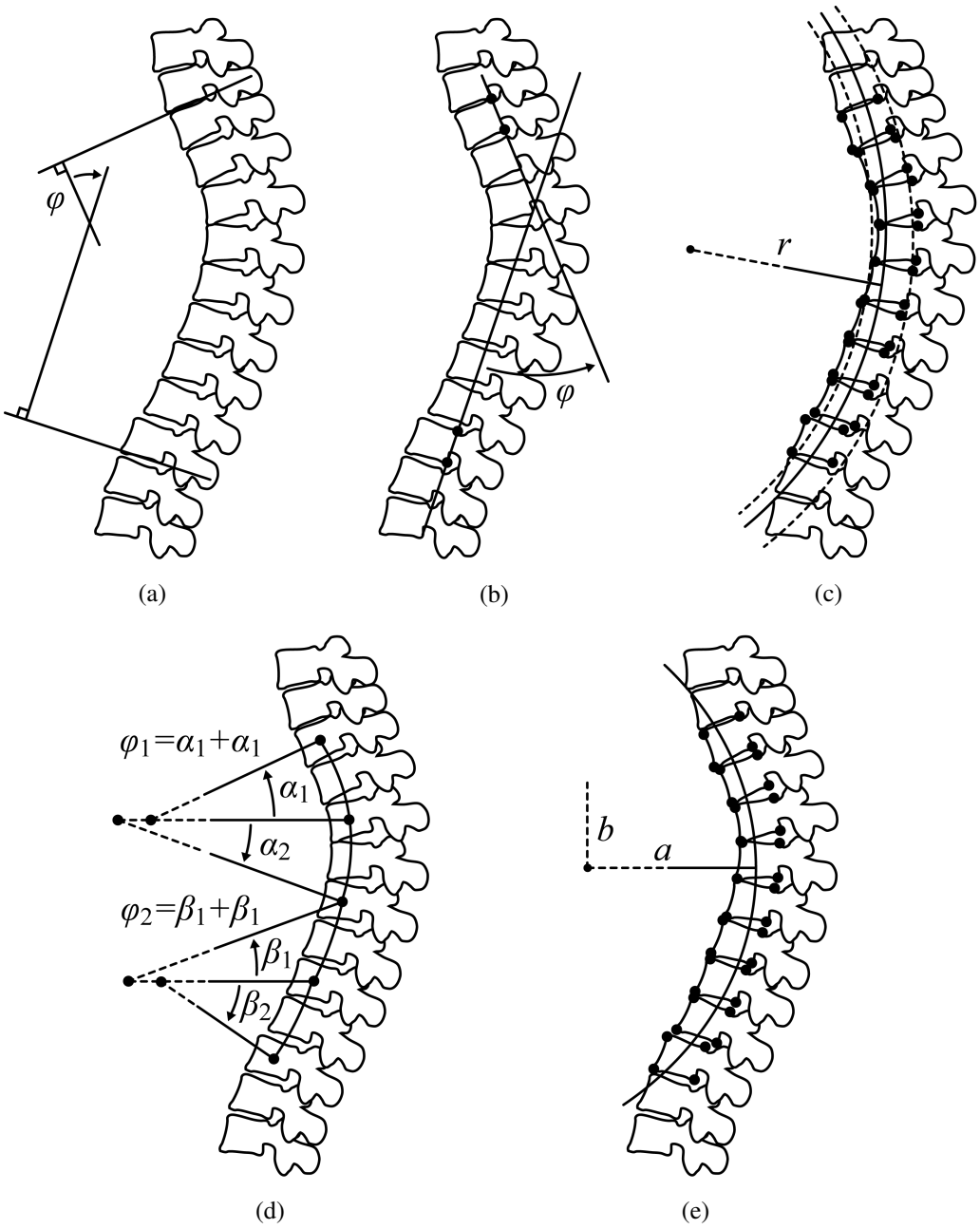

Figure 1.10. Measurement of sagittal vertebral rotation in sagittal radiographic images. (a) Method of Cobb (1948). (b) Posterior tangent method of Harrison et al. (2000). (c) Mean radius of curvature method of Goh et al. (2000a). (d) Tangent circles method of Pinel-Giroux et al. (2006). (e) Best-fit ellipses of Janik et al. (1998) and Harrison et al. (1998).

Slika 1.10. Določanje stranske rotacije vretenc v stranskih rentgenskih slikah. (a) Metoda po Cobbu (1948). (b) Metoda posteriornih tangent po Harrisonu in dr. (2000). (c) Povprečni polmer ukrivljenosti po Gohu in dr. (2000a). (d) Metoda tangentnih krožnic po Pinel-Girouxu in dr. (2006). (e) Metoda prilegajočih elips po Janiku in dr. (1998) ter Harrisonu in dr. (1998).

the angle between the two lines that were manually drawn tangently to the posterior wall of the selected vertebral bodies (figure 1.10b, p. 36). In the work presented by Goh et al. (2000a), the measure for the sagittal rotation was represented by the mean radius of curvature of the two circular arcs through the manually identified points at the corners of vertebral bodies (figure 1.10c, p. 36). Pinel-Giroux et al. (2006) constructed the spine curve from four circular arcs that were tangent to the centers of the selected vertebral bodies. The measured rotation was defined as the angle between the lines that connected the centers of the circular arcs with the centers of vertebral bodies and the reference horizontal line (figure 1.10d, p. 36). A similar approach was proposed by Janik et al. (1998) for lumbar lordosis and Harrison et al. (1998, 2002, 2004) for thoracic kyphosis, who defined ellipses that represented the best-fit to the points at the corners of vertebral bodies (figure 1.10e, p. 36). Prince et al. (2007) evaluated the sagittal vertebral rotation by measuring the kyphosis index, which was determined as the ratio between the maximal distance of the spine to the reference coronal plane and the length of the straight line that connected the measured points on the spine.

The measurement of axial vertebral rotation on axial cross-sections is the most intuitive measurement approach (Heithoff and Herzog, 1991), however, it only became possible with the development of 3D imaging techniques. CT proved to be the most accurate imaging technique for the determination of axial vertebral rotation (Krismer et al., 1996, Kuklo et al., 2005b). One of the first attempts for measuring axial vertebral rotation in axial CT cross-sections was proposed by Aaro and Dahlborn (1981). The rotation was determined by the angle between the line that connected the points at the two laminae[39] of the vertebral arch[40] with the center of the vertebral body and the reference sagittal plane (figure 1.11a, p. 38). A similar method was presented by Ho et al. (1993). The angle, defined between the two lines that connected the junction of each lamina and the pedicle with the junction of the two laminae, was first bisected by a third line. Axial rotation was then measured as the angle between the obtained line and the reference sagittal plane (figure 1.11b, p. 38). Krismer et al. (1996) proposed a more complex method that was based on the determination of five distinctive points, namely the points at the center of the vertebral body, at the tip of the spinous process, at the center of the spinal canal between both laminae and at the most anterior and posterior parts of the spinal canal. The points served to form lines that determined different axial rotation angles, measured against the reference sagittal plane (figure 1.11c, p. 38). Göçen et al. (1999) defined the axial rotation by the angle between the line that connected the most posterior points of the two pedicles and the reference sagittal plane of the CT image (figure 1.11d, p. 38).

Although the axial vertebral rotation was defined by precise procedures, the abovementioned methods ignored the fact that, due to spinal deformities, the vertebrae may be rotated also in sagittal and coronal direction, which may result in measurement errors in the form of an induced “virtual” axial rotation. Skalli et al. (1995) compared the measurements, performed in

[39] lamina of the vertebral arch: either of the pair of broad plates at the posterior part of the vertebral arch that provide a base for the spinous process (figure 1.4, p. 28)

[40] vertebral arch: the bony arch at the posterior aspect of a vertebra that supports the vertebral processes

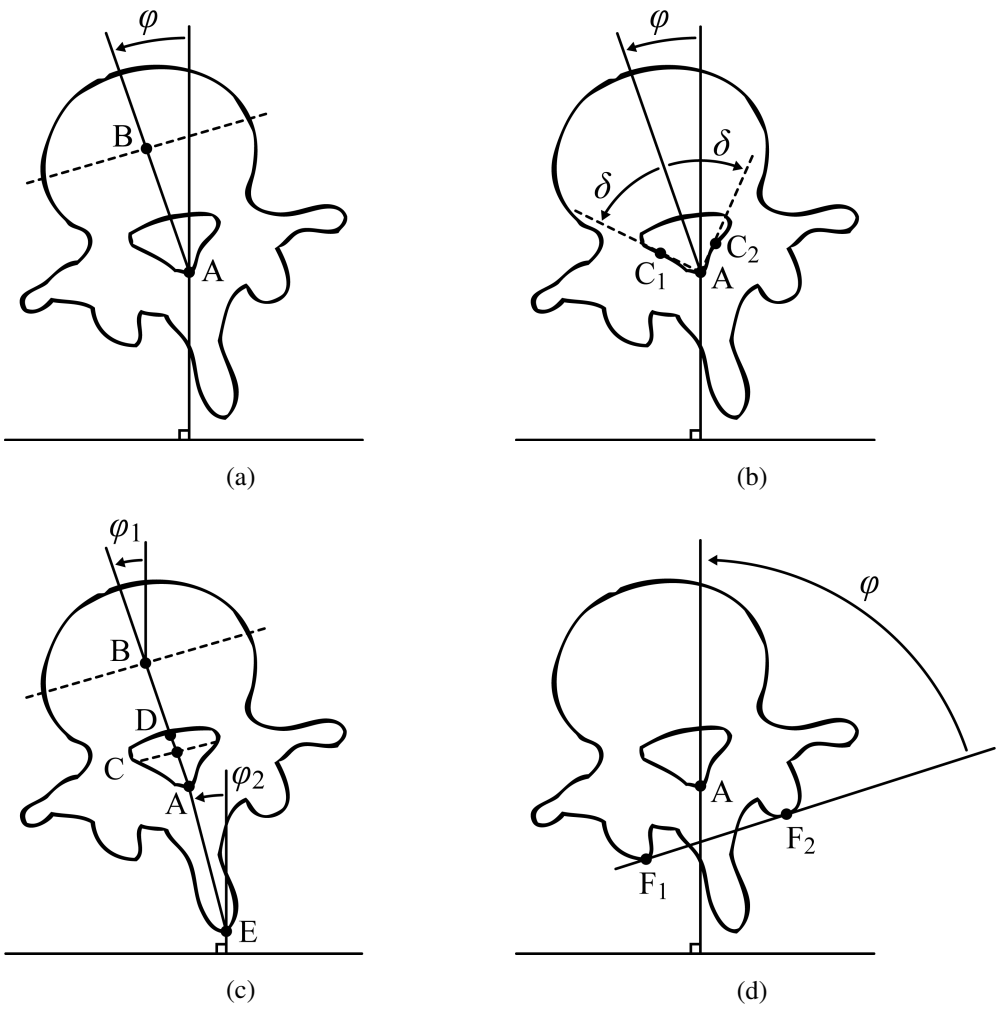

Figure 1.11. Measurement of axial vertebral rotation in axial CT cross-sections. (a) Method of Aaro and Dahlborn (1981). (b) Method of Ho et al. (1993). (c) Method of Krismer et al. (1996). (d) Method of Göçen et al. (1999).

Slika 1.11. Določanje prečne rotacije vretenc v prečnih CT prerezih. (a) Metoda po Aaroju in Dahlbornu (1981). (b) Metoda po Hoju in dr. (1993). (c) Metoda po Krismerju in dr. (1996). (d) Metoda po Göçenu in dr. (1999).

3D, with the measurements, performed in 2D, and concluded that the determination of axial vertebral rotation in axial cross-sections can be inaccurate, especially in the case of strong sagittal or coronal vertebral rotation. Krismer et al. (1996) reported that the measurement errors can also occur when the vertebrae are completely symmetrical and when the measurements in axial cross-sections are replaced with measurements in oblique cross-sections. Yazici et al. (2001) compared the measurements in axial CT cross-sections with the measurements in coronal radiographic images, which were acquired in patient's standing and supine positions. They concluded that patient positioning influences the measurements in both axial and coronal images, which can be considered as an additional rotation in 3D.

Computer-assisted methods for the evaluation of axial vertebral rotation in CT images were also proposed, however, they are considered to be semi-automatic as their initialization is based on manual interaction. Besides manual selection of the axial cross-section that was most appropriate for the measurements, the method proposed by Rogers et al. (2005) also required manual determination of the center of rotation at the anterior edge of the spinal canal. After initialization, the method automatically measured the rotation relative to a second cross-section by searching for the maximal correlation of the image intensities between the cross-sections (figure 1.12a, p. 40). Kouwenhoven et al. (2006) determined the axial vertebral rotation in manually selected axial cross-sections through the centers of the vertebral bodies in images of normal spines. The rotation was defined by the angle between the line that connected the center of the spinal canal with the center of vertebral mass, obtained by region growing segementation, and the line that connected the center of the spinal canal with the sternum at the T5 vertebra[41] (figure 1.12b, p. 40). Oblique cross-sections were used by Adam and Askin (2006), who measured the axial rotation in 3D by determining the orientation of the line that bisected the vertebral body. The orientation of the line was obtained by the maximal correlation of the image intensities between the bisected areas of the vertebral body (figure 1.12c, p. 40).

The evaluation of vertebral rotation in MR spine images was presented by Birchall et al. (1997), who used the technique proposed by Aaro and Dahlborn (1981) for the CT images (figure 1.13a, p. 41). Similarly have Birchall et al. (2005) evaluated the rotation on MR images with the method proposed by Ho et al. (1993), again developed for the CT spine images. The methods proposed by Haughton et al. (2002) and Rogers et al. (2002) required manual selection of the axial MR cross-section and manual determination of the center of rotation and circular areas that encompassed the vertebra. The axial rotation relative to a second vertebra was computed by searching for the maximal correlation of image intensities between circular areas that encompassed the two vertebrae (figures 1.13b, p. 41 and 1.13c, p. 41). A symmetry-based approach to the determination of the position and rotation of vertebrae in each axial MR cross-section was presented by Booth and Clausi (2001). After identifying the spinal cord as the center of rotation in each axial cross-section, the cross-sections were rotated around the spinal cord until

[41] the vertebral column consists of seven cervical vertebrae (from C1 to C7), twelve thoracic vertebrae (from T1 to T12), five lumbar vertebrae (from L1 to L5), the sacrum and the coccyx or the tailbone (figure 1.6, p. 30)

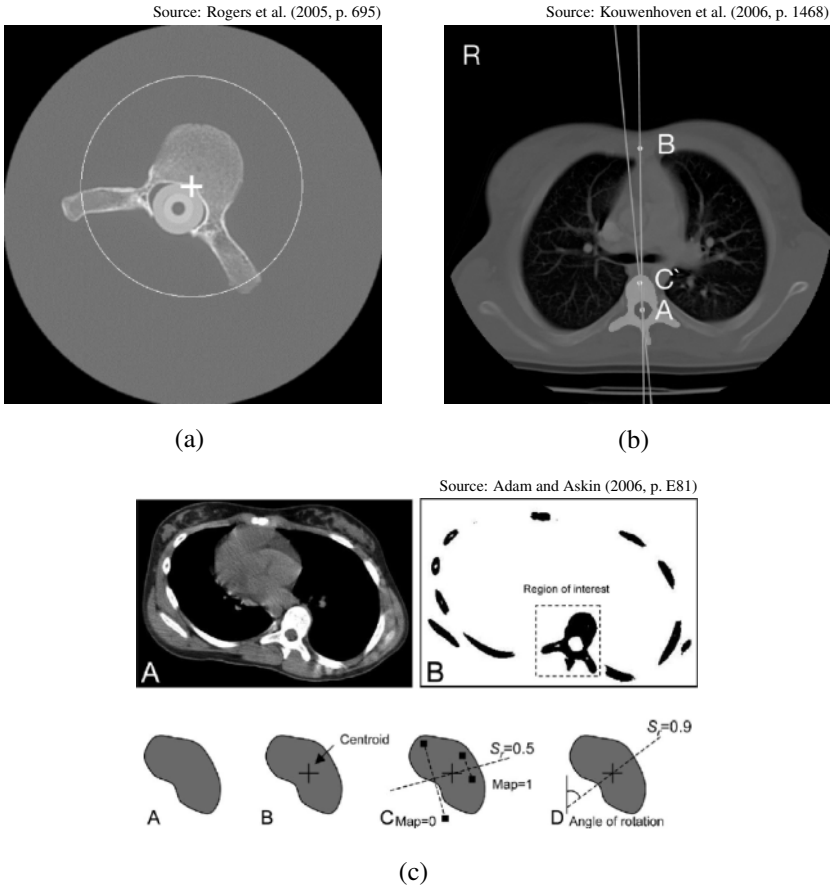

Figure 1.12. Automated measurement of axial vertebral rotation in CT spine images. (a) Method of Rogers et al. (2005). (b) Method of Kouwenhoven et al. (2006). (c) Method of Adam and Askin (2006).

Slika 1.12. Avtomatsko določanje prečne rotacije vretenc v CT slikah hrbtenice. (a) Metoda po Rogersu in dr. (2005). (b) Metoda po Kouwenhovenu in dr. (2006). (c) Metoda po Adamu in Askinu (2006).

obtaining the minimal mean square difference of image intensities in areas that were split by a vertical line through the spinal cord. Reisman et al. (2006) estimated the sagittal rotation of intervertebral discs in sagittal MR cross-sections by evaluating the similarity of the regions above and below each intervertebral disc.

Quantitative evaluation of spinal curvature and vertebral rotation is important in providing support to various image processing techniques and clinical measurements (Doi et al., 1997), and was therefore part of various spine-related studies, for example in measuring of the trunk balance (Berthonnaud et al., 2005b, Glassman et al., 2005a,b, Mac-Thiong et al., 2003), in the field of spine biomechanics (Cholewicki et al., 1996, Huysmans et al., 2004, Oda et al., 2002, Orchowski et al., 2000, Stokes, 1997, Teo et al., 2007, Wever et al., 1999),

Source: Birchall et al. (2005, pp. 124–125)

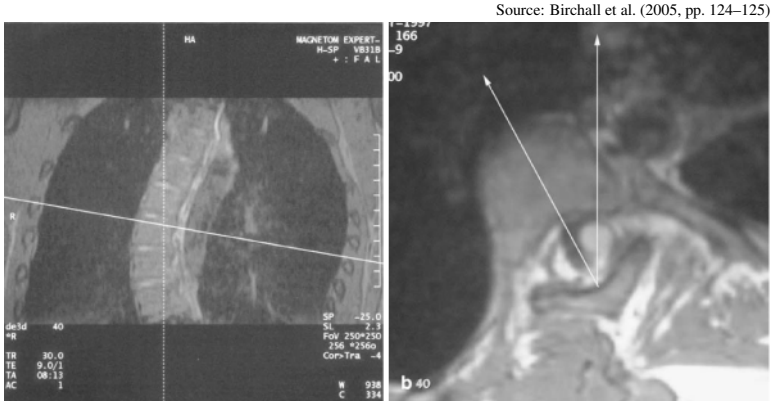

(a)

Source: Haughton et al. (2002, p. 1111)

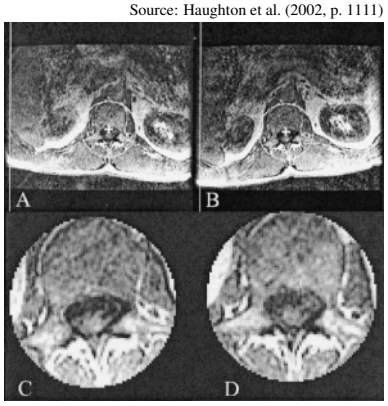

(b)

Source: Rogers et al. (2002, p. 1073)

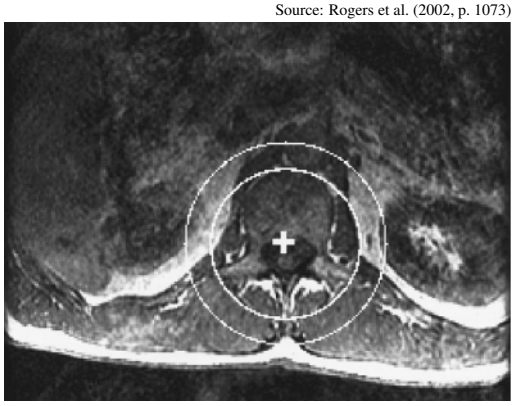

(c)

Figure 1.13. Measurement of axial vertebral rotation in MR spine images. (a) Method of Birchall et al. (2005). (b) Method of Haughton et al. (2002). (c) Method of Rogers et al. (2002).

Slika 1.13. Določanje prečne rotacije vretenc v MR slikah hrbtenice. (a) Metoda po Birchallu in dr. (2005). (b) Metoda po Haughtonu in dr. (2002). (c) Metoda po Rogersu in dr. (2002).

spine and vertebral morphometry (Goh et al., 2000b, Liljenqvist et al., 2000, Masharawi et al., 2004, Nojiri et al., 2005, Parent et al., 2002, Porter, 2000, Roberts et al., 2003b, Smyth et al., 1997, Tan et al., 2002, 2004), fusion of radiographic, CT and MR spine images (Chen and Wang, 2004, Hu and Haynor, 2004, Hu et al., 2005, Panigrahy et al., 2000), reconstruction of spine images (Benameur et al., 2005a,b, Bifulco et al., 2002, Chen and Wang, 2004, Gille et al., 2007, Huynh et al., 1997, Novosad et al., 2004, Perdriolle et al., 2001), and spine and vertebral segmentation (Carballido-Gamio et al., 2004, Ghebreab and Smeulders, 2004, Herring and Dawant, 2001, Hoad and Martel, 2002, Hoad et al., 2001, Muggleton and Allen, 1997, Peng et al., 2005, Yao et al., 2006, Zamora et al., 2003, Zheng et al., 2004).

1.3 Motivation

Despite all the reported limitations and difficulties, modern imaging techniques help clinicians in making more accurate diagnosis and planning more effective treatment strategies for spinal disorders. Methods of CAD are constantly developed to aid in the interpretation of the increasing amount of medical image data and clinical information (Giger, 2002). Increased efficiency in the interpretation, reduced human variability and error, and making the interpretation more quantitative are among the most important motivations for developing CAD systems (Doi et al., 1997). Computer-assisted visualization and quantitative evaluation of 3D spine images therefore remain challenging tasks in the field of medical image analysis and processing.

1.4 Contributions

The main contributions of this thesis are united under the design, development and validation of automated techniques that aim to improve the visualization of 3D spine images by generating curved cross-sections, and automated techniques for an improved quantitative evaluation of the most important parameters of the spine in 3D, namely the spinal curvature and vertebral rotation.

1.4.1 Definition of the spine-based coordinate system

CHAPTER 2: Automated curved planar reformation of 3D spine images

CHAPTER 3: Automated generation of curved planar reformations from MR images of the spine

The established techniques for 2D visualization of the spine are based on multiplanar cross-sections, obtained from 3D images. Multiplanar cross-sections are usually displayed in the

image-based (Cartesian) coordinate system (x, y, z), where the direction of each axis is determined along or orthogonal to the image acquisition plane. By navigating through the values on the x, y and z axis, corresponding image-based sagittal, coronal and axial planar cross-sections are displayed, respectively. The orientation of the coordinate system therefore depends on the position of the patient during image acquisition and is completely independent of the spine, which is the observed anatomical structure. To overcome these shortcomings, we propose a spine-based coordinate system (u, v, w) that is independent of patient positioning. The coordinate axes are oriented according to the spine and therefore can simultaneously describe geometrical and clinically relevant properties of the spine. The coordinate axis u is oriented in the direction of vertebral transverse processes, the coordinate axis v is oriented in the direction of vertebral spinous processes and the coordinate axis w is oriented along the longitudinal spine axis.

1.4.2 Development of an automated technique for curved planar reformation of CT spine images

CHAPTER 2: Automated curved planar reformation of 3D spine images

A method for automated CPR visualization of CT spine images, which is based on the transformation from the standard image-based to the spine-based coordinate system (section 1.4.1), is presented in this chapter. The transformation between the coordinate systems is determined on the curve that passes through the centers of vertebral bodies and on the rotation of the vertebrae around the spine curve, both of which are described by polynomial models. The parametrized spine curve is obtained by exploiting the anatomical property that vertebral bodies are locally the largest bone structures in the spine, which can be successfully segmented in CT images. The rotation of the vertebra around the spine curve is determined by the symmetry of the vertebra in cross-sections which are orthogonal to the spine curve in order to measure the rotation angle in 3D. The optimal polynomial parameters are obtained in an optimization framework. The proposed method was qualitatively and quantitatively evaluated on five CT spine images. The method performed well on both normal and pathological cases and was consistent with the manually obtained ground truth data.

1.4.3 Development of an automated technique for curved planar reformation of MR spine images

CHAPTER 3: Automated generation of curved planar reformations from MR images of the spine

A method for automated CPR visualization of MR spine images, which is based on the transformation from the standard image-based to the spine-based coordinate system (section 1.4.1), is

presented in this chapter. The 3D spine curve and the axial vertebral rotation, which determine the transformation, are described by polynomial functions. The 3D spine curve passes through the centers of vertebral bodies, while the axial vertebral rotation determines the rotation of vertebrae around the axis of the spinal column. The optimal polynomial parameters are obtained by a robust refinement of the initial estimates of the centers of vertebral bodies and axial vertebral rotation. The optimization framework is based on the automatic image analysis of MR spine images that exploits some basic anatomical properties of the spine. The centers of vertebral bodies and the vertebral rotation of vertebrae are determined by evaluating the symmetry of the vertebra and the fact that the vertebral body and intervertebral discs are homogeneous in image intensity when observed in axial cross-sections. The method was evaluated on 21 T_1- and T_2-weighted MR images from 12 patients and the results provided a good description of spine anatomy.

1.4.4 Development of a framework for quantitative evaluation of spinal curvature in 3D

CHAPTER 4: Quantitative analysis of spinal curvature in 3D: Application to CT images of normal spine

A framework for quantitative analysis of spinal curvature in 3D is presented in this chapter. Existing methods for measuring spinal curvature proved to be too complex for clinical environment and provide only 2D description of spinal deformity, while 3D descriptors may yield a more complete assessment of 3D spinal curvature. The 3D descriptors of spinal curvature, namely the geometric curvature (GC) and the curvature angle (CA), were measured on 30 CT images of normal spine in order to observe the characteristics of spine anatomy in 3D. The measurements were determined from 3D vertebral body lines, obtained by two different methods. The first method was based on the least squares techniques that approximated the manually identified vertebra centroids. The second method searched for vertebra centroids in an automated optimization scheme, based on computer-assisted image analysis. Polynomial functions of the fourth degree were used for describing normal spinal curvature in 3D. The main advantage of GC and CA features is that the measurements are independent of the orientation and size of the spine, thus allowing objective intra-subject and inter-subject comparisons. From the distributions of GC and CA, the locations of maximal thoracic kyphosis (TK), thoracolumbar junction (TJ) and maximal lumbar lordosis (LL) were also determined.

1.4.5 Development of an automated technique for the determination of the position and rotation of vertebra in CT and MR spine images

CHAPTER 5: Determination of 3D location and rotation of lumbar vertebrae in CT images by symmetry-based auto-registration

CHAPTER 6: Modality-independent determination of vertebral position and rotation in 3D

An automated method for the determination of position and rotation of vertebra in 3D from CT and MR spine images is presented in these two chapters. Many established techniques for measuring vertebral rotation do not exploit 3D image information, which may result in virtual axial rotation because of the sagittal and coronal rotations of vertebrae. Moreover, the measured parameters are estimated from planar cross-sections and the methods require a lot of manual interaction. The proposed automated approach to the measurement of the position and rotation of vertebrae in 3D does not require prior volume reformation, identification of appropriate cross-sections or knowledge in the form of statistical models. Different parts of the vertebra under investigation are encompassed by masks in the form of 3D elliptical cylinders. Their position and rotation in 3D is defined by six rigid parameters, namely the center of rotation (x, y, z) and rotation angles (α, β, γ). The natural symmetry of the vertebral body, vertebral column and vertebral canal is obtained by dividing the vertebral masks by their mid-axial, mid-sagittal and mid-coronal planes. The obtained mirror volume pairs are then simultaneously registered to each other by robust rigid auto-registration. In the first experiment, the method was quantitatively evaluated on 50 lumbar vertebrae from normal and scoliotic spine CT images. In the second experiment, the method was tested on 52 vertebrae; 26 were acquired by CT and 26 by MR imaging technique. The results show that by the proposed auto-registration of symmetrical vertebral parts, the 3D position and 3D rotation of vertebrae can be successfully determined in both CT and MR spine images.

One man's "magic" is another man's engineering. "Supernatural" is a null word.

Robert A. Heinlein, 1907 - 1988
(Time Enough for Love, 1973)

CHAPTER 2

Automated curved planar reformation of 3D spine images

Tomaž Vrtovec, Boštjan Likar and Franjo Pernuš

Physics in Medicine and Biology, 50(19):4257–4540, 2005

Abstract

Traditional techniques for visualizing anatomical structures are based on planar cross-sections from volume images, such as images obtained by computed tomography (CT) or magnetic resonance (MR) imaging. However, planar cross-sections taken in the coordinate system of the three-dimensional (3D) image often do not provide sufficient or qualitative enough diagnostic information, because planar cross-sections cannot follow curved anatomical structures (e.g. arteries, colon, spine, etc.). Therefore, not all of the important details can be shown simultaneously in any planar cross-section. To overcome this problem, reformatted images in the coordinate system of the inspected structure must be created. This operation is usually referred to as curved planar reformation (CPR). In this paper we propose an automated method for CPR of 3D spine images, which is based on the image transformation from the standard image-based to a novel spine-based coordinate system. The axes of the proposed spine-based coordinate system are determined on the curve that represents the vertebral column, and the rotation of the vertebrae around the spine curve, both of which are described by polynomial models. The optimal polynomial parameters are obtained in an image analysis based optimization framework. The proposed method was qualitatively and quantitatively evaluated on five CT spine images. The method performed well on both normal and pathological cases and was consistent with manually obtained ground truth data. The proposed spine-based CPR benefits from reduced structural complexity in favour of improved feature perception of the spine. The reformatted images are diagnostically valuable and enable easier navigation, manipulation and orientation in 3D space. Moreover, reformatted images may prove useful for segmentation and other image analysis tasks.

2.1 Introduction

Traditional techniques for visualizing anatomical structures are based on planar cross-sections from volume images, such as images obtained by computed tomography (CT) or magnetic resonance (MR) imaging. Modern scanners enable acquisition of high-resolution image data for visualization of bony anatomy and soft tissue. However, visualization of a structure of interest is difficult in the standard reformation (axial, sagittal and coronal), and thus planar cross-sections taken in the coordinate system of the three-dimensional (3D) image often do not provide sufficient or qualitative enough diagnostic information. The reason is that because planar cross-sections generally do not follow curved or tubular anatomical structures (e.g. arteries, colon, spine, etc.), not all of the important details can be shown simultaneously in any planar cross-section. For a better visualization of curved structures, reformatted images orthogonal or tangent to a curve along a tortuous 3D structure, i.e. images in the coordinate system of the structure, must be created. This operation is called curved planar reformation (CPR) and can be used to overcome the shortcomings of standard reformation.

In CT angiography, curved planar reformation has been widely used for visualization of blood vessels and evaluation of vascular abnormalities. Different CPR methods for visualization of blood vessels, such as projected, stretched and straightened CPR, were described and evaluated by Kanitsar et al. (2002). The authors also proposed a number of enhancements to the existing methods in order to overcome some of their limitations, and continued their work by introducing two advanced CPR methods (Kanitsar et al., 2003). The helical CPR was used to visualize the interior of a blood vessel within a single image, whereas the untangled CPR produced an unobscured display of a vascular tree regardless of the viewing direction. In Raman et al. (2002), a method capable of automatically producing and interactively displaying curved planar reformations from volumetric image data of blood vessels has been presented. The boundaries of the arteries and branches, found by simple thresholding, were morphologically thinned to obtain the medial centreline between user-specified start and end points. Saroul et al. (2003) extended the notion of CPR to extraction of free form surfaces, defined by user-placed surface boundary curves. While focusing on the visualization of blood vessels, they also mentioned the possibility of using free form surfaces for following non-tubular structures, such as the sternum and the costal cartilage, and irregular anatomical structures, such as the pelvis and the jaw. Their results were, however, limited to the Visible Human data. Recently, these new CPR techniques have been applied to other structures of interest than blood vessels. Gong and Xu (2004) showed that the generation of curved planar reformations could be used for evaluating pancreatic and peripancreatic diseases. However, the curved lines that follow the course of the bile–duct system and peripancreatic vessels were drawn manually on stacks of transverse cross-sections. Common to all of the reported methodologies is that the most important issue for CPR visualization is the appropriate and accurate estimation of the centreline of a tubular structure. Besides in angiography (He et al., 2001, Maddah et al., 2003, Raman et al., 2003), centreline extraction is an important issue in virtual colonoscopy (Ge et al., 1999, Samara et al., 1999, Wan et al., 2002), bronchoscopy (Law and Heng, 2000, Perchet et al., 2004), and can be considered as a common problem (Bitter et al., 2000). General issues were presented by Aylward and Bullitt (2002), who evaluated the effects of initialization, noise and singularities on centreline extraction of tubular objects.

In the analysis of spinal structures, a model of the curvature of the vertebral column which describes the spatial relationship between vertebrae may assist high level image analysis, such as segmentation. Ghebreab and Smeulders (2004) stacked models of single vertebrae to construct a model of the spine, which was used to assist segmentation. Determination of the spinal curvature was based on the assumption that surface landmarks occur at approximately the same position on each vertebra and can be therefore connected by a curve. In Benameur et al. (2003b), an a priori geometric model of the whole spine was presented. The model, based on a set of simple cubic templates, whose parameters were given by statistical knowledge on deformations in a scoliotic population, provided an estimation of position and orientation of each vertebra, from which the spine curve could be defined. Different approaches to reformation of CT spine data have been introduced and reported to be useful in assisting the evaluation of spine defor-

mities. Roberts et al. (2003a) reformatted the image data perpendicular to the long axis of both the left and right neural foramina of the cervical spine segment. They showed that by oblique reformation, consistency in the interpretation of neural foraminal stenosis between observers was improved and suggested that such an approach should be considered in routine evaluation. Congenital spine abnormalities were examined by Newton et al. (2002), who showed that advanced visualization improved the identification of deformities that were inherently difficult to interpret and understand by conventional visualization. By manually outlining the boundaries of the spine curve, they generated curved multiplanar reformatted images that showed the whole spine. The benefit of these images, in comparison with multiplanar (oblique) images, is most valuable in the case of significant sagittal or coronal bending of the spine, as they may help spine surgeons to achieve a more complete understanding and evaluation of spine deformity. Kaminsky et al. (2004) proposed a protocol for spine segmentation composed of standard and novel interactive segmentation tools that were applied on reformatted data. A 3D spline, placed through vertebrae centres, was defined either manually by determining centrelines on sagittal and coronal planes, or automatically by dropping spheres of maximum possible radius through the vertebral bodies or the spinal canal. In order to overcome the problems of orientation in standard reformation, the initial image was reformatted in such a way that the centre spline formed the centre axis of the rotated images.

The motivation for the present work was to design, develop and test an automated CPR method for CT spine images with minimal human intervention. We introduce a transformation that converts the standard image-based to a novel spine-based coordinate system. The proposed algorithm automatically extracts the vertebral column curve and the rotation of individual vertebrae around this curve. The algorithm works well on both normal and deformed (e.g. scoliotic) spines. The information gained from the spine curve is then used to reformat the images. The spine curve and the rotation of vertebrae around the curve are not only important for extracting diagnostically important images, but also for easier navigation, manipulation and orientation in 3D space, and for easier identification of the marginal structures of the spine.

2.2 Method

2.2.1 Spine-based coordinate system

Usually, 3D images of the spine are inspected and analysed in the standard image-based reformation, represented by the Cartesian coordinate system, where the x, y, and z axes determine the standard sagittal, coronal and axial view, respectively. To inspect the structures in the coordinate system of the spine and to create CPR images, a new spine-based (i.e. spine-specific) coordinate system must be introduced. To render a complete 3D representation of the space, the new coordinate system requires three directional variables, i.e. axes, say u, v and w. The axes

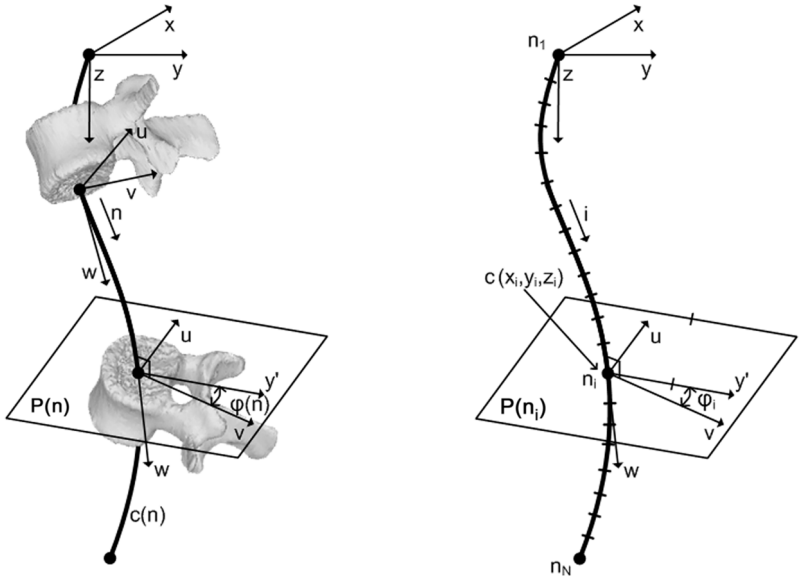

(a) (b)

Figure 2.1. Spine-based coordinate system (u, v, w) (a), determined by the course $c(n)$ and orientation $\varphi(n)$ of the spine curve, and the corresponding discretization of the spine domain (b).

are defined by a continuous curve $c(n) = (x(n), y(n), z(n))$ that goes through the same anatomical landmarks on individual vertebrae and represents the spine (vertebral column) curve. The continuous independent variable n parametrizes the curve. The coordinate axis w of the spine-based coordinate system (figure 2.1, p. 51) is tangent to the spine curve. The axis v is orthogonal to w, i.e. to the spine curve, and oriented in the direction of vertebral spinous processes. The rotation of the axis v around the curve is determined by the angle $\varphi(n) = \varphi(v(n), y'(n))$ between v and the corresponding projection y' of the Cartesian coordinate y onto the plane $P(n)$, i.e. the plane orthogonal to the spine curve, which is determined by the tangent to the curve (figure 2.1, p. 51). The u axis is orthogonal to v and therefore extends in the direction parallel to the vertebral transverse processes. Both u and v axes lie in the normal plane $P(n)$; hence the axis u is also orthogonal to the axis w. As a result, the direction of the spine-based coordinates (u, v, w), when observed in the Cartesian coordinate system (x, y, z), depends on the spine curve and the vertebrae rotation around the spine curve.

To inspect the structures in the spine-based coordinate system we define three spine-based views, which are analogous to the standard sagittal, coronal and axial views in the imagebased Cartesian coordinate system. A spine-based view is a curved two-dimensional (2D) cross-section of the 3D original image, defined by any two of the (u, v, w) axes for a chosen value on the third axis:

- The spine-based sagittal view is defined by the v and w axes for a chosen value on the u axis.
- The spine-based coronal view is defined by the u and w axes for a chosen value on the v axis.
- The spine-based axial view is defined by the u and v axes for a chosen value on the w axis.

Using any of these views, we can create a 3D spine-based reformatted image by stacking the corresponding 2D cross-sections. For example, if we stack spine-based axial 2D cross-sections, obtained for a selected set of values on the w axis, we obtain the 3D spine-based reformatted image.

2.2.2 Coordinate system parametrization

Since the spine curve $c(n)$ and the rotation $\varphi(n)$ of the vertebrae around the spine curve are expected to be smooth functions of n, we parametrize them by the following polynomial functions:

$$x(n) = \sum_{k=0}^{K_x} b_{x,k} \frac{n^k}{\hat{b}_k} \quad y(n) = \sum_{k=0}^{K_y} b_{y,k} \frac{n^k}{\hat{b}_k} \quad z(n) = \sum_{k=0}^{K_z} b_{z,k} \frac{n^k}{\hat{b}_k}$$
$$\varphi(n) = \sum_{k=0}^{K_\varphi} b_{\varphi,k} \frac{n^k}{\hat{b}_k}, \tag{2.1}$$

where K_x,K_y,K_z and K_φ. are the degrees and $b_x = \{b_x, k; k = 0, 1, \ldots, K_x\}$, $b_y = \{b_y, k; k = 0, 1, \ldots, K_y\}$, $b_z = \{b_z, k; k = 0, 1, \ldots, K_z\}$ and $b_\varphi = \{b_\varphi, k; k = 0, 1, \ldots, K_\varphi\}$ are the parameters of polynomials $x(n)$, $y(n)$, $z(n)$ and $\varphi(n)$, respectively. The polynomial parameters are normalized over the spine domain Ω_n, so that a modification of each parameter has the same impact on the absolute variation of the corresponding polynomial term:

$$\hat{b}_k = \int_{\Omega_n} \left| n^k \right| \mathrm{d}n. \tag{2.2}$$

The crucial part of the proposed automated spine-based CPR is estimation of the spine-specific parameters $b = b_x \cup b_y \cup b_z \cup b_\varphi$, which by equation 2.1 (p. 52) define the parametrized spine curve and the vertebrae rotation. We address this issue in the following sections. For the purpose of implementation, the continuous variable n is discretized. The discrete spine domain consists of N samples, $n_i, i = 1, 2, \ldots, N$ (figure 2.1, p. 51), which can be transformed

to the Cartesian coordinate system by using the discrete form of equation 2.1 (p. 52). After discretization, a discrete spine curve $c(n_i) = c(x_i, y_i, z_i), i = 1, 2, \ldots, N$ and a discrete rotation of vertebrae $\varphi(n_i), i = 1, 2, \ldots, N$ are obtained.

2.2.3 Estimation of spine curve parameters

In order to locate the spine curve, we exploit the anatomical fact that vertebral bodies are locally the largest bone structures along the vertebral column. We create a 3D distance map D by computing the Euclidean distances from the edges of the bone structures, which are separated from other structures in the CT image by simple thresholding. Distances are positive inside and negative outside the bone structures. The values of the distance map are therefore expected to be the highest in geometrical centres of vertebral bodies and smoothly decreasing by moving away from the centres. Let the spine curve be described by a curve $c(n)$ that passes through the centres of vertebral bodies, and let this curve be parametrized by the spine curve parameters $b_c = b_x \cup b_y \cup b_z$. The parameters are found by an optimization procedure that searches for the parameters b_c^{opt} that maximize the cost function, which is the sum of values in the distance map D along the spine curve:

$$b_c^{opt} = \arg\max_{b_c} \sum_{i=1}^{N} D(P(n_i)\big|b_c). \tag{2.3}$$

In order to increase the robustness of optimization, we consider for each sample n_i of the discrete spine domain distance map values within a circle, centred at $c_i = c(n_i)$ in the plane $P(n_i)$, both of which are determined by the current spine curve parameters b_c. The radius of the circle is chosen to be smaller than the radius of the smallest vertebral body. The optimization procedure is hierarchical, initiated by the polynomial functions of a specified degree. When the termination criterion is reached, the polynomial degree is increased and the procedure is restarted at the next level, using the resulting polynomial parameters as the new initialization values (figure 2.2, p. 54).

2.2.4 Estimation of rotational parameters

The rotation $\varphi(n)$ of vertebrae around the spine curve, which is parametrized by the rotational parameters b_φ, is obtained by maximizing the in-plane intensity symmetry in planes $P(n)$ normal to the spine curve. The projection y' of the Cartesian coordinate axis y onto the plane $P(n)$ (figure 2.1, p. 51) serves to define the rotation. An in-plane straight line that passes through the centre of the plane, represented by the spine curve sample c_i, declined for an angle φ_i (equation 2.1, p. 52) from y', halves the plane (figure 2.3, p. 55). For a given angle φ, the

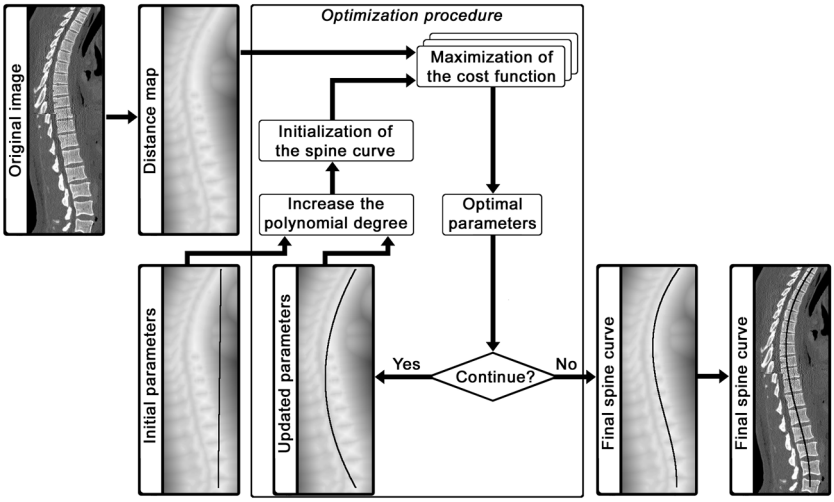

Figure 2.2. Hierarchical optimization of the spine curve parameters. The curve is initialized with the first-degree polynomial functions (i.e. a 3D straight line). The parameters that maximize the cost function at each level are used to initialize the polynomials at the next level of the optimization procedure.

in-plane similarity between the two halves is evaluated by the correlation coefficient $R_i(\varphi)$:

$$R_i(\varphi) = \frac{\sum_{j=1}^{L} (f_{i,j}(\varphi) - \bar{f}_i(\varphi))(g_{i,j}(\varphi) - \bar{g}_i(\varphi))}{\sqrt{\sum_{j=1}^{L} (f_{i,j}(\varphi) - \bar{f}_i(\varphi))^2 \sum_{j=1}^{L} (g_{i,j}(\varphi) - \bar{g}_i(\varphi))^2}}, i = 1, 2, \ldots, N, \tag{2.4}$$

where $f_{i,j}$ and $g_{i,j}$ represent the L mirror intensity pairs of each half of the ith plane (figure 2.3, p. 55), while $\bar{f}_i$ and $\bar{g}_i$ are the corresponding mean intensity values. The evaluation of similarity is performed on a rotationally invariant circular domain. The in-plane similarity values represent the cost function used to optimize the rotational polynomial parameters b_φ. The optimization procedure searches for the rotational parameters b_φ^{opt} that maximize the sum of all N in-plane similarities along the spine curve:

$$b_\varphi^{opt} = \arg\max_{b_\varphi} \sum_{i=1}^{N} R_i(\varphi). \tag{2.5}$$

The in-plane similarity is the highest when the line that splits the plane equals the axis of intensity symmetry. The optimization of rotational parameters is performed by the same hierarchical optimization scheme that is used for the spine curve parameters.

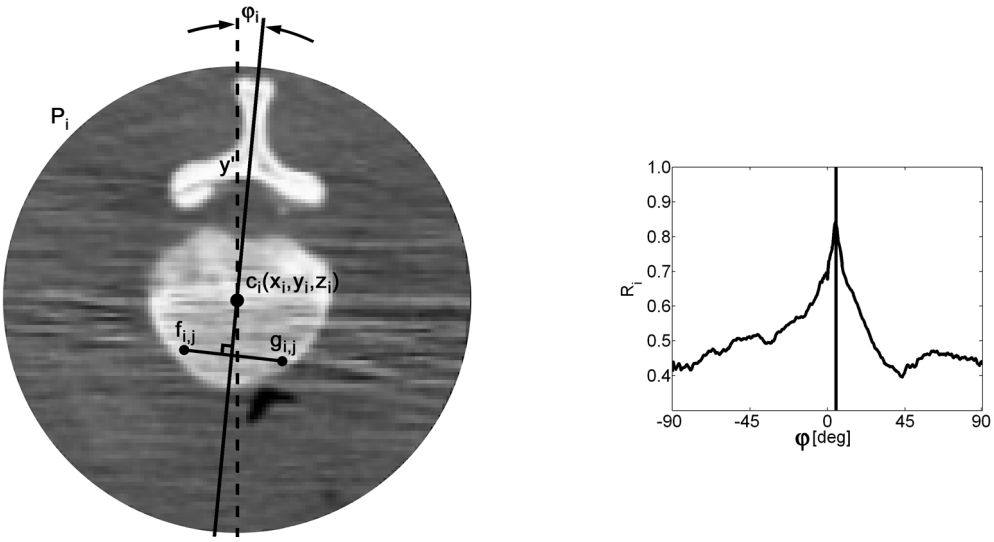

(a) (b)

Figure 2.3. Rotation φ_i is defined by the axis of in-plane intensity symmetry (solid line) (a) that maximizes the correlation between the halves of the normal plane (right) (b).

2.2.5 Additional spine features

Radius of vertebral bodies. The vertebral bodies, together with the intervertebral discs, form a tubular structure with a central axis that represents the spine curve. The size of vertebral bodies, however, is not constant along the vertebral column, so we parametrize the radius r of the tubular structure similarly as the spine curve (equation 2.1, p. 52), i.e. by a polynomial function of degree K_r:

$$r(n) = \sum_{k=0}^{K_r} b_{r,k} \frac{n^k}{\hat{b}_k}, \tag{2.6}$$

where the polynomial parameters $b_r = \{b_r, k; k = 0, 1, \ldots, K_r\}$ are normalized as in equation 2.2 (p. 52). The parameters are determined using an optimization procedure that, similarly as for the spine curve, searches for the maximum of the sum of positive and negative distance map values inside the resulting tubular structure (equation 2.3, p. 53).

Spinal curvature. An interesting feature that has already been reported to be relevant, especially the value and the location of its maximum, is the spinal curvature (Aykroyd and Mardia 2003). The spinal curvature is an inherent spine feature that can be used to evaluate interesting anatomical properties (e.g. the strength of the spinal deformity). The curvature of a parametrized curve in 3D space is defined at any point along the curve as the reciprocal of the

radius of the osculating circle (Weisstein, 1999):

$$\kappa(n) = \frac{\left| \frac{\mathrm{d}c(n)}{\mathrm{d}n} \times \frac{\mathrm{d}^2 c(n)}{\mathrm{d}n^2} \right|}{\left| \frac{\mathrm{d}c(n)}{\mathrm{d}n} \right|^3}, \tag{2.7}$$

which can be solved analytically for the given polynomial parameters of the 3D curve $c(n)$ (the sign $\times$ denotes the vector cross product). The curvature at any point on the curve can be interpreted as the tendency of the curve to depart from the tangent to the curve at that point.

2.3 Experiments

2.3.1 Experimental data

The experiments were performed on five CT spine segments, including the spine segment of the Visible Human Male (VH) data table 2.1 (p. 56).

Table 2.1. Properties of the spine segments used in the experiments.

Spine segment	Number of vertebrae	Segment dimensions (voxel)	Voxel size (voxel/mm^{-1})	Segment dimensions (mm)
VH	18	573×330×774	1.000×1.000×1.000	573.0×330.0×774.0
01	11	512×512×448	0.732×0.732×1.000	374.8×374.8×448.0
02	15	512×512×545	0.702×0.702×1.000	359.4×359.4×545.0
03	14	512×512×444	0.732×0.732×1.000	374.8×374.8×444.0
04	14	512×512×472	0.601×0.601×1.000	307.7×307.7×472.0

2.3.2 Implementation details

To extract the spine curve, user interaction was limited to pinpointing two points that correspond to approximate centres of the upper- and lower-most vertebral bodies, respectively, which determined the section of interest of the vertebral column. The two selected points initialized a first-degree spine curve, i.e. a straight line. During the optimization procedure, the polynomial degree was gradually increased from 1 upwards. The degree of the polynomial $z(n)$ (equation 2.1, p. 52) was fixed to the initial value $K_z = 1$, constraining the course of the z-coordinate

to be linear. The number of samples N was set to the approximate value of the number of voxels between the selected points in the z-direction, which proved to be sufficient for describing a spine curve and extracting CPR images. 3D spine-based reformatted images were created by stacking spine-based 2D cross-sections, using trilinear interpolation to obtain the corresponding intensity values. On the whole sample domain, the rotational function was initialized by a polynomial of 0 degree, i.e. a constant. Fifth degree polynomial functions were used to describe the spine curves and rotations of vertebrae around the spine curves. The optimizations were performed by the downhill simplex method in multidimensions (Press et al., 2002) with the parameters $f_{tol} = 10^{-4}$ and $n_{max} = 500$. The fast marching method (Sethian, 1999) was used to compute distance maps.

2.4 Results

2.4.1 Qualitative results

Figure 2.4 (p. 58) shows the image-based and reformatted spine-based coronal and sagittal views. In standard image-based reformation, the whole course of the spine segment cannot be seen in any planar cross-section as, due to the spinal curvature, the spine is generally 'coming in' and 'going out' of the plane. In the spine-based reformation, however, the whole course of the spine segment can be seen as the cross-section follows the spinal curvature. The spine curve and the corresponding radii of the vertebral bodies for the normal VH and a scoliotic spine, along with the spine-based cross-sections in image-based coordinate system, are illustrated in figure 2.5 (p. 58).

2.4.2 Quantitative results

The course of the spine curve coordinates $x(n)$ and $y(n)$, and the corresponding rotation of vertebrae $\varphi(n)$, described by polynomial functions (equation 2.1, p. 52), are shown in figure 2.6 (p. 59). The course of the spine curve of VH reflects the curvature of a normal spine with a relatively small coronal bend $x(n)$ in comparison with the natural S-shaped sagittal bend $y(n)$. The rotation $\varphi(n)$ of vertebrae is also small. For the scoliotic spine, on the other hand, a large deviation from normality can be observed. The sagittal bend $y(n)$ is very small, whereas the coronal bend $x(n)$ is large. The difference between the scoliotic and normal spine is also well demonstrated by the large rotation $\varphi(n)$ of vertebrae around the spine curve, which ranges from -15° to 12°.

Figure 2.7 (p. 59) shows the course of the spinal curvature along the spine. For the normal spine, the spinal curvature well expresses the natural S-shape. The course of the curvature

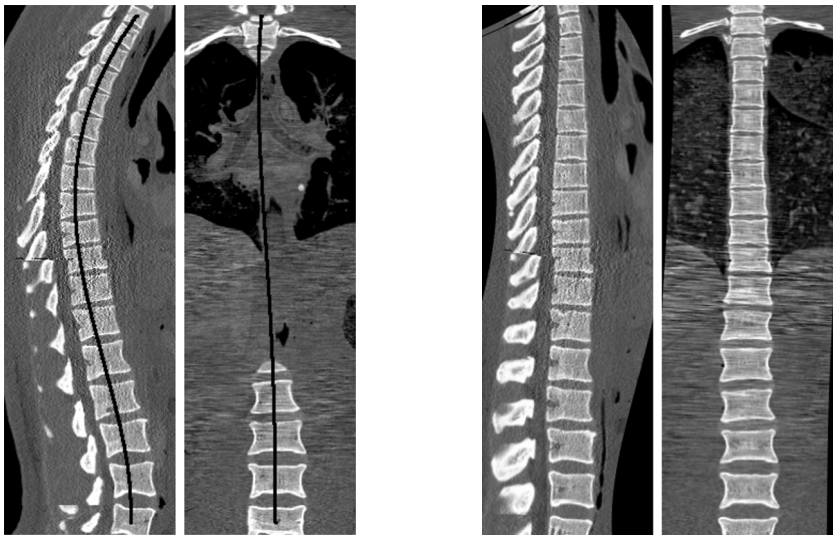

(a) (b)

Figure 2.4. Image-based (a) and reformatted spine-based (b) sagittal and coronal views. The projection of the obtained 3D spine curve is superimposed on the image-based 2D views.

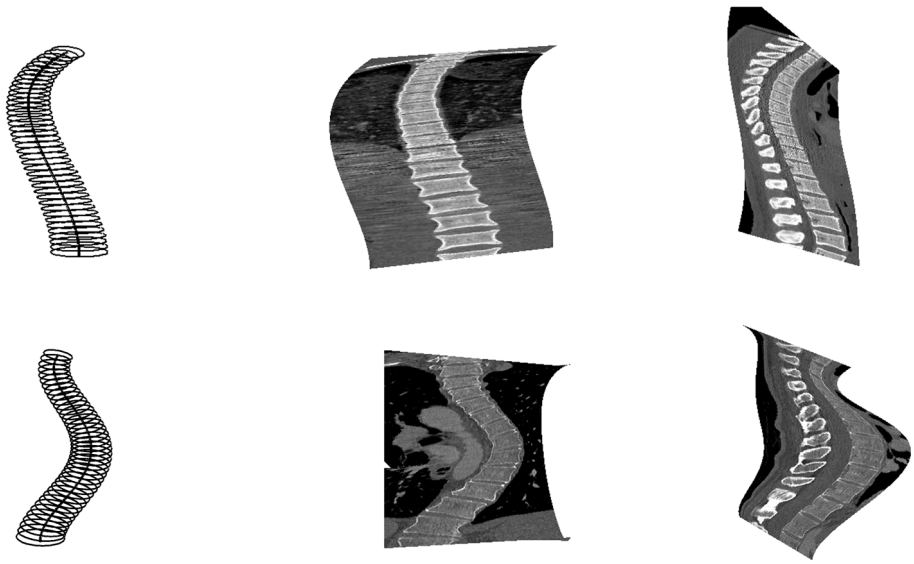

(a) (b) (c)

Figure 2.5. Graphical illustration of the spine curve and the corresponding radii of vertebral bodies (a), coronal (b) and sagittal (c) spine-based cross-sections viewed in the image-based coordinate system for the normal VH spine (top) and for a scoliotic spine (bottom).

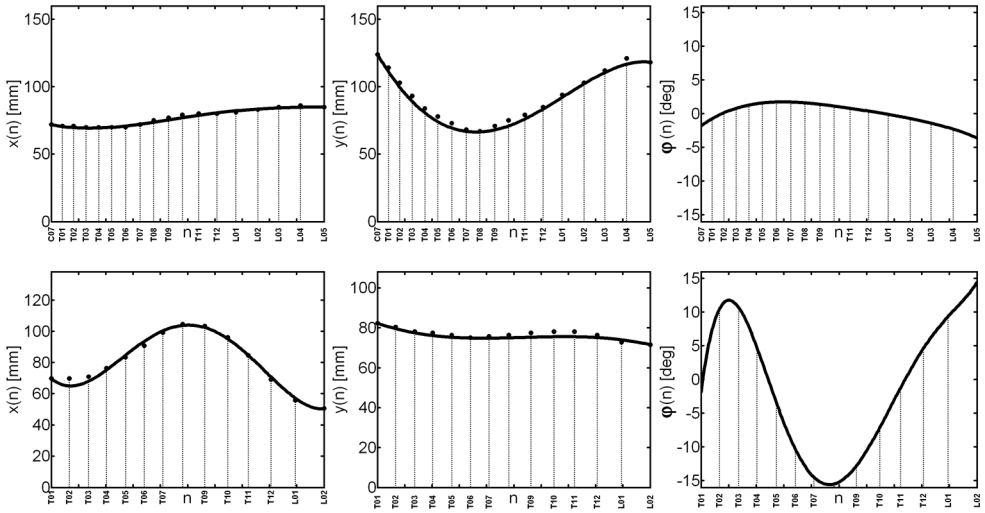

Figure 2.6. The course of the spine curve coordinates $x(n)$ and $y(n)$, and the corresponding rotation of vertebrae $\varphi(n)$ for the normal VH spine (top) and for a scoliotic spine (bottom). The vertical lines represent the locations of the centres of vertebral bodies (ground truth data).

of the scoliotic spine, however, exhibits unnatural variations that are mostly due to the large coronal bend (figure 2.6, p. 59). By the mapping from the spine domain onto the image-based coordinate system, the location of any spinal curvature can be easily identified in the original image.

The performance of the spine curve detection algorithm was also assessed quantitatively using ground truth data, obtained from landmarks that were placed in 3D (standard axial, sagittal and coronal planes) by an expert radiologist at centres of vertebral bodies. The spine curve positional error was expressed as the Euclidean distances from ground truth points to the spine curve. The obtained mean positional errors for the five spine segments are tabulated in table 2.2

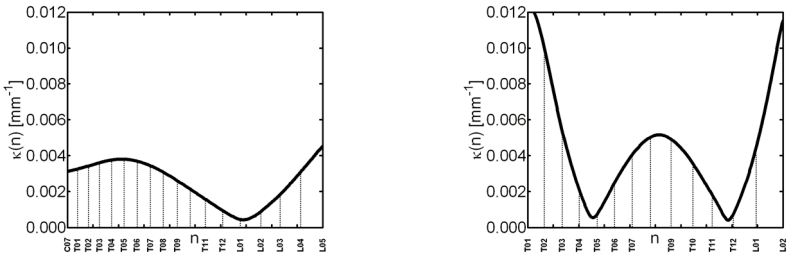

(a) (b)

Figure 2.7. Spinal curvature $\kappa(n)$ for the normal VH spine (a) and for a scoliotic spine (b). The vertical lines represent the locations of the centres of vertebral bodies (ground truth data).

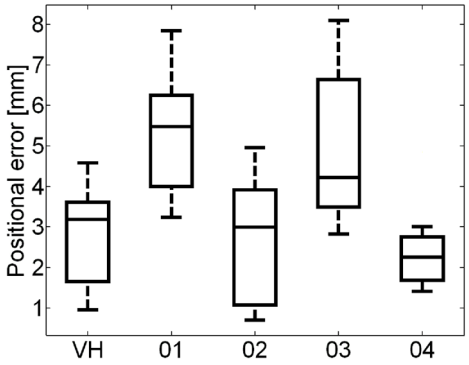

Figure 2.8. Distributions of positional errors.

(p. 60). The mean positional errors range from 2 to 6 mm for normal and pathological spines. The distributions of positional errors are illustrated in figure 2.8 (p. 60) by the box-whiskers diagram, showing the medians, first and third quartiles, and minimal and maximal errors for each spine segment.

Table 2.2. Mean positional errors.

Spine segment	Mean error (mm)
VH (normal)	2.82
01 (normal)	5.46
02 (normal)	2.68
03 (normal)	5.97
04 (scoliotic)	2.39

2.5 Discussion

A valuable contribution of the presented reformation of 3D spine images is the ability to inspect and analyse 3D images in the coordinate system of the spine. Displaying the whole vertebral column length within a single image makes the inspection of images quicker and more precise while the probability of overlooking certain important features of the spine is reduced. The proposed method was qualitatively and quantitatively evaluated on five CT spine images. It was shown that the method finds both natural and pathological spine curves and that it is consistent with manually obtained ground truth data. As such, the method can be used for objective evaluation of pathology, especially for significant coronal (i.e. scoliosis) or sagittal (i.e. kyphosis

or lordosis) spinal bends, and may provide additional support for segmentation and other image analysis tasks.

The CPR technique does, however, have some limitations. For example, the determination of rotation of vertebrae depends on the prior estimation of the spine curve. The better the estimation of the spine curve, the more accurate the determination of vertebrae rotation. Hence, the accuracy of spine curve extraction is of significant importance for further analysis. Another limitation that has to be stressed out is that the curved transformation does not preserve distances. However, by applying the inverse transformation, the structures identified in CPR images can be mapped onto the standard reformation in which distances are simply measured.

The introduced spine-based coordinate system (u, v, w) is inconsistent with the Frenet frame in differential geometry (Weisstein, 1999), which is determined by the intrinsic parameters of the curve, i.e. the curvature and torsion. However, a spine-curve-based coordinate system, consistent with the Frenet frame, depends solely on the geometrical properties of the spine curve and therefore incorporates solely anatomical information on the spinal curvature and not the anatomical information on the direction of the vertebral spinous processes. Therefore, we have proposed an alternative spine-anatomy-based coordinate system by which the anatomical spine shape is described by the spine curve $c(n)$ and the rotation $\varphi(n)$ of vertebrae around the spine curve. We believe that the proposed spine-anatomy-based coordinate system is clinically more relevant.

In general, the presented method can facilitate image manipulation and computer-assisted applications. For example, in the spine-based coordinate system, pathological anatomy is oriented comparable to healthy anatomy, thus facilitating image interpretation. Furthermore, quantitative assessment of the 3D spinal curvature (equation 2.7, p. 56) can improve diagnosis of spinal deformities. The Cobb technique is the accepted standard for measuring scoliosis on a single 2D radiograph (Cassar-Pullicino and Eisenstein, 2002). However, the rotation of vertebrae, which is a major factor determining changes in the body shape, is not taken into account. This drawback can be avoided by implementing the Cobb technique on the 3D spine curve. Automatic extraction of the spine curve may also prove useful for removing the spine before creating maximum intensity projections (MIPs) of CT angiographic data, especially when the structures under investigation, located in the vicinity of the spine (e.g. the abdominal aorta or the thoracic aorta), are obscured or overlapped by the high-attenuating bone structures (Raman et al., 2003). Knowledge on the course of the spine and rotation of vertebrae may facilitate advanced spine analysis techniques. For example, in approaches to segmentation that model the spinal curvature by taking into account spatial relationships between vertebrae (Benameur et al., 2003b, Ghebreab and Smeulders, 2004) and/or in statistical shape analysis of vertebrae (Benameur et al., 2003a, Kaus et al., 2003, Lorenz and Krahnstover, 2000, Vrtovec et al., 2004a,b). The estimation of rotation of vertebrae around the spine curve is not only useful for the assessment of the rotation of a vertebra relative to the neighbouring vertebrae (i.e. inter-vertebral rotation), but it also allows the determination of the rotation present within

individual vertebrae, i.e. between their superior and inferior end-plates (i.e. intra-vertebral rotation). This is of extreme importance, especially in the case of scoliotic spines, each having its own slightly different and slightly unpredictable shape. The inter-vertebral rotations are potentially correctable by surgical intervention, whereas the intra-vertebral rotations are designated to be non-correctable (Cassar-Pullicino and Eisenstein, 2002). However, although a number of different methods for quantitative spine analysis were proposed in the past (Cheung et al., 2002, Drerup and Hierholzer, 1996, Göçen et al., 1999, Verdonck et al., 1998), the methodological approaches are quite inconsistent and there are no universal solutions. An important problem that will need special attention in the future is the definition of a generally accepted spine-based coordinate system. Such a system should be invariant to rigid body transformation and scale, and at the same time it should be simple, intuitive, easy to interpret, and should explicitly provide clinically relevant information on spine anatomy.

The assessment of the spine curve and rotation of vertebrae of an individual subject may improve surgical and therapeutic procedures. The proposed CPR is modality-independent, constructed on the spine-based coordinate system. However, the automatic estimation of the transformation parameters was developed for CT, which is a standard orthopaedic modality, providing a good bone contrast but a relatively large dose of radiation. On the other hand, MR imaging is a non-invasive alternative, especially for frequent and whole-body scanning. Our further research will therefore focus on the automatic extraction of the spine curve and rotation of vertebrae from the MR data.

2.6 Conclusion

An automatic approach to CPR of CT spine images has been proposed. The curvature of the spine and the rotation of vertebrae around the spine curve were obtained automatically and used to transform a 3D spine image from the image-based to the spine-based coordinate system. As a result, structural complexity of the spine was reduced in favour of improved feature perception and image analysis.

Acknowledgments

This work has been supported by the Slovenian Ministry of Higher Education, Science and Technology under grant P2-0232. We would like to thank M Medved from University of Ljubljana, Faculty of Electrical Engineering, Slovenia, for the implementation of the 3D distance map algorithm. Part of the utilized CT images is from the Segmented Inner Organs Data of the Visible Human Male, VOXEL-MAN project, purchased from the Institute of Medical Informatics, University Hospital Hamburg-Eppendorf, Germany.

If you don't stand for something, you'll fall through anything.

EDDIE VEDDER
(Pearl Jam in Raleigh, NC, USA, July 15th 2003)

CHAPTER 3

Automated generation of curved planar reformations from MR images of the spine

TOMAŽ VRTOVEC, SÉBASTIEN OURSELIN, LAVIER GOMES, BOŠTJAN LIKAR AND FRANJO PERNUŠ

PHYSICS IN MEDICINE AND BIOLOGY, 52(10):2865–2878, 2007

Abstract

A novel method for automated curved planar reformation (CPR) of magnetic resonance (MR) images of the spine is presented. The CPR images, generated by a transformation from image-based to spine-based coordinate system, follow the structural shape of the spine and allow the whole course of the curved anatomy to be viewed in individual cross-sections. The three-dimensional (3D) spine curve and the axial vertebral rotation, which determine the transformation, are described by polynomial functions. The 3D spine curve passes through the centres of vertebral bodies, while the axial vertebral rotation determines the rotation of vertebrae around the axis of the spinal column. The optimal polynomial parameters are obtained by a robust refinement of the initial estimates of the centres of vertebral bodies and axial vertebral rotation. The optimization framework is based on the automatic image analysis of MR spine images that exploits some basic anatomical properties of the spine. The method was evaluated on 21 MR images from 12 patients and the results provided a good description of spine anatomy, with mean errors of 2.5 mm and 1.7 degrees for the position of the 3D spine curve and axial rotation of vertebrae, respectively. The generated CPR images are independent of the position of the patient in the scanner while comprising both anatomical and geometrical properties of the spine.

3.1 Introduction

Images of three-dimensional (3D) anatomical structures, obtained by computed tomography (CT) or magnetic resonance (MR) imaging, are usually presented to clinicians in the form of a series of two-dimensional (2D) planar cross-sections in the standard axial, sagittal and coronal image reformation. However, because structures of interest may have curved 3D morphology, they can not be completely visualized in individual multiplanar or oblique cross-sections. In the examination of spine images, for example, the spine may intersect the sagittal or coronal cross-sections due to its natural curved shape, while the axial cross-sections may not always be positioned at the same level of the vertebral bodies or intervertebral discs. Not all of the important details can therefore be shown simultaneously in any planar cross-section, which may be even more explicit in case of significant coronal or sagittal spinal curvature, i.e. scoliosis and kyphosis or lordosis, respectively. To enable an effective clinical evaluation and quantitative analysis of such cases, images should be created in the coordinate system of the curved 3D anatomical structure, in which cross-sections are either orthogonal or tangent to a curve along the structure. This type of image reformation is referred to as curved planar reformation (CPR), or curved sectioning, and is often used (e.g. in angiography, diagnostics of colon and pancreas) to overcome the difficulties of conventional representations.

Several approaches to reformation of CT images of the spine have already been presented and reported to be useful for evaluation of spinal deformities. Rothman et al. (1984) demonstrated that curved images of the coronal spine region, obtained by connecting manually selected points into a continuous curve, are useful in evaluation of anatomical relationships. After reformation, structures such as nerve roots, facet joints and spinal cord could be observed in a single 2D image. By generating oblique sagittal images, Rabassa et al. (1993) showed that visualization of the vertebral facets improved, while oblique axial images allowed views parallel to the intervertebral discs in case of scoliosis or an increased lumbosacral curvature of the spine. Although the reformation was limited to oblique cross-sections, the authors concluded that in certain clinical situations, such as in evaluation of neural foraminal stenosis or localization of spinal lesions, the reformatted images could supplement the acquired CT images. Congenital spinal deformities were examined by Newton et al. (2002), who manually outlined the boundaries of the spine in standard reformation and created CPR images that improved the identification and interpretation of abnormalities. The benefit of CPR images, in comparison with multiplanar or oblique cross-sections, was most valuable in case of significant sagittal or coronal curvature of the spine, as CPR images might help spine surgeons to achieve a more complete understanding of spinal deformity. Roberts et al. (2003a) reformatted the images orthogonally to the long axis of both left and right neural foraminae of the cervical region of the spine. By oblique reformation, they improved the consistency in the interpretation of neural foraminal stenosis between observers. They also suggested that such an approach should be considered in routine evaluation. In order to improve the definition of congenital abnormalities of the spine, Menten et al. (2005) described a planospheric reformation method that was based on a reconstruction from a cylindrical plane, defined around the approximate boundary of the spinal canal within an axial CT cross-section. As a result, the anterior and posterior elements of the spine were visualized in the same plane. Manual determination of the curve points was required in all of the studies reported above. A semi-automated method was presented by Kaminsky et al. (2004), who performed segmentation of the spine on reformatted CT images in order to overcome the problems of orientation in the standard reformation. The transformation axis was determined by a 3D spline, obtained either manually by delineating centrelines in sagittal and coronal planes, or automatically by dropping spheres of maximum possible radius through the vertebral bodies or spinal canal. Recently, an automated CPR method for 3D CT spine images was presented by Vrtovec et al. (2005), which required manual determination of just two points at both ends of the spinal section of interest. By introducing the notion of the spine-based coordinate system, they represented the spinal curvature and the rotation of vertebrae as polynomial functions, which formed the transformation axes for the reformation procedure. However, the method was developed for CT images and is therefore modality-dependent.

Over the past years, MR has become a more dominant modality in spine imaging, providing high-quality 3D images of soft tissues and bone structures of the spine, including the spinal cord, by a correct selection of imaging parameters. The poor resolution of early MR scanners has been improved by dedicated multichannel spine coils with better signal-to-noise ratio (SNR).

Visualization of abnormalities, injuries and diseases in the spinal region is often superior in MR imaging than in other imaging methods, such as CT or myelography. Moreover, as there is no exposure to ionizing radiation, MR is considered to be the modality of choice for follow up examinations and longitudinal studies. Image reformation has already been identified as a valuable technique in MR imaging of the spine. Apicella and Mirowitz (1995) reported that image reformation could compensate for the apparent asymmetry of 3D anatomical structures, caused by improper patient positioning or patient motion during image acquisition, and that reformatting can be applied to different anatomical structures, including the spine, where it can be used to improve the visualization of the spinal canal and neural foraminae. Liljenqvist et al. (2002) focused their study on vertebral morphology, which is of significant importance in pedicle-screw placement for the treatment of scoliosis. In order to obtain true values of the pedicle width, length and angle, the MR spine images were manually reformatted so that the measurements could be performed in cross-sections perpendicular to the vertebral bodies. Very recently, in a study of automated survey of MR spine images Weiss et al. (2006), it was reported that automated reformation of 3D spine images along the true sagittal, coronal or axial axis of the vertebral bodies and discs may potentially facilitate the radiologist's image interpretation. On the other hand, dedicated commercial software and packages provided by CT/MR scanner vendors enable generation of multiplanar and curved cross-sections. However, the points that are connected into a continuous curve also have to be manually selected by the user, which requires navigation through complex 3D (spine) anatomy. Although the MR scanners allow acquisition of images in arbitrary planes (i.e. in a rotated standard reformation), they are selected by the machine operator and dependent on the position of the patient in the scanner. The possibility of obtaining a curved slice from the MR scanner (Börnert, 2003, Jochimsen and Norris, 2002) was achieved by the application of spatially selective 2D radio-frequency (RF) pulses, thus allowing the imaged slice to be curved only in one dimension. Poor spatial resolution in initial experiments was improved, however, the image quality was still not satisfying due to intensity modulation artifacts.

In this paper we present a novel method for automated CPR of MR images of the spine. The reformation framework is based on the transformation from the standard image-based to the spine-based coordinate system, which we proposed for automated CPR of CT images (Vrtovec et al., 2005). The main contribution of this work is the automated extraction of the 3D spine curve and axial vertebral rotation from MR images. The method is based on automated detection of spine bone structures from MR images, which is far more difficult than the detection of these structures from CT images. For this purpose, we exploit some of the basic anatomical features of the spine, i.e. the mid-sagittal symmetry and circularity of the vertebral column. Besides being diagnostically valuable, the resulting CPR images are independent of the position of the patient in the scanner, as they are referenced to the location of the vertebral bodies and the relative orientation of vertebrae while comprising both anatomical and geometrical properties of the spine.

3.2 Problem description

In order to generate CPR images of the spine, information on individual vertebrae and intervertebral discs and their spatial relationship has to be properly extracted from MR images of the spine. The standard image-based reformation is represented by the Cartesian coordinate system, in which the x, y and z axes represent the standard sagittal, coronal and axial directions, respectively. With the introduction of the spine-based coordinate system (Vrtovec et al., 2005), the spine domain Ω_n is mapped from the image-based to the spine-based coordinate system by applying the transformation $\mathbb{T}$:

$$\mathbb{T}: (x, y, z) \xrightarrow{\Omega_n} (u, v, w), \tag{3.1}$$

where u, v and w are the axes of the spine-based coordinate system, defined by continuous parametric functions $c(n)$ and $\varphi(n)$, which are specific for the spine. The 3D spine curve $c(n)$ is a curve that passes through the centres of vertebral bodies and intervertebral discs and represents the central axis of the spinal column. The axial vertebral rotation $\varphi(n)$ represents the rotation of the vertebral spinous processes around the axis of the spinal column. The continuous variable n parameterizes the spine domain Ω_n. For an arbitrary position on the spine, the axes of the spine based-coordinate system (figure 3.1, p. 68) can be therefore defined as:

- The axis w is tangent to the 3D spine curve $c(n)$ and points in the direction of the axis of the spinal column.
- The axis v is orthogonal to axis w and points in the direction of the vertebral spinous processes. The rotation of the axis v around the axis w is determined by the angle $\varphi(n) = \angle(v, y_\perp)$, which is defined as the angle between the axis v and the projection $y_\perp$ of the Cartesian axis y onto the plane $P_\perp(n)$, in which the axis v lies.
- The axis u is orthogonal to both axes w and v.

The key problem in automated generation of CPR is the determination of the 3D spine curve $c(n)$ and axial vertebral rotation $\varphi(n)$, which is especially demanding for MR spine images in which bone structures, needed to define $c(n)$ and $\varphi(n)$, are difficult to extract. The major contribution of this paper is a novel solution to this challenging problem, which is addressed in the following subsections.

3.3 Methods

In order to automatically detect the centres of vertebral bodies and intervertebral discs, which will serve to define the 3D spine curve $c(n)$ and axial vertebral rotation $\varphi(n)$, we exploit some

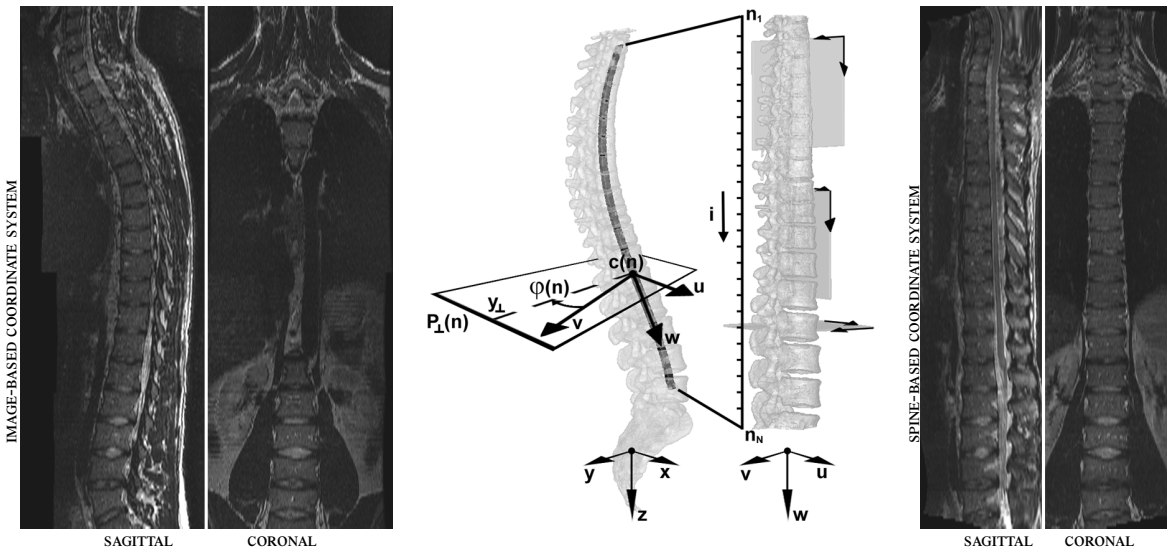

(a) (b) (c)

Figure 3.1. In the image-based coordinate system, the spine intersects sagittal and/or coronal cross-sections (a). The transformation from image-based to spine-based coordinate system is determined by the 3D spine curve $c(n)$ and axial vertebral rotation $\varphi(n)$ (c). In the spine-based coordinate system, the whole course of the spine can be observed in sagittal and coronal cross-sections (b).

of the basic anatomical properties of the spine. First, when observed in axial cross-sections, the vertebral bodies and intervertebral discs are nearly circular in shape and the vertebrae are symmetric over the lines that pass through the centres of vertebral bodies (or intervertebral discs) and vertebral spinous processes. These anatomical properties are used for initial estimation of the centres of vertebral bodies and axial vertebral rotation in each 2D axial cross-section of the original 3D MR spine volume. Second, assuming that the 3D spine curve and axial vertebral rotation are smooth functions, the initial estimates are refined in 3D by robust nonlinear regression.

3.3.1 Initial estimation of centres and rotations of vertebrae

In each axial cross-section $P_{ax}(z = z_j);\ j = 1, 2, \ldots, Z$ of the 3D image, an in-plane line of symmetry $y_j(x) \subset P_{ax}(z_j)$ that passes through the centre of vertebral body and spinous process is defined. The line $y_j(x)$, which splits the corresponding vertebral body into two halves, is obtained by maximizing the similarity function $sim(\cdot)$ between the two half-images (figure 3.2, p. 69):

$$\{\hat{\gamma}_j, \hat{\lambda}_j\} = \underset{\{\gamma_j, \lambda_j\}}{\arg\max}\ sim\begin{pmatrix} P_{ax}(z_j);\ y<y_j(x) \\ P_{ax}(z_j);\ y>y_j(x) \end{pmatrix}, \tag{3.2}$$

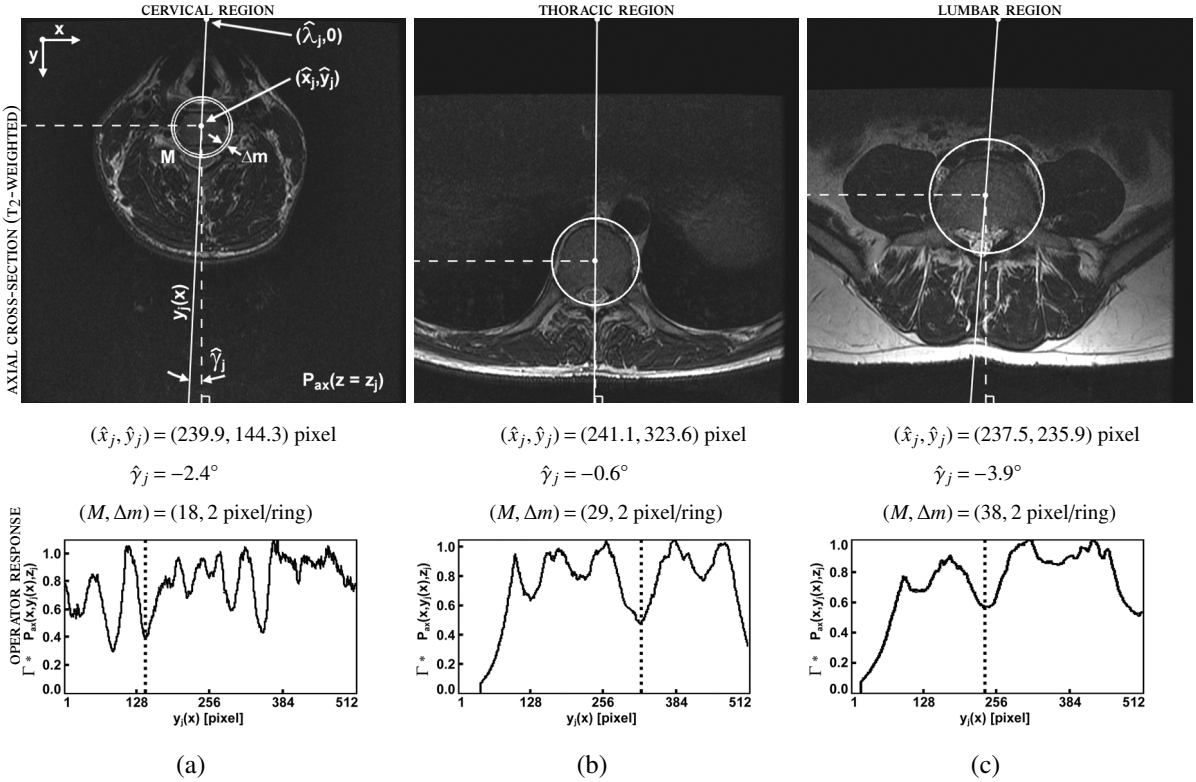

Figure 3.2. Detection of the centres of vertebral bodies in cross-sections of the cervical (a), thoracic (b) and lumbar (c) spinal region. The response of the operator Γ has a (local) minimum in the centre of the vertebral body.

where $tan(90° - \hat{\gamma}_j)$ is the slope and $\hat{\lambda}_j$ is the intersection of the optimal in-plane line of symmetry $y_j(x) = tan(90° - \hat{\gamma}_j)\,(x - \hat{\lambda}_j)$ with the axis x.

Next, the centre of the vertebral body is searched for along the obtained optimal in-plane line of symmetry $y_j(x)$ by an operator, sensitive to the circular structure of the vertebral body in the axial cross-section. For a circular structure, a certain intensity variation along any radial direction is always present, while the intensity variation in the direction perpendicular to the radial direction should be relatively small. To estimate these properties of a circular structure, the proposed operator is made of concentric rings. Intensity variation in the direction perpendicular to the radial direction is estimated by the sum of entropies of pixel intensities in individual concentric rings. On the other hand, to estimate the intensity variation along radial directions and to penalize the homogeneous regions, the entropy of the entire operator is also computed. The operator Γ, which consists of M concentric rings of radii r_m; $r_m < r_{m+1}$; $m = 0, 1, \ldots, M - 1$, is

defined as:

$$\Gamma = \frac{\sum_{m=0}^{M-1} w_m H_m}{H \sum_{m=0}^{M-1} w_m}; \quad w_m = e^{-\frac{1}{2}\left(\frac{m}{M} \cdot S\right)^2}, \tag{3.3}$$

where H_m; $H_m = -\sum_{q=1}^{Q} p_{q,m} \log p_{q,m}$ is the entropy defined by the probability distribution $p_{q,m}$ of intensities in the m^{th} ring, H; $H = -\sum_{q=1}^{Q} p_q \log p_q$ is the entropy defined by the probability distribution p_q of intensities within the entire operator, and Q is the number of bins used for probability estimation. The ring weights w_m are chosen to be within S standard deviations of the Gaussian distribution (equation 3.3, p. 70), so that the inner rings have a relatively larger impact to the operator response than the outer ones. The centre $(\hat{x}_j, y_j(\hat{x}_j)) = (\hat{x}_j, \hat{y}_j)$ of the vertebral body is found by minimizing the response of the entropy-based operator Γ along the line of symmetry $y_j(x)$ in plane $P_{ax}(z_j)$:

$$\hat{x}_j = \arg\min_x \left(P_{ax}(z_j) | \Gamma(x, y_j(x), z_j) \right). \tag{3.4}$$

Initial estimates of the centres of vertebral bodies $\{c\} = \{c_j = (\hat{x}_j, \hat{y}_j, z_j); j = 1, 2, \ldots, Z\}$ and axial vertebral rotations $\{\hat{\gamma}\} = \{\hat{\gamma}_j; j = 1, 2, \ldots, Z\}$ along the spine are obtained by applying the above procedure (equations 3.2, p. 68 and 3.4, p. 70) to all axial cross-sections $P_{ax}(z = z_j)$; $j = 1, 2, \ldots, Z$ of the original 3D spine image.

3.3.2 Robust refinement of centres and rotations of vertebrae

The initial estimates of the centres of vertebral bodies and axial vertebral rotations, obtained by procedure above, are refined in 3D by robust nonlinear regression. For this purpose, we introduce the continuous 3D spine curve $c(n) = (x(n), y(n), z(n))$ and axial vertebral rotation $\varphi(n)$ in the form of polynomial functions:

$$\{x, y, z, \varphi\}(n) = \sum_{k=0}^{K_{\{x,y,z,\varphi\}}} b_{\{x,y,z,\varphi\},k} \frac{n^k}{\tilde{b}_k}, \tag{3.5}$$

where K_x, K_y, K_z and K_φ are the degrees and $b_x = \{b_{x,k}\}$, $b_y = \{b_{y,k}\}$, $b_z = \{b_{z,k}\}$ and $b_\varphi = \{b_{\varphi,k}\}$ are the parameters of polynomials $x(n)$, $y(n)$, $z(n)$ and $\varphi(n)$, respectively. The parameters are normalized over the spine domain Ω_n:

$$\tilde{b}_k = \int_{\Omega_n} |n^k| \, \mathrm{d}n, \tag{3.6}$$

so that the modification of each parameter has the same impact on the absolute variation of the corresponding polynomial term. For the purpose of implementation, the continuous spine

domain Ω_n is discretized into N samples; $\{\Omega_n\} = \{n_i; i = 1, 2, \ldots, N\}$. The discretization yields a discrete 3D spine curve $c(n_i) = (x(n_i), y(n_i), z(n_i))$; $i = 1, 2, \ldots, N$ and a discrete axial vertebral rotation $\varphi(n_i)$; $i = 1, 2, \ldots, N$.

The parametric form of the 3D spine curve $c(n)$, determined by the 3D spine curve parameters $b_c = b_x \cup b_y \cup b_z$, is obtained by fitting a polynomial curve (equation 3.5, p. 70) to the set $\{c\}$ of the centres of vertebral bodies in the discrete spine domain $\{\Omega_n\}$. Nonlinear least trimmed squares (LTS) regression method (Rousseeuw and Leroy, 2003) is used to determine the optimal parameters $\hat{b}_c$:

$$\hat{b}_c = \arg\min_{b_c} \sum_{i=1}^{h_c} r^2_{c,[i]}(b_c), \tag{3.7}$$

where $r^2_{c,[i]}(b_c)$; $r^2_{c,[1]}(b_c) \leq r^2_{c,[2]}(b_c) \leq \ldots \leq r^2_{c,[N]}(b_c)$ represent the ordered squared residuals $r^2_{c,i}(b_c) = (c_i - c(n_i))^2$, and h_c is the trimming constant that satisfies the condition $0.5 < \frac{h_c}{N} \leq 1$ and determines the number of ordered residuals that are used in the computation.

The initial estimates of rotations $\{\hat{\gamma}\} = \{\hat{\gamma}_j; j = 1, 2, \ldots, Z\}$ of vertebral spinous processes, which are obtained from the lines of symmetry $\hat{y}_j(x)$, serve to initialize the computation of the axial vertebral rotations $\{\varphi\} = \{\varphi_j; j = 1, 2, \ldots, Z\}$. The rotations $\{\varphi\}$ are recomputed in planes $P_\perp(n)$ orthogonal to the 3D spine curve $c(n)$ (figure 3.1, p. 68). The optimal parameters $\hat{b}_\varphi$ that determine the parametric form of the axial vertebral rotation $\varphi(n)$ (equation 3.5, p. 70) are obtained by applying the nonlinear LTS regression method to the set $\{\varphi\}$ in the discrete spine domain $\{\Omega_n\}$:

$$\hat{b}_\varphi = \arg\min_{b_\varphi} \sum_{i=1}^{h_\varphi} r^2_{\varphi,[i]}(b_\varphi). \tag{3.8}$$

Similarly as for the 3D spine curve (equation 3.7, p. 71), the trimming constant h_φ; $0.5 < \frac{h_\varphi}{N} \leq 1$ determines the number of ordered squared residuals $r^2_{\varphi,[i]}(b_\varphi)$; $r^2_{\varphi,i}(b_\varphi) = (\varphi_i - \varphi(n_i))^2$ that are used in the computation.

3.3.3 Curved planar reformation

Curved surfaces are obtained from original MR images of the spine by following the computed 3D spine curve $c(n)$ and axial vertebral rotation $\varphi(n)$, which determine the transformation $\mathbb{T}$ from image-based to spine-based coordinate system (equation 3.1, p. 67). The curved transformation does not preserve distances. However, by applying the inverse transformation $\mathbb{T}^{-1}$, distances can be measured in the image-based coordinate system. By folding the obtained curved surfaces onto a plane, CPR images of the spine are generated. Similarly as the axial, sagittal and coronal cross-sections determine the position of the anatomy relative to imaging planes in the image-based coordinate system (x, y, z), cross-sections that determine the position

of the anatomy relative to the spine can be determined in the spine-based coordinate system (u, v, w) (figure 3.1, p. 68). A spine-based axial, sagittal and coronal cross-section is any plane which is parallel to the axes u and v, v and w, and u and w of the spine-based coordinate system, respectively.

3.4 Experiments and results

3.4.1 MR spine images

The proposed method was tested on 21 axial MR scans of the spine from 12 patients, acquired by a spine array coil. T_1-weighted (average repetition time $T_R = 550$ ms, average echo time $T_E = 15$ ms) and T_2-weighted (average repetition time $T_R = 4560$ ms, average echo time $T_E = 110$ ms) images of the lumbar and thoracic spinal regions from 9 patients were obtained by a 1.5T (tesla) MR scanner (General Electric Signa Excite). The matrix size was $X \times Y = 512 \times 512$ pixels, the average voxel size $S_x \times S_y = 0.398 \times 0.398$ mm^2 (field of view $FOV = 200 \times 200$ mm^2), the cross-section thickness $S_z = 3 \div 6$ mm, and the number of axial cross-sections $Z = 23 \div 31$. In addition, 3 whole-length T_2-weighted spine images were acquired ($S_z = 3$ mm, $Z = 208 \div 230$, one on a 1.5T and two on a 3T GE Signa Excite scanner) using the same imaging protocol in order to test the performance of the algorithm on the whole course of the spine. The whole-length spine images were acquired in three separate acquisitions and joined into one image by using the information in the header of the DICOM files. Landmarks, manually placed in 3D at the centres of vertebral bodies and corresponding tips of vertebral spinous processes in each original MR image (i.e. in the image-based coordinate system), served as ground truth data. Ground truth data was used to quantitatively evaluate the performance of the proposed automated CPR method.

3.4.2 Implementation details

User interaction, required by the automated CPR method, was limited to pinpointing the approximate centre of the vertebral body in only one axial cross-section of each MR spine image in either cervical, thoracic or lumbar region. The centre of the vertebral body served for initializing the search of the sets $\{c\}$ (equation 3.2, p. 68) and $\{\varphi\}$ (equation 3.4, p. 70), while the radius of the entropy-based operator Γ (equation 3.3, p. 70) was automatically adjusted from $M = 15$ rings in the cervical region, to $M = 20$ rings in the thoracic region, and to $M = 30$ rings in the lumbar region of the spine (the ring size was $\Delta m = 1 \frac{\text{mm}}{\text{ring}}$, the weights w_m were within $S = 2$ standard deviations of the Gaussian distribution, the probability distributions were computed using $Q = 16$ bins). Standard mutual information (Weisstein, 1999) was used as the similarity measure (function $sim(\cdot)$ in equation 3.2 (p. 68)) and the simplex method in multi-

dimensions (Press et al., 2002) was used for the optimization procedure (equations 3.2, p. 68 and 3.4, p. 70). The number of samples N in the discrete spine domain $\{\Omega_n\}$ was set to the number of axial cross-sections Z; $N = Z$. For describing the 3D spine curves and axial vertebral rotations (equation 3.5, p. 70), polynomials of degree $K_{\{x,y,\varphi\}} = 4$ were used in images of spine segments and polynomials of degree $K_{\{x,y,\varphi\}} = 6$ in whole-length spine images. The degree K_z of the polynomials $z(n)$ (equation 3.5, p. 70) was fixed to 1. The trimming constants of the nonlinear LTS regression method (Rousseeuw and Leroy, 2003) were set to $h_c = h_\varphi = \frac{2N}{3}$ (equations 3.7, p. 71 and 3.8, p. 71). The summary of parameter values used in the experiments is presented in table 3.1 (p. 73).

Table 3.1. Summary of parameter values used in the experiments.

Entropy-based operator Γ	
Number of rings	$M = 15 \div 20 \div 30$[a]
Ring size	$\Delta m = 1 \frac{\text{mm}}{\text{ring}}$
St. deviation of weights	$S = 2$
Number of bins	$Q = 16$
Spine domain Ω_n	
Number of samples	$N = Z$
3D spine curve $c(n)$	
Polynomial degree	$K_{\{x,y\}} = 4 \div 6$[b], $K_z = 1$
LTS trimming constant	$h_c = \frac{2N}{3}$
Axial vertebral rotation $\varphi(n)$	
Polynomial degree	$K_\varphi = 4 \div 6$[b]
LTS trimming constant	$h_\varphi = \frac{2N}{3}$

[a] cervical region ÷ thoracic region ÷ lumbar region
[b] spine segment ÷ whole-length spine

3.4.3 Results

The whole course of the spine can not be observed in the image-based coordinate system, as the spine intersects with sagittal and coronal cross-sections. This shortcoming is overcome by CPR images, which allow the inspection of the whole course of the spine in single spine-based cross-sections (figure 3.1, p. 68). By following the course of the computed 3D spine curve $c(n)$ and the course of the computed axial vertebral rotation $\varphi(n)$ in the spine domain Ω_n (equation 3.5,

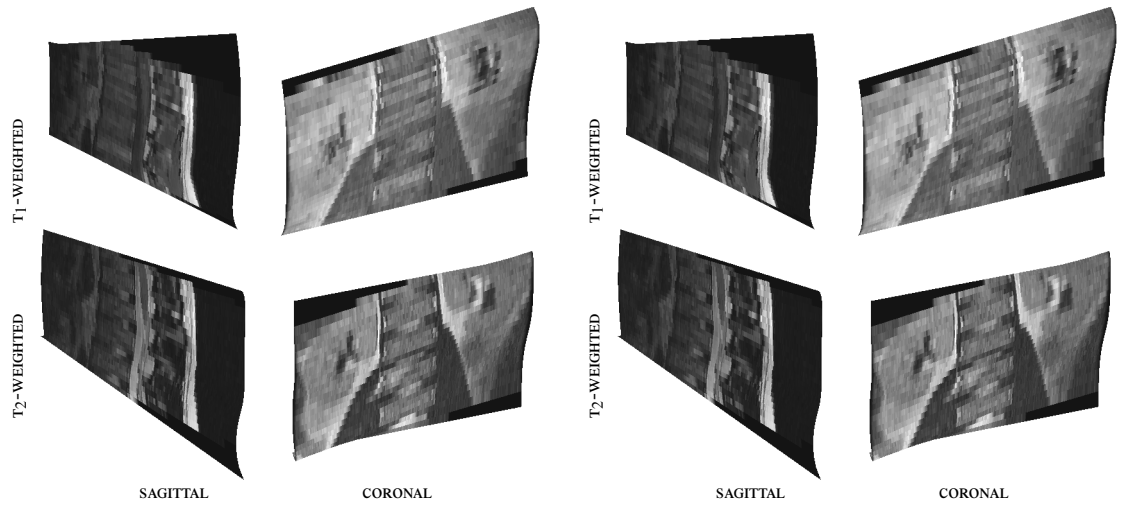

(a) (b)

Figure 3.3. CPR T_1-weighted images (top row) and T_2-weighted (bottom row) images of a spine segment, created by folding curved surfaces (a) onto a plane (b).

p. 70), and by folding the obtained curved surfaces onto a plane, CPR images were successfully generated from images of spine segments (figure 3.3, p. 74) and from whole-length spine images (figure 3.4, p. 77).

The courses of the sagittal spine curve $x(n)$ and coronal spine curve $y(n)$ are shown in figure 3.5 (p. 78). Since the images used in this study represented normal spine anatomy, the coronal spine curves show the natural coronal curvatures of the spine, while the sagittal spine curves reflect the relatively small natural sagittal curvatures. Such results were expected and also confirmed by the close match to the ground truth data. On the other hand, the courses of axial vertebral rotation $\varphi(n)$ (figure 3.5, p. 78) indicate that there may be no common course of axial vertebral rotation in normal spines but only a slight natural fluctuation that is specific for the observed spine anatomy.

Since axial vertebral rotation is computed in planes orthogonal to the 3D spine curve, the estimation of the axial rotation parameters depends on the previous estimation of the 3D spine curve parameters. This makes the procedure inconsistent with the Serret-Frenet reference frame in differential geometry (Weisstein, 1999), i.e. the axis v of the spine-based coordinate system does not equal the Frenet normal vector, but is oriented in the direction of vertebral spinous processes. However, such an approach assures that besides geometrical also the anatomical properties of the spine are incorporated in the resulting CPR images. The curvature, which is defined in differential geometry as an intrinsic property of the curve, can nevertheless be observed. For a parameterized curve $c(n)$ it is defined in 3D as (the sign $\times$ denotes vector cross product):

Table 3.2. Quantitative comparison between the computed 3D spine curve and axial vertebral rotation, and ground truth data. The results are shown separately for T_1- and T_2-weighted images. Overall mean values and the corresponding standard deviations are shown in the bottom rows.

	Spine segments									Whole spines				
Images	1	2	3	4	5	6	7	8	9	10	11[a]	12[a]	mean	std
Mean 3D spine curve error $\Delta c(n)$ [mm]														
T_1-weighted	2.7	4.1	1.0	1.5	4.3	3.7	2.7	2.8	1.9	-	-	-	2.8	1.1
T_2-weighted	3.2	3.9	1.2	1.1	1.7	1.7	1.4	1.5	2.0	2.6	3.6	3.7	2.3	1.0
Mean axial vertebral rotation error $\Delta\varphi(n)$ [deg]														
T_1-weighted	3.1	1.3	1.5	0.9	2.6	0.8	0.9	2.2	1.6	-	-	-	1.7	0.8
T_2-weighted	3.9	2.5	0.9	1.3	2.6	1.7	0.8	2.0	0.9	1.4	2.1	1.2	1.8	0.9
3D spine curve error $\Delta c(n)_\Sigma$ [mm]													2.5	1.1
Axial vertebral rotation error $\Delta\varphi(n)_\Sigma$ [deg]													1.7	0.9

[a] images acquired on a 3T MR scanner

$$\kappa(n) = \frac{\left| \frac{\mathrm{d}c(n)}{\mathrm{d}n} \times \frac{\mathrm{d}^2 c(n)}{\mathrm{d}n^2} \right|}{\left| \frac{\mathrm{d}c(n)}{\mathrm{d}n} \right|^3}. \tag{3.9}$$

The spinal curvature $\kappa(n)$ at an arbitrary position n on the spine has a magnitude equal to the reciprocal value of the radius of an osculating circle to the 3D spine curve at that position. As a result, the 3D spine curve can be presented by a one-dimensional curve that captures the characteristics of the spine in 3D. The computed courses of the spinal curvature for the whole-length spine images are shown in figure 3.5 (p. 78).

Ground truth data was used to quantitatively evaluate the performance of the proposed automated CPR method. The 3D spine curve error was estimated as the Euclidean distance between the computed 3D spine curve and the ground truth landmarks. The axial vertebral rotation error was estimated as the difference between the computed values and the rotations from ground truth data, obtained as the angles between the lines through the centres of vertebral bodies and the corresponding tips of vertebral spinous processes, and the sagittal reference plane. The results are presented in table 3.2 (p. 75) and indicate that the method performed well both for T_1- and T_2-weighted images. For all images used in this study, the mean 3D spine curve error was $\Delta c(n)_\Sigma = 2.5$ mm (standard deviation $\sigma = 1.1$ mm) and the mean axial vertebral rotation error was $\Delta\varphi(n)_\Sigma = 1.7$ degrees (standard deviation $\sigma = 0.9$ degrees).

3.5 Discussion and conclusion

The proposed automated method for generating CPR images from MR images of the spine allows the visualization and inspection of images in the coordinate system of the spine. Most of the existing reformation techniques for 3D spine images require manual determination of the spinal curvature and/or vertebral rotations and are usually determined in 2D. With minimal user interaction (i.e. by identifying the centre of only one vertebral body), the proposed method automatically extracts the 3D spine curve and axial vertebral rotation, which determine the transformation from image-based to spine-based coordinate system (equation 3.1, p. 67). The measured quantities are described continuously along the whole spinal length in a low-parametric form by polynomials of degree 4÷6. The proposed method was qualitatively and quantitatively evaluated on 18 MR images of spine segments (9 T_1- and 9 T_2-weighted) and 3 T_2-weighted whole-length MR images of normal spines. The computed 3D spine curves and axial vertebral rotations are consistent with the manually defined ground truth data, and comparable to the results obtained on CT images (Vrtovec et al., 2005).

Quantitative assessment of spinal curvature and axial vertebral rotation is important for surgical planning, analysis of surgical results, and monitoring of the progression of spinal deformities (Aronsson et al., 1996, Birchall et al., 1997). Describing spinal curvatures with mathemat-

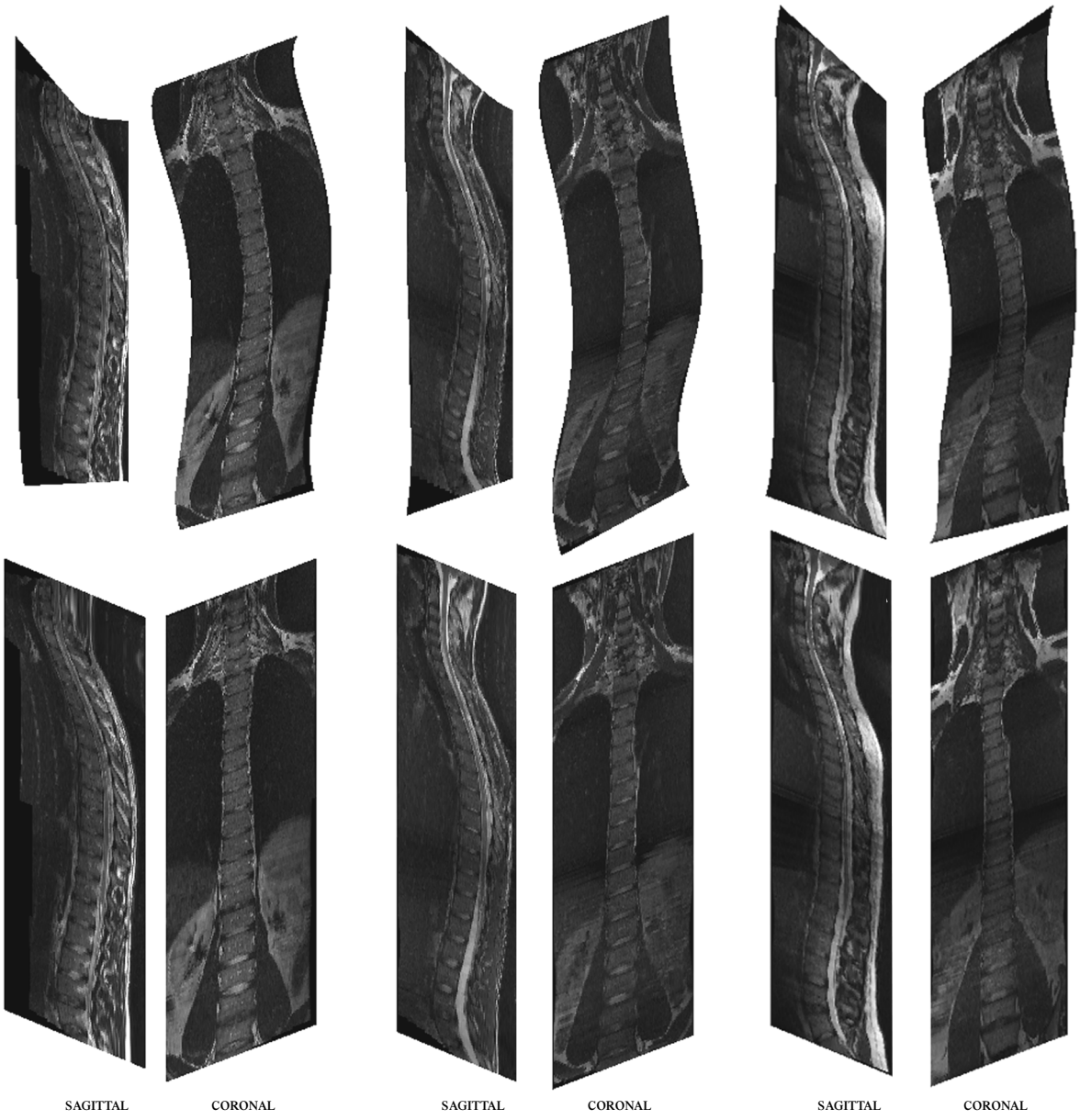

Figure 3.4. The sagittal and coronal CPR images of the three whole-length images of the spine ((a), (b) and (c), respectively), obtained by folding the sagittal and coronal curved surfaces (top row) onto a plane (bottom row).

ical functions is not a new concept, and functions such as sinusoids (Drerup and Hierholzer, 1996), splines (Kaminsky et al., 2004, Verdonck et al., 1998), and polynomials (Peng et al., 2005, Vrtovec et al., 2005) were used for that purpose. For measuring the axial vertebral rotation, CT is the most accurate imaging modality (Krismer et al., 1996, Kuklo et al., 2005b). Different techniques for CT were developed (Aaro and Dahlborn, 1981, Göçen et al., 1999, Ho et al., 1993) and later improved by taking into account sagittal and coronal inclinations of vertebrae (Hecquet et al., 1998, Krismer et al., 1996, Skalli et al., 1995). Similar techniques were also applied to MR images of the spine. Birchall et al. (1997) computed the axial vertebral rotation from the position of landmarks that were manually placed in each oblique axial cross-section, defined through superior and inferior end-plates of each vertebra in the acquired axial MR images. In order to assess inter-vertebral rotations, Rogers et al. (2002) registered pairs of axial cross-sections that captured most of the transverse, spinous and superior articular processes of each vertebra. However, the initial centre of rotation was manually defined at the dorsal edge of the vertebral body on each cross-section.

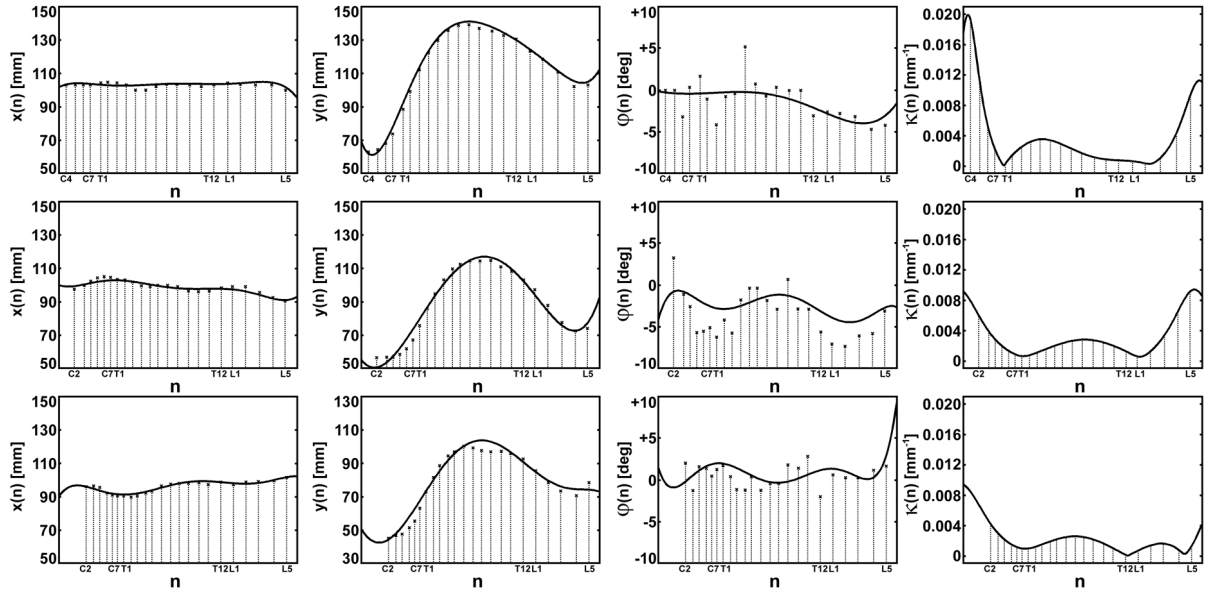

Figure 3.5. Course of the sagittal spine curve $x(n)$ (a), coronal spine curve $y(n)$ (b), axial vertebral rotation $\varphi(n)$ (c), and spinal curvature $\kappa(n)$ (d) of the three (top to bottom row, respectively) whole-length images of the spine. The vertical lines represent the position of the ground truth landmarks.

The spinal curvature $\kappa(n)$, which is relative to the osculating circle to the 3D spine curve, and the axial vertebral rotation $\varphi(n)$, which is the rotation of vertebrae around the 3D spine curve, are inherent properties of the spine (i.e. spine-specific) and therefore not affected by rigid body

transformations. The generated CPR images are independent of the position of the patient in the MR scanner and of the orientation of the imaging planes. Moreover, healthy anatomy is represented in the same coordinate system as abnormal anatomy, which may allow a more objective evaluation and diagnosis of the abnormalities. Displaying the whole course of the spinal column within a single 2D image may be of significant importance in case of increased coronal (i.e. scoliosis) or sagittal (i.e. kyphosis, lordosis) spinal curvature. The vertebral rotation is determined by taking into consideration sagittal and coronal inclinations of vertebrae, which are known to significantly influence the measurements. However, the vertebral rotation can not be always uniquely defined, as it is affected by the natural bending of spinous and transverse vertebral processes. The same observation can be made for vertebral rotations, obtained by manually defined landmarks. The major limitation of the presented method is that the determination of axial vertebral rotation depends on prior estimation of the 3D spine curve, as the rotation is measured in planes that are centred in the computed spine curve samples.

Among the most significant parameters that may assist an orthopaedic surgeon in evaluating spinal deformities, is the length of the spinal axis, the Cobb angle, the locations of the centres of vertebral bodies, and vertebral rotation angles, i.e. axial rotation, sagittal and coronal inclination (Stokes, 1994). Besides direct automated localization of the centres of vertebral bodies, i.e. the 3D spine curve, and measurement of axial vertebral rotation (equation 3.5, p. 70), the proposed method implicitly allows automated measurement of the remaining parameters. The length of the spinal axis can be computed from the arc length, which is a geometrical property of the polynomial function that represents the 3D spine curve. In case of a scoliotic spinal deformity, the location of the end vertebrae (i.e. the vertebrae with maximal slant towards the concavity of the curve above and below its apex) could be extracted from the course of curvature (equation 3.9, p. 76) and axial vertebral rotation, allowing the measurement of the Cobb angle (Cassar-Pullicino and Eisenstein, 2002). The sagittal and coronal vertebral inclinations can be associated with the inclination of the planes, orthogonal to the 3D spine curve. Moreover, the identification of the superior and inferior end-plate on individual vertebral bodies would allow the determination of inter-segmental (i.e. between neighboring vertebrae) and intra-segmental (i.e. within individual vertebrae) rotation angles (Birchall et al., 1997). These are of a significant importance, since only the inter-segmental rotations can be corrected by surgical intervention (Cassar-Pullicino and Eisenstein, 2002). Automated measurement of the significant spine-specific parameters may therefore provide a complete quantitative representation of the spine in 3D, which may improve preoperative planning and postoperative evaluation.

The main purpose of the proposed automated CPR method is, however, to reduce the structural complexity in favor of an improved feature perception of the spine, and to provide clinically relevant quantitative analysis of the 3D spine anatomy. However, the knowledge on the location and orientation of the spine in 3D can be exploited by other image analysis techniques and applied in a clinical environment, e.g. for the identification and measurement of dimensions of the spinal canal and the spinal cord. The notion of the spine-based coordinate system is

modality-independent and can therefore be used for data fusion, i.e. merging of CT and MR images of the same patient. We will focus our future research on some of these topics.

Acknowledgments

This work has been supported by the Slovenian Ministry of Higher Education, Science and Technology under grant P2-0232, and by a six-month fellowship from the Commonwealth Scientific and Industrial Research Organisation (CSIRO), Australia.

"My dear Watson, try a little analysis yourself,"
said he, with a touch of impatience.
"You know my methods. Apply them,
and it will be instructive to compare results."

SHERLOCK HOLMES
(The Sign of the Four, 1890)

CHAPTER 4

Quantitative analysis of spinal curvature in 3D: Application to CT images of normal spine

TOMAŽ VRTOVEC, BOŠTJAN LIKAR AND FRANJO PERNUŠ

Submitted for journal publication.

Abstract

Study Design. Three-dimensional (3D) descriptors of spinal curvature were measured on images of normal spine to observe the characteristics of spine anatomy in 3D. **Objective.** To present a framework for quantitative analysis of spinal curvature in 3D. **Summary of Background Data.** Existing methods for measuring spinal curvature proved to be too complex for clinical environment and provide only two-dimensional (2D) description of spinal deformity, while 3D descriptors may yield a more complete assessment of 3D spinal curvature. **Methods.**The 3D descriptors of geometric curvature (GC) and curvature angle (CA) were measured in 3D on 30 computed tomography (CT) images of normal spine. The measurements were determined from 3D vertebral body lines, obtained by two different methods. The first method is based on the least squares techniques that approximates the manually identified vertebra centroids. The second method searches for vertebra centroids in an automated optimization scheme, based on computer-assisted image analysis. **Results.** Polynomial functions of the fourth degree were used for describing normal spinal curvature in 3D. The mean distance to vertebra centroids was 1.1 mm (± 0.6mm) for the first and 2.1 mm (± 1.4mm) for the second method. The distributions of GC and CA show that the maximal thoracic kyphosis (TK), thoracolumbar junction (TJ) and maximal lumbar lordosis (LL) on average occur at T3/T4, T12/L1 and L4/L5, respectively. **Conclusions.** The main advantage of GC and CA is that the measurements are independent of the orientation and size of the spine, thus allowing objective intra- and inter-subject comparisons. Positions of maximal TK, TJ and maximal LL can be easily identified by observing the distributions of GC and CA. The proposed framework may therefore improve the understanding of spine anatomy and aid in clinical quantitative evaluation of spinal deformities.

4.1 Introduction

Quantitative analysis of the spinal curvature is important for understanding of the nature of normal and pathological spine anatomy, monitoring of the progression of spinal deformities, surgical planning, and analysis of surgical results (Asazuma et al., 2004, Duke et al., 2005, Mac-Thiong et al., 2000). The Cobb technique (Cobb, 1948) is the most established method for quantifying spinal curvature in coronal plane in case of scoliotic deformities (Adam et al., 2005, Cheung et al., 2002, Chockalingam et al., 2002, Morrissy et al., 1990, Shea et al., 1998, Stokes and Aronsson, 2006), as well as in sagittal plane to measure lordosis and kyphosis (Bernhardt and Bridwell, 1989, Goh et al., 2000a, Harrison et al., 2000, Korovessis et al., 1998, Pinel-Giroux et al., 2006). Several limitations of this technique were reported (Harrison et al., 2000, Polly et al., 1996, Stokes et al., 1987) and stimulated the development of new methods for measuring the degree of spinal deformity (Goh et al., 2000a, Harrison et al., 2000, 2002, Pinel-Giroux et al., 2006). Besides that most of the proposed methods proved to be too complex for routine use in clinical environment, they provide only two-dimensional (2D) geometric

descriptors of spinal deformity, although it was already emphasized that three-dimensional (3D) descriptors may yield a more complete assessment of 3D spinal curvatures (Duong et al., 2006, Stokes et al., 1987, Villemure et al., 2001).

In this paper we present a framework for quantitative analysis of the spinal curvature in 3D. The observed 3D descriptors of spinal curvature are the geometric curvature (GC) and curvature angle (CA), both of which are independent of the orientation of spine anatomy, moreover, CA is also independent of the size of spine anatomy. The evaluation of the descriptors is straightforward for a given 3D vertebral body line in a parametric form, which can be easily obtained by identifying vertebra centroids. We also present an approach to the determination of a 3D vertebral body line that is based on automated image analysis techniques and can replace the identification of vertebra centroids when applied to computed tomography (CT) images of the spine. We show results of applying the proposed framework to images of normal spine. Knowledge of the normal spine may improve the understanding of spinal deformities (Bernhardt and Bridwell, 1989, Berthonnaud et al., 2005a, Harrison et al., 2002, Korovessis et al., 1998, Kouwenhoven et al., 2006, Roussouly et al., 2005), while computer-assisted analysis of spine images may allow a faster, more objective and more reliable evaluation of spine anatomy. The terms in this paper follow the convention on 3D terminology of spinal deformity, proposed by the Scoliosis Research Society (Stokes, 1994).

4.2 Materials and Methods

4.2.1 Subjects

CT spine images (Tomoscan AVE and MX 8000, Philips Medical Systems, The Netherlands) of 30 adult patients (gender and exact age was not considered relevant) that were treated for reasons other than spinal pathology were used in this study. The image voxel size was $0.6 \times 0.6 \times 4$ mm. Reference anatomical landmarks, required for the proposed evaluation of the spinal curvature, were identified by an expert, well experienced in manipulation and shape analysis of 3D spine images. By using dedicated computer software that allowed simultaneous navigation through axial, sagittal and coronal image planes, reference vertebra centroids from T1 to L5 were identified in 3D on each image and their spatial coordinates were recorded (figure 4.1, p. 84).

4.2.2 Three-dimensional (3D) vertebral body line

The 3D vertebral body line is a continuous curve that passes through vertebra centroids. For the given vertebra centroids, the 3D vertebral body line can be determined by fitting a curve to

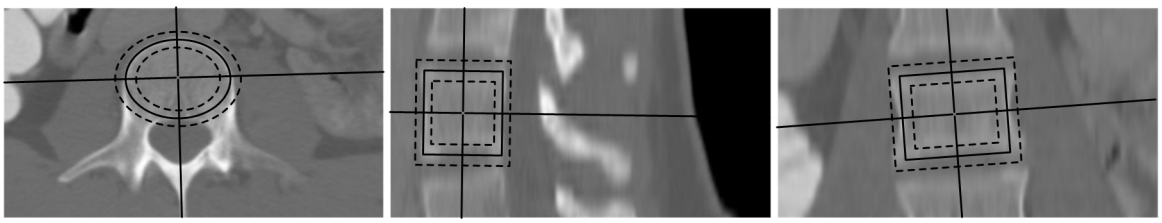

Figure 4.1. Dedicated software for identification of vertebra centroids.

the spatial coordinates of vertebra centroids using the least squares method (Bjõrck, 1996). In order to ensure the continuity and preserve the generality of the description, we represent the 3D vertebral body line with a parametric polynomial function in 3D (equations 4.1, p. 93 and 4.2, p. 93). The least squares coefficients of the parametric 3D vertebral body line are obtained by minimizing the sum of square distances between the 3D vertebral body line and vertebra centroids. The optimal values are computed by relatively simple matrix operations, which can be performed by dedicated computer software such as Matlab (Mathworks Inc., USA). We will refer to this method as the least squares fitting (LSF) method.

Alternative approaches to the determination of the 3D vertebral body line can be used when vertebra centroids are not available. In this study we present an automated method for analyzing CT spine images that is derived from the method used for curved planar reformation (CPR) of whole-length spine images (Vrtovec et al., 2005). The method exploits the anatomical property of the spine that vertebral bodies represent the largest bony regions in a spine image and that regions with bone structures can be coarsely determined by intensity thresholding of the CT image. If the distance between an arbitrary point in the image and the nearest bone edge is positive when the point is located inside and negative when the point is located outside a bony region, then the distance is expected to be the largest at vertebra centroids. The 3D vertebral line is initialized as a parametric polynomial function of the first degree in 3D, i.e. as a straight line, where vertebra centroids at T1 and L5 can serve as initialization points. The polynomial degree is gradually increased in an optimization scheme that searches for those polynomial coefficients that maximize the sum of distances between points located on the 3D vertebral body line and the edges of the regions with bone structures. For more details on the method, which is developed as a computer program in C++ language (C++ Builder, Borland Inc., USA), the reader is referred to reference (Vrtovec et al., 2005). We will refer to this method as the edge distance optimization (EDO) method.

Irrespective of the applied method for 3D vertebral body line extraction, the 3D vertebral body line is represented by a parametric polynomial function. It is the geometric property of a polynomial function that the number of its flexion points is equal to the polynomial degree, decreased by one. As three distinctive flexion points exist in normal spinal curvature, i.e. the thoracolumbar junction (TJ), the maximal thoracic kyphosis (TK) and the maximal lumbar lordosis (LL),

polynomial functions of the fourth degree were chosen to describe normal spine anatomy in sagittal and coronal image planes. Along axial image planes, polynomial functions of the first degree (i.e. straight lines) were used to represent the natural cranial-caudal length of the spine.

4.2.3 Geometric curvature and curvature angle

The geometric properties of a spine can be described by 3D descriptors that capture the 3D spinal curvature in coronal and sagittal plane as functions of the position on the spine. As a result, the strength of the spinal curvature is given quantitatively for a specific position on the spine. GC and CA are the 3D descriptors with such properties, moreover, their evaluation is straightforward for a given parametric 3D vertebral body line. GC is defined for an arbitrary position on the spine as the reciprocal to the radius of the osculating circle at that position, and represents the amount by which the 3D vertebral body line deviates from being flat (equation 4.3, p. 93). Hence, the smaller is the radius of the osculating circle, the higher is GC. Since GC is an inherent property of the 3D vertebral body line, it is independent of the spatial orientation of spine anatomy and is therefore not affected by the position of the patient in the scanner nor by the orientation of image acquisition planes.

The descriptor CA is defined as the angular magnitude of GC on an arbitrary spine section. CA can be considered as the angular representation of GC, normalized to the specified spine section (equation 4.4, p. 93). In case that the specified section is relatively small, the arc of the osculating circle that is used for computation of CA can be approximated with the length of the 3D vertebral body line on that section (equation 4.5, p. 93). For example, vertebra centroids of two adjacent vertebrae may represent a section where such an approximation can be applied (figure 4.2, p. 86). Therefore, besides inheriting all the properties of GC, normalization to a specified section makes CA independent of the size of the spine.

4.3 Results

In order to obtain the GC and CA values, the 3D vertebral body line in the form of a parametric polynomial function of the fourth degree has to be extracted first. We have applied two methods, the LSF and EDO method, to the studied 30 spine images. The small distances between the obtained 3D vertebral body lines and manually identified vertebra centroids indicate that the selection of polynomial function of the fourth degree was appropriate (figure 4.3, p. 88). On average, the EDO method is only slightly less accurate and slightly more variable than the LSF method which requires known vertebra centroids (Table 1).

We first present a detailed analysis for two illustrative cases, chosen among the images used in this study (namely images 4 and 25). Clinically relevant features that are located at flexion

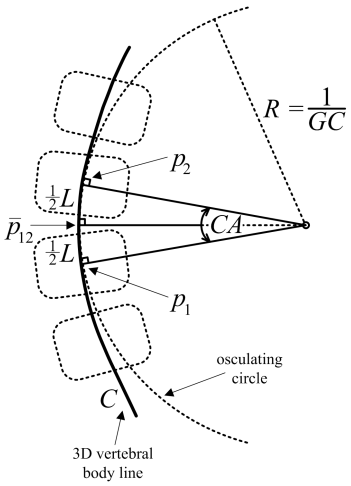

Figure 4.2. Geometric representation of geometric curvature (GC) and curvature angle (CA).

points can be extracted from the course of GC. The flexion point where the course of GC reaches its minimal value represents the position where the spine is most straight in 3D, i.e. the position of TJ. For the first case (figure 4.4c, p. 89), the TJ occurs approximately at T11 (Table 1). Since the minimal value of GC is not equal to zero, the spine at TJ is not completely straight. It can be observed in figures 4.4a (p. 89) and 4.4b (p. 89) that although the 3D vertebral body line is straight at TJ in the sagittal, it is curved in the coronal image plane. The true nature of the observed spine would therefore be overlooked if observed in sagittal image plane only, i.e. in 2D. Similarly, the TJ can be identified and evaluated for the second illustrative case (figure 4.5c, p. 90), where it occurs approximately at T12 (table 4.1, p. 87). Since GC at that point is almost equal to zero, the TJ is almost completely straight in 3D, what can be also observed from the obtained 3D vertebral body lines (figures 4.5a, p. 90 and 4.5b, p. 90). The flexion point where the course of GC reaches the maximal value towards the cranial and caudal direction represents the position of maximal TK and maximal LL, respectively. For the two illustrative cases, the maximal TK occurs approximately at T3 in the first and approximately at T5/T6 in the second case, while the maximal LL occurs at L5 in both cases (Table 1).

The GC descriptor can be evaluated continuously along the whole spine, on the other hand, the CA descriptor can be evaluated only on specified spine sections (figure 4.4c, str. 89 in 4.5c, str. 90). The exact positions of TJ, maximal TK and maximal LL can therefore not be determined using CA. Moreover, CA directly depends on GC (equation 4.4, p. 93) and can be therefore viewed upon as an alternative descriptor to GC. For these reasons, CA is less appropriate for the analysis of spinal curvature in a single image. On the other hand, CA is more suitable for evaluation of spinal curvature along a series of images where spine may differ in size, as two spines with equal spinal curvatures but different sizes have different GC but equal CA values. We evaluated the distribution of CA along the 30 images of normal spines, which

Table 4.1. Distance *d* to the 3D vertebral body line (VL) and the geometric curvature (GC) and curvature angle (CA) at the thoracic kyphosis (TK), thoracolumbar junction (TJ) and lumbar lordosis (LL), obtained by applying the least squares fitting (LSF) and edge distance optimization (EDO) method to illustrative cases 1 and 2, and to all the 30 images used in this study.

		LSF method	**EDO method**
VL	Mean *d* (± std) [1]	1.3 mm (± 0.7 mm)	2.4 mm (± 1.7 mm)
	Mean *d* (± std) [2]	1.5 mm (± 0.9 mm)	3.5 mm (± 1.2 mm)
	Mean *d* (± std) [all]	1.1 mm (± 0.6 mm)	2.1 mm (± 1.4 mm)
TJ	Minimal *GC* (*R*) [1]	0.6 m^{-1} (1.67 m) [~T11]	0.6 m^{-1} (1.67 m) [~T11]
	Minimal *GC* (*R*) [2]	0.03 m^{-1} (33.3 m) [~T12]	0.14 m^{-1} (7.14 m) [~T12]
	Mean *CA* (± std) [all]	1.2° (± 1.0°) [T12/L1]	1.0° (± 0.8°) [T12/L1]
TK	Maximal *GC* (*R*) [1]	2.9 m^{-1} (0.35 m) [~T3]	3.4 m^{-1} (0.29 m) [~T1]
	Maximal *GC* (*R*) [2]	5.6 m^{-1} (0.18 m) [~T5/T6]	5.1 m^{-1} (0.19 m) [~T5/T6]
	Mean *CA* (± std) [all]	3.4° (± 1.3°) [T3/T4]	3.5° (± 1.2°) [T3/T4]
LL	Maximal *GC* (*R*) [1]	5.7 m^{-1} (0.17 m) [~L5]	4.6 m^{-1} (0.22 m) [~L5]
	Maximal *GC* (*R*) [2]	4.3 m^{-1} (0.23 m) [~L5]	5.6 m^{-1} (0.18 m) [~L5]
	Mean *CA* (± std) [all]	6.5° (± 4.4°) [L4/L5]	5.0° (± 3.4°) [L4/L5]

was obtained by grouping CA values on spine sections from T1/T2 to L4/L5 (figure 4.6, p. 91). The CA is on average the lowest at section T12/L1, which means that generally, TJ will occur at this section. The maximal TK occurs on average at section T3/T4 and the maximal LL at section L4/L5 (Table 1). A number of other features characteristic for the normal spine can also be observed. The course of normal TK is represented by a gradual increase of CA in cranial direction from section T12/L1 to T3/T4, followed by a slight decrease towards section T1/T2, while the course of normal LL is represented by a gradual increase of CA in caudal direction from section T12/L1 to L4/L5. Furthermore, the obtained average CA values along the spine (figure 4.6, p. 91) are comparable to the normal sagittal angulations measured in 2D radiographic images acquired in standing position (Bernhardt and Bridwell, 1989).

4.4 Discussion

The purpose of this study is to present a framework for quantitative analysis of spinal curvature in 3D. Spinal deformities occur in axial, sagittal and coronal image planes, or in a combination

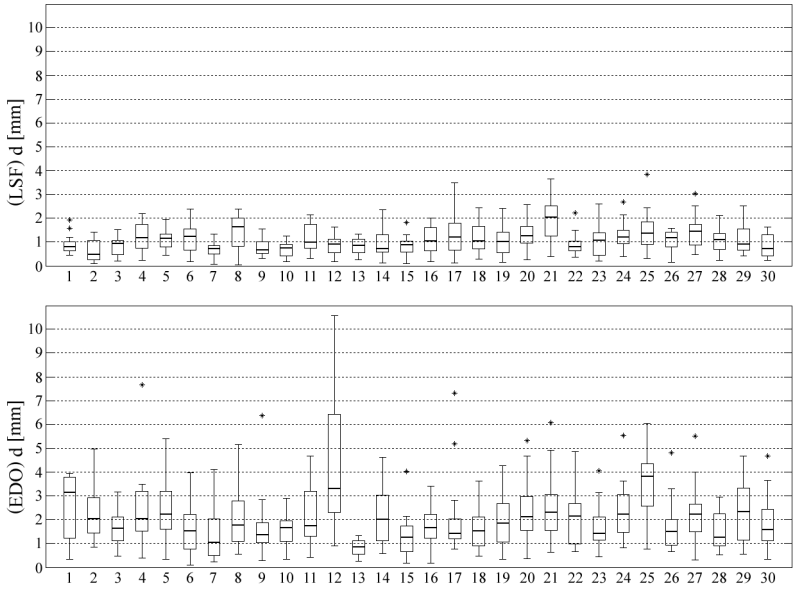

Figure 4.3. Distribution of distances between the 3D vertebral body line, obtained by the least squares fitting (LSF, top) and edge distance optimization (EDO, bottom) method, and vertebra centroids for each of the 30 spine images. For each image, the results are presented as a box-whiskers diagram, which shows the median, first and third quartile, minimal and maximal distance and outliers (values that are more than 1.5 times the interquartile range away from the first or third quartile).

of any of these planes. In order to study the properties of such complex 3D structures, descriptors that capture the characteristics of the spine in 3D should be applied. Although the Cobb angle (Cobb, 1948) is the established method for quantifying spinal deformities, its measurement depends on various factors. Among the most significant are the correct identification of the end vertebrae of the spinal curvature and the determination of vertebral end-plate inclination (Chockalingam et al., 2002), both of which may be affected by the lower visibility (separability) of anatomical structures in the thoracic region and by the variable shape of vertebral end-plates (Polly et al., 1996). Moreover, since the measurement is based solely on the inclination of vertebral end-plates, the method is unable to describe global spine geometry (Harrison et al., 2000, Pinel-Giroux et al., 2006, Stokes et al., 1987). The described limitations induce a high variability in the measurement of the Cobb angle, which stimulated the development of new techniques for evaluation of spinal curvature. Descriptors such as posterior tangent lines (Harrison et al., 2000), best-fit ellipses (Harrison et al., 2002), mean radius of curvature (Goh et al., 2000a), geometric torsion (Poncet et al., 2001) or tangent circles (Pinel-Giroux et al., 2006) are either associated with a large number of clinically unintuitive parameters or require a relatively high degree of user interaction (e.g. precise outlining or drawing tangent lines to vertebral bodies). As complicated models do not help surgeons and clinicians in understanding the spinal deformity, such techniques are too complex for routine use in clinical environment. Moreover, all techniques focus on spinal curvature separately in either coronal or sagittal image plane, i.e. in

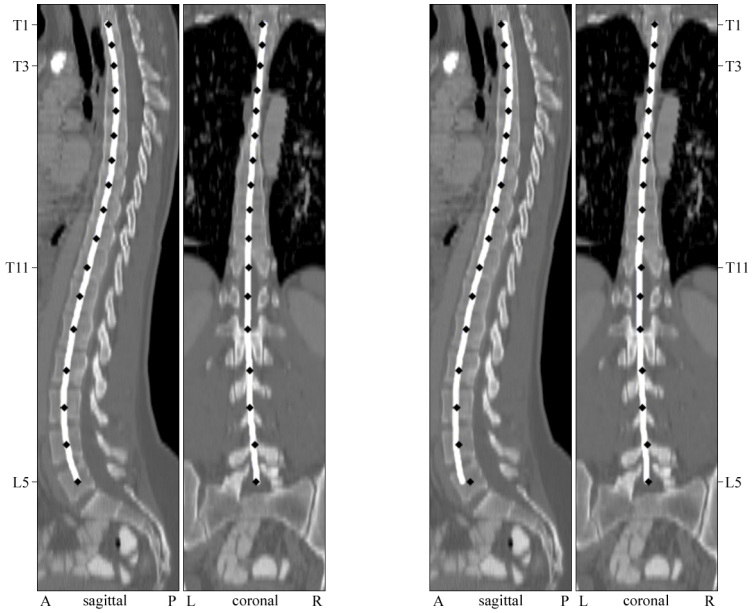

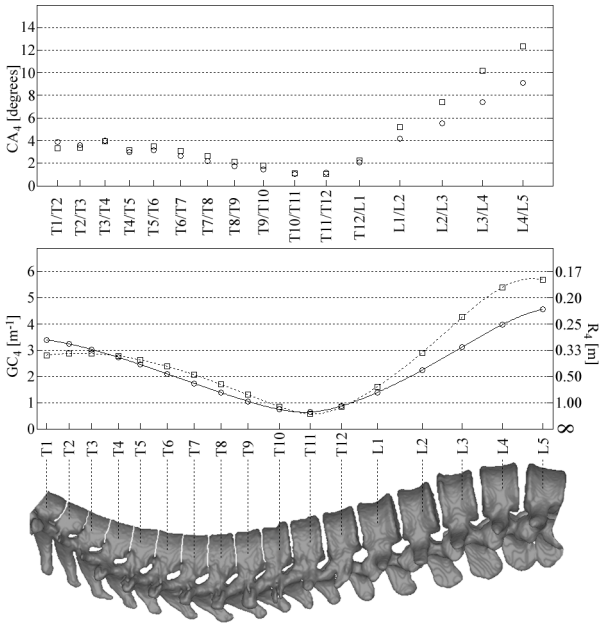

Figure 4.4. Case 1. (a) The 3D vertebral body line (white line), obtained by the least squares fitting (LSF) method and (b) by the edge distance optimization (EDO) method. Black diamonds represent the vertebra centroids. (c) Geometric curvature (GC) and curvature angle (CA), evaluated along the spine by applying the LSF (squares, dotted lines) and EDO (circles, solid lines) method.

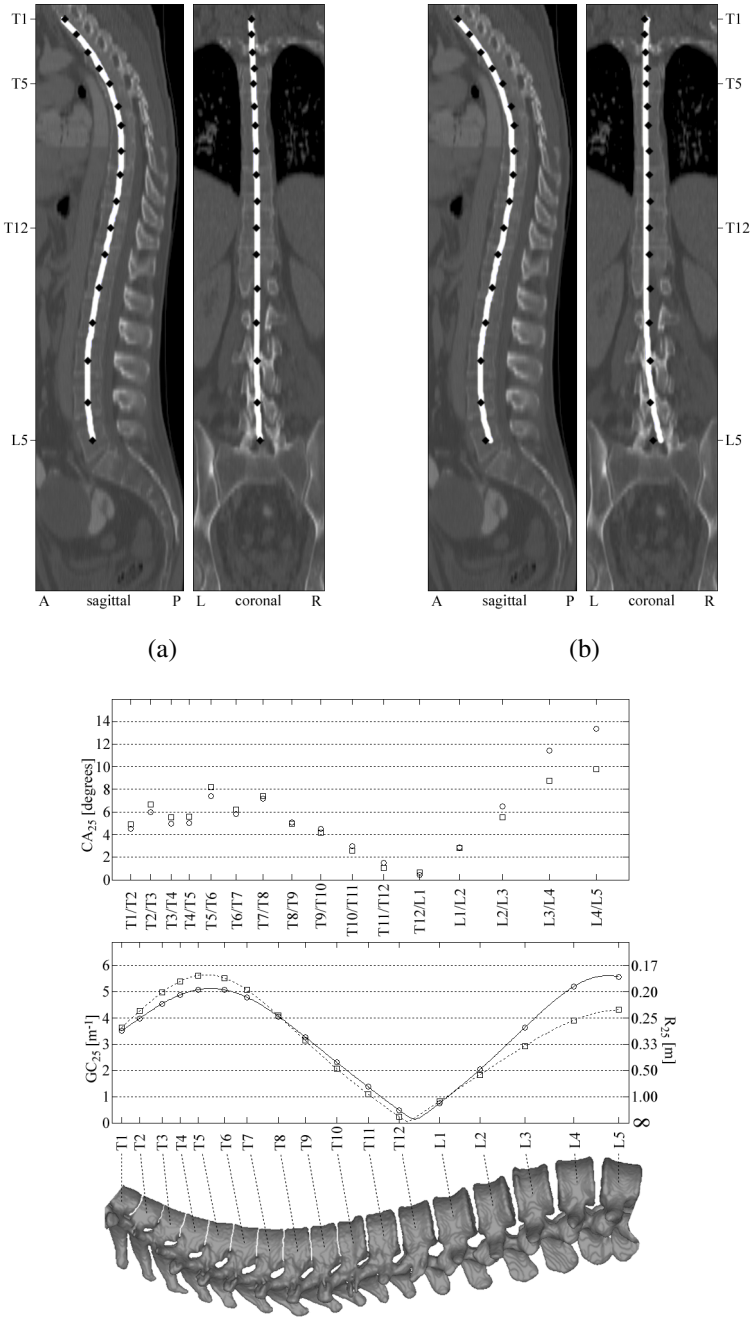

Figure 4.5. Case 2. (a) The 3D vertebral body line (white line), obtained by the least squares fitting (LSF) method and (b) by the edge distance optimization (EDO) method. Black diamonds represent the vertebra centroids. (c) Geometric curvature (GC) and curvature angle (CA), evaluated along the spine by applying the LSF (squares, dotted lines) and EDO (circles, solid lines) method.

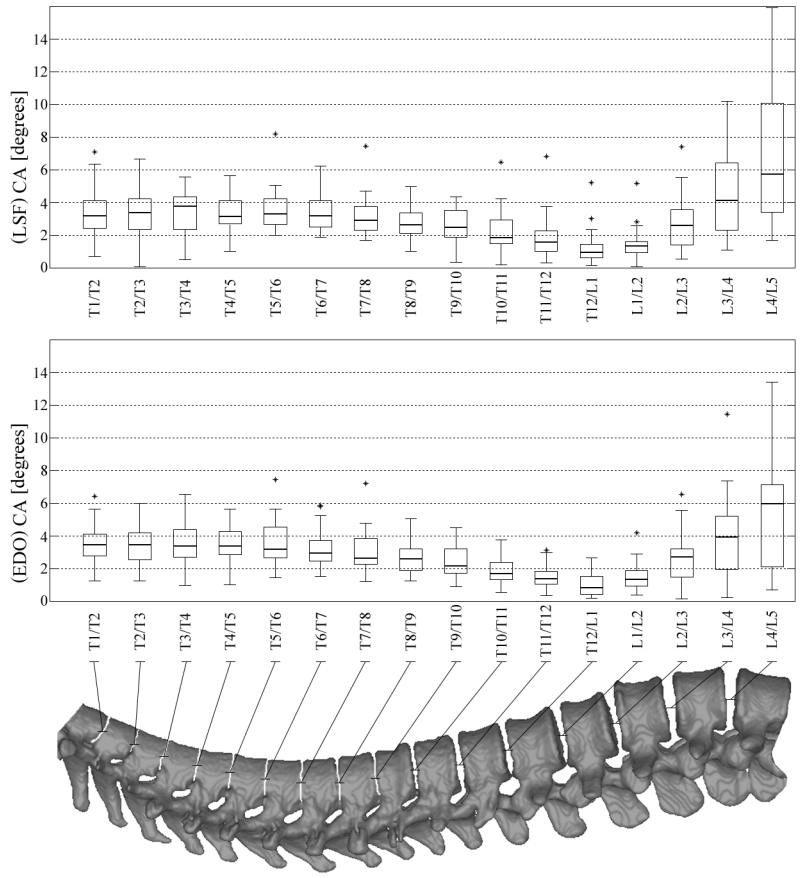

Figure 4.6. Distribution of curvature angle (CA) for different spine segments, obtained by applying the least squares fitting (LSF, top) and edge distance optimization (EDO, bottom) method to 30 CT spine images. For each segment, the results are presented as a box-whiskers diagram, which shows the median, first and third quartile, minimal and maximal values, and outliers (values that are more than 1.5 times the interquartile range away from the first or third quartile).

2D, although they can occur in an arbitrary plane. This requires the images to be uniform in orientation and size, which can be achieved by a standardized image acquisition process. On the other hand, descriptors that measure the spinal curvature in 3D and are independent of the orientation and size of the spine may allow a more general (e.g. using images of different modality) and more objective (e.g. measuring the curvature in multiple image planes) evaluation of spinal deformities.

The presented GC and CA descriptors of spinal curvature in 3D are evaluated straightforwardly from the 3D vertebral body line. The LSF method for the determination of 3D vertebral body line is based solely on spatial coordinates of vertebra centroids, which are clinically intuitive and can be unambiguously defined on images of different size, dimensionality (e.g. 2D or 3D images) and modality (e.g. radiographs, CT or magnetic resonance (MR) images). Although

a polynomial function that would pass exactly through vertebra centroids could be determined by adequately higher polynomial degrees, smaller degrees help in compensating the variability in the identification of vertebra centroids. However, the identification of vertebra centroids is a process that requires clinical experience and a relatively high amount of user interaction. The EDO method is an example of how computer-assisted image analysis techniques can be used to overcome these problems. The amount of user interaction is limited to the approximate determination of the two end points of the 3D vertebral body line. The identification of vertebra centroids from T1 to L5 in 3D equals to 51 spatial coordinates, i.e 17 coordinates for each vertebra in each of the 3 image planes (axial, sagittal and coronal). This number represents the number of input parameters for the LSF method, while for the EDO method, just 2 initialization points are required, therefore the number of input parameters reduces to 6.

The main advantage of the 3D descriptors of GC and CA is that the measurements are independent of the orientation and size of the spine. The acquisition of images is therefore not required to be standardized, thus allowing a comparison between images with different properties (e.g. different scanners, acquisition parameters, patient orientation, spinal deformities, clinical environments). The measures also do not depend on vertebral body or intervertebral disc shape, or vertebral end-plate tilt, but solely on the global properties of the obtained 3D vertebral body line. The parametric description of the 3D vertebral body line may be useful in different applications and studies, for example, it can be applied straightforwardly to measurements of spine torsion (Poncet et al., 2001) or to the automated spine survey technique (Weiss et al., 2006). Moreover, the analysis can be reduced to 2D without losing the independence of the orientation and size by observing the 3D vertebral body line separately in sagittal and coronal image planes (equation 4.1, p. 93). If the exact location of TJ was automatically identified, automated evaluation of total TK (CA between T1 and TJ) and total LL (CA between TJ and L5) may be possible. Normal TK and normal LL are of significant importance in the maintenance of an adequate sagittal spinal balance and evaluation of the low back pain (Berthonnaud et al., 2005a, Vedantam et al., 1998). By comparing an arbitrary spine anatomy to the mean GC and CA values over a healthy population, the presence and exact location of hyperkyphosis and/or hyperlordosis may be easily identified and more objectively evaluated. Although this study is focused on normal spine anatomy, pathological spines could also be analyzed. The LSF method is designed for application to an arbitrary form of spinal curvature, while the EDO method proved to be capable of describing scoliotic curvatures (Vrtovec et al., 2005). The automated detection of all characteristic spine regions (i.e. flexion points of the 3D vertebral body line) may be further used to classify spinal deformities (King et al., 1983, Lenke et al., 2001, Roussouly et al., 2005). To conclude, the application of the proposed framework to the analysis of spinal curvatures in 3D may improve the understanding of spine anatomy and aid in clinical quantitative evaluation of spinal deformities.

Appendix

A curve C (figure 4.2, p. 86) that represents the 3D vertebral body line

$$C(p) = \Big[x(p),\, y(p),\, z(p) \Big] \tag{4.1}$$

is parameterized by the arbitrary position p on the spine and defined as a polynomial function of degree K:

$$C(p) = \left[\sum_{k=0}^{K} a_{x,k}\, p^k,\, \sum_{k=0}^{K} a_{y,k}\, p^k,\, \sum_{k=0}^{K} a_{z,k}\, p^k \right], \tag{4.2}$$

where $a_{x,k}$, $a_{y,k}$ and $a_{z,k}$; $k = 0, 1, \ldots, K$ are the coefficients of the polynomials $x(p)$, $y(p)$ and $z(p)$ that represent the sagittal, coronal and axial component of the 3D vertebral body line, respectively. The geometric curvature GC of the parameterized 3D vertebral body line

$$GC(p) = \frac{\left| \frac{dC(p)}{dp} \times \frac{d^2C(p)}{dp^2} \right|}{\left| \frac{dC(p)}{dp} \right|^3} = \frac{1}{R(p)} \tag{4.3}$$

is defined as the reciprocal value to the radius R of the osculating circle in 3D, i.e. the circle that best approximates the 3D vertebral body line at an arbitrary position p on the spine ($\times$ denotes the vector cross product). The curvature angle CA (in radians) of the parameterized geometric curvature

$$CA(p_1, p_2)\,[rad] = \frac{L(p_1, p_2)}{R(\bar{p}_{12})} = L(p_1, p_2) \cdot GC(\bar{p}_{12}) \tag{4.4}$$

is determined as the angle that spans two given positions p_1 and p_2 on the spine with the arc L of the osculating circle, which is defined at the mean position $\bar{p}_{12} = \frac{1}{2}(p_2 - p_1)$ on the spine (figure 4.2, p. 86). The arc L of the osculating circle can be approximated by the arc length of the parameterized 3D vertebral body line:

$$L(p_1, p_2) = \int_{p_1}^{p_2} \left| \frac{dC(p)}{dp} \right| dp\,. \tag{4.5}$$

The representation of CA in degrees is given by:

$$CA\,\big[degrees\big] = \frac{180^\circ}{\pi}\, CA\,[rad]\ . \tag{4.6}$$

Acknowledgments

This work has been supported by the Slovenian Ministry of Higher Education, Science and Technology under grant P2-0232. The authors would like to thank the Images Sciences Institute, Medical University Utrecht, The Netherlands, for providing the CT images used in this study.

A good rotation. A rotation I define as the experiencing of the new beyond the expectation of the experiencing of the new.

WALKER PERCY, 1916 - 1990
(The Moviegoer, 1961)

CHAPTER 5

Determination of 3D location and rotation of lumbar vertebrae in CT images by symmetry-based auto-registration

TOMAŽ VRTOVEC, BOŠTJAN LIKAR AND FRANJO PERNUŠ

SPIE MEDICAL IMAGING 2007: IMAGE PROCESSING CONFERENCE
SAN DIEGO, CALIFORNIA, USA, FEB 17-22 2007
PROCEEDINGS OF SPIE, 6512:65121Q–1

(text slightly modified)

Abstract

Quantitative measurement of vertebral rotation is important in surgical planning, analysis of surgical results, and monitoring of the progression of spinal deformities. However, many established and newly developed techniques for measuring axial vertebral rotation do not exploit three-dimensional (3D) information, which may result in virtual axial rotation because of the sagittal and coronal rotation of vertebrae. We propose a novel automatic approach to the measurement of the location and rotation of vertebrae in 3D without prior volume reformation, identification of appropriate cross-sections or aid by statistical models. The vertebra under investigation is encompassed by a mask in the form of an elliptical cylinder in 3D, defined by its center of rotation and the rotation angles. We exploit the natural symmetry of the vertebral body, vertebral column and vertebral canal by dividing the vertebral mask by its mid-axial, mid-sagittal and mid-coronal plane, so that the obtained volume pairs contain symmetrical parts of the observed anatomy. Mirror volume pairs are then simultaneously registered to each other by robust rigid auto-registration, using the weighted sum of absolute differences between the intensities of the corresponding volume pairs as the similarity measure. The method was evaluated on 50 lumbar vertebrae from normal and scoliotic computed tomography (CT) spinal scans, showing relatively large capture ranges and distinctive maxima at the correct locations and rotation angles. As such, the proposed method may aid the measurement of the dimensions of vertebral pedicles, foraminae and canal, and may be a valuable tool for clinical evaluation of the spinal deformities in 3D.

5.1 Introduction

Quantitative assessment of vertebral rotation is important in surgical planning (Aronsson et al., 1996), analysis of surgical results (Lee et al., 2004, Petit et al., 2004), and monitoring of the progression of spinal deformities (Stokes and Aronsson, 2001). Many established techniques were developed for measuring the axial vertebral rotation from frontal and/or lateral radiographs (Cobb, 1948, Nash and Moe, 1969, Stokes and Aronsson, 2001, Stokes et al., 1986), however, sagittal and coronal inclination (rotation) of vertebrae, which can significantly influence the measurements by introducing a virtual axial rotation, were rarely taken into account (Hecquet et al., 1998, Skalli et al., 1995). As axial cross-sections can be easily extracted from computed tomography (CT) images, CT proved to be the most accurate imaging modality for evaluating axial vertebral rotation (Krismer et al., 1996). Various angles, such as the inclination of the line between the posterior central aspect of the vertebral foramen and the middle of the vertebral body (Aaro and Dahlborn, 1981, Chi et al., 2006), the inclination of the line that bisects the angle of lines between the junctions of inner surfaces of the two laminae and the midpoint of the posterior surface of the vertebral body (Ho et al., 1993), the inclination of the line between the most posterior points of the two pedicles (Göçen et al., 1999), or

the inclination of the line between the center of the spinal canal and the center of the vertebral body (Kouwenhoven et al., 2006) have been proposed to express the vertebral rotation. However, axial cross-sectional measurements can still be misleading for vertebrae that are rotated in space (Skalli et al., 1995) and affected by mechanical vertebral torsion, i.e. different axial rotations at different cross-sections of the same vertebra. The error induced by vertebral torsion can be reduced by performing measurements in axial cross-sections that pass through the center of the vertebral body and have clearly visible posterior vertebral structures (Krismer et al., 1996) or pedicles (Kouwenhoven et al., 2006) or, in case of magnetic resonance (MR) images, in cross-sections reformatted through the superior and inferior vertebral end-plates (Birchall et al., 1997). The Cobb technique (Cobb, 1948) is the most established method for measuring vertebral rotation in the coronal plane in case of scoliotic deformities (Cheung et al., 2002, Shea et al., 1998, Stokes and Aronsson, 2006) and in the sagittal plane to measure thoracic kyphosis and lumbar lordosis (Bernhardt and Bridwell, 1989, Korovessis et al., 1998, Pinel-Giroux et al., 2006, Vedantam et al., 1998). However, correct identification of end vertebrae, determination of vertebral end-plate inclination and the variable end-plate shape induce high variability in the estimation of the Cobb angle (Cheung et al., 2002, Chockalingam et al., 2002, Polly et al., 1996). On the other hand, newly developed techniques for evaluation of sagittal vertebral rotation, such as posterior tangent lines (Harrison et al., 2000), best-fit ellipses (Harrison et al., 2002), mean radius of curvature (Goh et al., 2000a), or tangent circles (Pinel-Giroux et al., 2006) require a relatively high degree of user interaction and are associated with a large number of clinically unintuitive parameters. Although the determination of the center of rotation is inherently included in the estimation of vertebral rotation, few studies address it explicitly. The center of vertebral rotation is reported to be located in the mid-sagittal plane at the anterior wall of the vertebral canal (Molnár et al., 2006, Nash and Moe, 1969) approximately at the superior vertebral end-plate (Petit et al., 2004).

The problem of estimating the rotation of vertebrae was also approached by computer-assisted, mainly semi-automated techniques that involved low-level image analysis (Cheung et al., 2002, Chockalingam et al., 2002, Kouwenhoven et al., 2006, Shea et al., 1998, Stokes and Aronsson, 2006). Rogers et al. (2002) measured axial vertebral rotation by registering circular areas in two MR axial cross-sections, which were selected manually in order to show as much as possible of the transverse, spinous and superior articular process of the vertebra. Benameur et al. (2005b) modeled the vertebral bodies with cubic shapes, which were initialized in positions that were obtained from statistical knowledge over a representative scoliotic population. After rigid registration to pre-segmented vertebral bodies in frontal and lateral radiographs, the cubic shapes were replaced by statistical shape models of the vertebrae and deformed according to first modes of shape variation in the population. An automatic method for measuring the axial vertebral rotation in CT images was proposed by Adam and Askin (2006), who defined axial vertebral rotation as the axis of maximum symmetry in axial cross-sections, either manually selected at the center of the vertebral body or manually reformatted through vertebral end-plates.

All of the abovementioned methods either operate on two-dimensional (2D) data, do not exploit three-dimensional (3D) information, or avoid the determination of the center of rotation in 3D. As a result, manual selection of the correct axial cross-section in the middle of the vertebrae, manual reformation of the image so that the axial cross-section is perpendicular to the spine (i.e. manual definition of sagittal and coronal vertebral rotation), or manual determination of the exact center of rotation is required. To the best of our knowledge, an attempt to determine the location and rotation angles of vertebrae in 3D automatically has not yet been presented. In this paper, we propose an automatic approach to the determination of the location and rotation of vertebrae in 3D that is based on registration of symmetrical vertebral parts. Although the method was developed for arbitrary vertebrae, this study is focused on the estimation of 3D location and rotation of lumbar vertebrae, which may provide important clinical information for patients with low back pain, e.g. diagnosis of spinal instability (Berthonnaud et al., 2005a) and evaluating the integrity of a spinal fusion (Vedantam et al., 1998). The obtained values may aid the measurement of the dimensions of vertebral pedicles, vertebral foraminae and vertebral canal, provide considerable information on the nature of spinal deformity, and assist other image analysis tasks.

5.2 Methodology

5.2.1 Vertebral parameters

The location of the center of rotation and the rotation angles of a vertebra in the 3D image space $\mathcal{I}$ is defined by three translation and three rotation parameters $t = (x, y, z)$ and $\varphi = (\alpha, \beta, \gamma)$, respectively, i.e. by the vertebral parameters p:

$$p = (t, \varphi) = (x, y, z, \alpha, \beta, \gamma)\,. \tag{5.1}$$

The translation parameters t represent the sagittal, coronal and axial position of the vertebral center of rotation (coordinates x, y and z, respectively), while the rotation parameters represent the vertebral rotation angles around coordinate axes x, y and z (angles α, β and γ, respectively). When the translation parameters coincide with the center of the vertebral canal and when the rotation parameters resemble the rotation of the vertebra, the vertebral parameters best describe the vertebra under investigation.

5.2.2 Symmetry of the vertebral anatomy

By dividing a vertebra by its mid-axial, mid-sagittal and mid-coronal planes, volume pairs that contain symmetrical parts of the observed vertebral anatomy can be obtained:

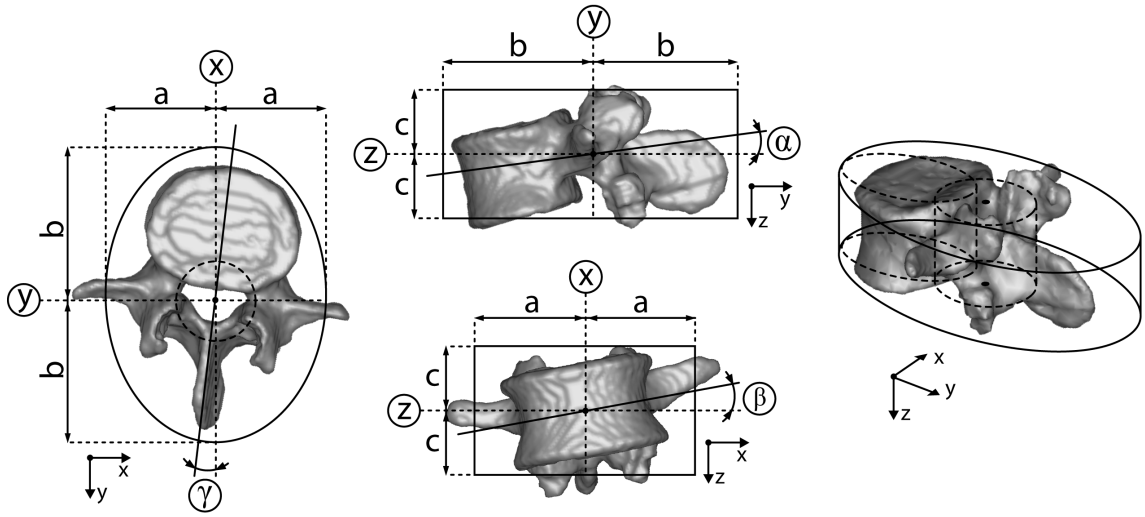

Figure 5.1. The position of the center of rotation $t = (x, y, z)$ and the rotation angles $\varphi = (\alpha, \beta, \gamma)$ of a vertebra are represented by vertebral parameters $p = (t, \varphi)$. A vertebra (or parts of the vertebra) is encompassed by 3D vertebral masks (e.g. in the form of elliptical cylinders) that are used to evaluate the natural symmetry of vertebral anatomy. The figure shows a schematic axial (left), left sagittal (middle, top), anterior coronal (middle, bottom), and a 3D (right) view of a lumbar vertebra, encompassed by two 3D vertebral masks.

- Symmetrical parts of the vertebral body and the adjacent intervertebral discs, which can be observed in cranial-to-caudal direction along the vertebral column, are obtained by dividing the vertebra by its mid-axial plane (symmetry $S^{[\text{axial}]}$).
- Symmetrical parts of the whole vertebra, which can be observed in left-to-right direction along the vertebra, are obtained by dividing the vertebra by its mid-sagittal plane (symmetry $S^{[\text{sagittal}]}$).
- Symmetrical parts of the vertebral canal, which can be observed in anterior-to-posterior direction along the vertebra, are obtained by dividing the vertebra by its mid-coronal plane (symmetry $S^{[\text{coronal}]}$).

5.2.3 Symmetry-based auto-registration

In order to capture the natural symmetry of the vertebral anatomy, each vertebra or parts of the vertebra under investigation is encompassed by 3D geometrical shapes, i.e. 3D vertebral masks. By dividing the 3D vertebral masks with the corresponding mid-axial, mid-sagittal and/or mid-coronal planes, mirror volume pairs can be determined. However, symmetrical mirror volume pairs are obtained only when the vertebral masks are positioned and rotated according to the vertebral parameters p (figure 5.1, p. 99):

- The symmetry $S^{\,[\text{axial}]}$ determines the translation parameter z and the rotation parameters (α, β).
- The symmetry $S^{\,[\text{sagittal}]}$ determines the translation parameter x and the rotation parameters (β, γ).
- The symmetry $S^{\,[\text{coronal}]}$ determines the translation parameters (x, y) and the rotation parameters (α, β).

The natural symmetry of the vertebral anatomy can therefore be exploited to determine the joint symmetry S, which is composed of the symmetries along different mirror volume pairs, obtained from M vertebral masks:

$$S = \sum_{m=1}^{M} S_m^{\,[\text{axial}]} + \sum_{m=1}^{M} S_m^{\,[\text{sagittal}]} + \sum_{m=1}^{M} S_m^{\,[\text{coronal}]}, \tag{5.2}$$

The joint symmetry represents the similarity measure between the corresponding mirror volume pairs and depends on the vertebral parameters p, therefore $S = S(p)$. The maximal joint symmetry is achieved at optimal vertebral parameters p^{opt}, which can be obtained by a rigid registration of the corresponding mirror volume pairs:

$$p^{opt} = \arg\max_{p} S(p). \tag{5.3}$$

5.3 Experiments and results

5.3.1 Experimental data

The proposed method for the determination of vertebral parameters p (equation 5.1, p. 98) was evaluated on 50 vertebrae, which were obtained from 10 CT scans of normal lumbar spine (vertebrae L1 to L5). The image size was $512 \times 512 \times 123 \div 191$ voxels and the voxel size was $0.488 \times 0.488 \times 2.0$ mm. In addition, one L1 vertebra was selected from a scoliotic spine (image size $512 \times 512 \times 472$ voxels, voxel size $0.6 \times 0.6 \times 1.0$ mm) to evaluate the method on vertebrae with relatively high rotation angles. In order to quantitatively assess the performance of the method, a visualization software was developed that provided a fixed cross-sectional reference display of the vertebra under investigation in its mid-axial, mid-sagittal and mid-coronal plane. Two observers were independently appointed to manually translate and rotate each vertebra in 3D until it was considered to be aligned with the fixed reference display, which resulted in manually determined vertebral parameters $p_{1[m]}$ and $p_{2[m]}$.

5.3.2 Implementation details

Basing on the characteristics of the vertebral anatomy, the 3D vertebral masks were initialized in the form of elliptical cylinders. For each vertebra, $M = 2$ masks were initialized with size $(2a_1, 2b_1, 2c_1) = (35, 49, 25)$ mm and $(2a_2, 2b_2, 2c_2) = (13, 13, 25)$ mm, where parameters a and b denote the ellipse axes and the parameter c denotes the cylinder half-height (figure 5.1, p. 99). The first mask encompassed the whole vertebra and was used to evaluate the symmetry $S^{[\text{sagittal}]}$ of the whole vertebra and, when only the anterior half of the mask was taken into account, also the symmetry $S^{[\text{axial}]}$ of the vertebral body. The second mask encompassed the area around the vertebral canal and was used to evaluate the symmetries $S^{[\text{coronal}]}$ and $S^{[\text{sagittal}]}$ of the vertebral canal.

The symmetry-based similarity measure (equation 5.2, p. 100) was estimated by a robust, weighted sum of absolute intensity differences (SAD) (Hajnal et al., 2001) between the voxels in corresponding mirror volume pairs, obtained from the 3D vertebral masks:

$$S^{[*]} = -\sum_{k=1}^{K} \begin{cases} |i_{k1} - i_{k2}| & \texttt{if} \quad |i_{k1} - i_{k2}| \leq T \\ T & \texttt{if} \quad |i_{k1} - i_{k2}| > T \end{cases}, \tag{5.4}$$

where K is the number of voxels in each volume, i_1 and i_2 are the corresponding voxel intensities in a volume and in its mirror pair, respectively, $T = 30$ represents the intensity threshold and $S^{[*]}$ denotes the chosen $S^{[\text{axial}]}$, $S^{[\text{sagittal}]}$ or $S^{[\text{coronal}]}$ symmetry. The maximal joint symmetry, which determines the optimal vertebral parameters p^{opt}, was obtained by rigid registration of the mirror volume pairs (equation 5.3, p. 100). Simulated annealing (Press et al., 2002) combined with the simplex method in multidimensions (Press et al., 2002) was used as the registration optimization method ($T_0 = 3$, $K = 500$, $\alpha = 2$, $N_{iter} = 4$).

Quantitative evaluation of registration results was achieved by mapping the vertebral parameters p from the 3D image space $\mathcal{I}$ into normalized vertebral parameters p_n in a six-dimensional (6D) parameter space $\mathcal{I}_n$. After normalization, the $(x, y, z) = (1, 1, 1)$ mm translation and $(\alpha, \beta, \gamma) = (2, 2, 2)$ degrees rotation in $\mathcal{I}$ (equation 5.1, p. 98) were represented as a $p_n = (1, 1, 1, 1, 1, 1)$ mm translation in $\mathcal{I}_n$.

5.3.3 Experiments

Manual determination of vertebral parameters in 3D is a difficult and error-prone task, affected by many factors, such as the mechanical vertebral torsion, asymmetrical vertebral transverse and spinous processes, low resolution in axial image direction and subjective interpretation of each observer. Moreover, a relatively high variability can be induced by interparameter dependency, since the relatively small $\Delta x = 1$ mm translation of the center of rotation causes an average

difference of $\Delta\gamma \approx 2$ degrees in the rotation angle (mask size $2b_1 = 49$ mm is taken into account). The manually determined vertebral parameters $p_{1[m]}$ and $p_{2[m]}$ can therefore not be directly used as the reference for quantitative evaluation of the proposed method. In order to obtain the reference vertebral parameters, an initial experiment of $N_1 = 100$ symmetry-based auto-registrations was first performed on each of the 50 lumbar vertebrae. The registration starting positions were defined by uniformly distributed displacements with maximal length of 5 mm in the normalized parameter space $\mathcal{I}_n$ that were randomly generated from the mean $p_{\overline{12}[m]}$ of the manually determined vertebral parameters. The median vertebral parameters of the displacements that resulted from the registration were then presented to the observers for final verification. If the observers identified that a parameter did not provide a good description of the center of rotation and/or rotation of the vertebrae, the parameter was replaced by the mean of the manually determined parameters. The resulting configuration represented the reference vertebral parameters $p_{[r]}$ that were used for quantitative evaluation of the proposed method in the main registration experiment.

The main registration experiment was performed similarly, however, in this case $N_2 = 1000$ uniformly distributed displacements with maximal length of 25 mm in the normalized parameter space $\mathcal{I}_n$ were randomly generated from the reference vertebral parameters $p_{[r]}$. The displacements were used as starting positions for the proposed symmetry-based auto-registration of the mirror volume pairs, which were obtained from 3D vertebral masks and contained symmetrical parts of vertebral anatomy. The vertebral parameters that corresponded to the median resulting displacements after registration were quantitatively and qualitatively assessed by comparison to the reference parameters and by the verification by the observers, respectively.

In order to simulate manual initialization of the registration starting positions, an additional registration experiment was performed on the scoliotic vertebra L1. The translation parameters t that represent the position of the vertebral center of rotation (equation 5.1, p. 98) were initialized in the vertebral canal, which was simulated by displacing each of the translation parameter independently for ±2.5 mm. The rotation parameters φ that represent the vertebral rotation angles (equation 5.1, p. 98) were, on the other hand, always initialized as zero, which corresponds to the manual determination of a point in the 3D image (i.e. pinpointing) approximately at the vertebral center of rotation. The experiment was applied to the scoliotic vertebra because the rotation angles are relatively high when compared to those in normal spines.

5.3.4 Results

The differences between the manually determined vertebral parameters $p_{1[m]}$ and $p_{2[m]}$ are presented in table 5.1 (p. 106) as distances in the normalized parameter space $\mathcal{I}_n$. The mean difference between observers along all 50 vertebrae is approximately 2.2 mm, which can be considered as an estimate of the uncertainty. This means that the manually determined parameters on average differ for a 2.2 mm translation in a single direction or for a 4.4 degrees

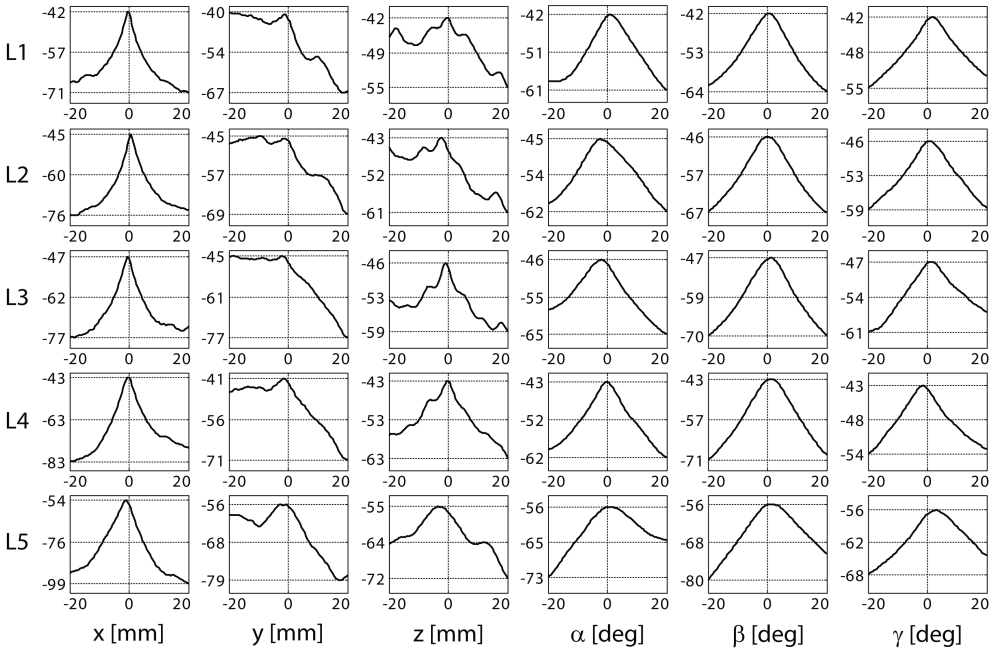

Figure 5.2. Courses of the symmetry-based similarity measure S for lumbar vertebrae in image 8, evaluated by displacing each of the vertebral parameters $p = (x, y, z, \alpha, \beta, \gamma)$ from the manually determined parameters $p_{1[m]}$.

rotation around a single axis in the 3D image space $\mathcal{I}$. However, by observing the courses of the similarity measure (figure 5.2, p. 103), it can be concluded that the manually determined parameters can nevertheless be used to roughly determine the reference vertebral parameters $p_{[r]}$. Most courses have relatively large capture ranges and distinctive maxima in the proximity of the manually determined center of rotation and rotation angles of the vertebrae, which indicates that the proposed symmetry-based similarity measure (equations 5.2, p. 100 and 5.4, p. 101) is feasible for the determination of the 3D location and rotation of vertebrae in CT images.

The reference rotation parameters $p_{[r]}$ were obtained from the results of $N_1 = 100$ symmetry-based auto-registrations, where the starting positions were defined by the displacements from the mean $p_{\overline{12}[m]}$ of the manually determined parameters, and are presented in table 5.1 (p. 106) for all 50 vertebrae. The parameters that did not provide a good description of the center of rotation and/or rotation angles of the vertebrae (10 out of 50) and were therefore replaced by the mean of the manually determined parameters, were the translation parameters y or z. This can be explained by the fact that, besides in the center of the vertebral body, the symmetry $S^{\text{[axial]}}$ may reach local maxima in adjacent intervertebral discs or even in the adjacent vertebral bodies, which affects directly the translation parameter z. For the parameter y, the symmetry $S^{\text{[coronal]}}$ may reach a local maximum when the mask that encompasses the area around the vertebral canal is positioned on the vertebral body (figure 5.2, p. 103). Visual assessment of the results confirmed this explanation. However, this problem could be solved by isolating each vertebra

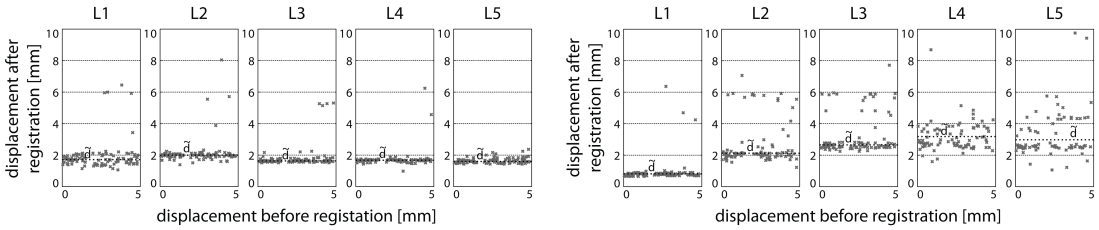

Figure 5.3. Scatter plots of the vertebral parameters before and after registration of $N_1 = 100$ displacements from the mean $p_{\overline{12}[m]}$ of the manually determined vertebral parameters, presented as distances in the normalized parameter space $\mathcal{I}_n$ for vertebrae in images 8 (left) and 9 (right).

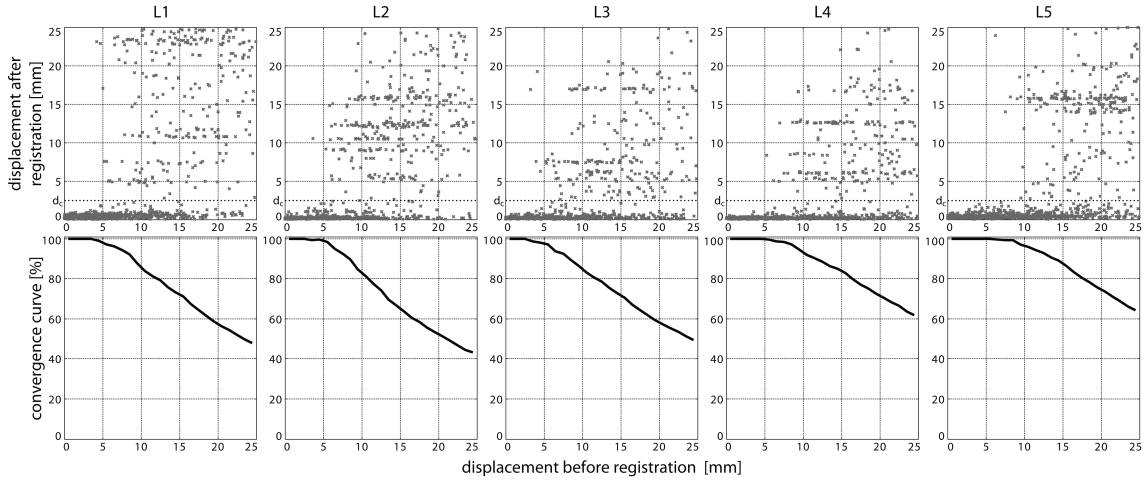

Figure 5.4. Scatter plots of the vertebral parameters before and after regsitration of $N_2 = 1000$ displacements from the reference vertebral parameters $p_{[r]}$, presented as distances in the normalized parameter space $\mathcal{I}_n$ for vertebrae in image 8 (top row). The corresponding convergence curves (bottom row) represent the ratio of the successful registration results, defined by the threshold distance $d_c = \sqrt{6} \approx 2.45$ mm.

in the 3D image or by initializing additional 3D vertebral masks that would contribute to the distinctiveness of the correct symmetry maxima. Nevertheless, most of the resulting reference vertebral parameters passed the verification by the observers (40 out of 50) and their normalized values were comparable to the uncertainty of the manually determined parameters. For all 50 vertebrae, the mean of the median displacements $\tilde{d}_{[1]}$ of the parameters that provided a good description of the vertebrae after registration was 2.3 mm. Figure 5.3 (p. 104) shows the results of this initial registration experiment in the normalized parameter space $\mathcal{I}_n$ for the CT scans 8 and 9. Although the results for the vertebrae in CT image 9 are more dispersed, especially for vertebrae L4 and L5, the resulting median parameters provided a good description of the vertebral location and rotation, which confirms that a relatively high variability may be induced in the manual determination of vertebral parameters.

The results of the main registration experiment, which consisted of symmetry-based auto-registrations of $N_2 = 1000$ displacements from the reference vertebral parameters $p_{[r]}$, are presented in table 5.1 (p. 106) and shown in figures 5.4 (p. 104) and 5.5 (p. 108) as distances in the normalized parameter space $\mathcal{I}_n$. The parameters that did not provide a good description of the center of rotation and/or rotation angles of the vertebrae in the initial experiment also failed do provide such a description in the main experiment. For all 50 vertebrae, the mean of the median displacements $\tilde{d}_{[2]}$ of the parameters that provided the correct description of the vertebrae after registration was 0.4 mm. Convergence curves (figures 5.4, p. 104 and 5.5, p. 108) represent the cumulative ratio of successful registrations against the number of all registrations. We considered a registration successful when the displacement after registration was less than the threshold distance $d_c = \sqrt{6} \approx 2.45$ mm, which represents a 1 mm unit translation of each vertebral parameter in the 6D normalized parameter space $\mathcal{I}_n$ and corresponds to $(x, y, z) = (1, 1, 1)$ mm translation and $(\alpha, \beta, \gamma) = (2, 2, 2)$ degrees rotation in the 3D image space $\mathcal{I}$. It can be observed that displacements result in successful registrations if they are approximately inside the 5 mm radius of a sphere in the normalized parameter space, centered in the reference vertebral parameters $p_{[r]}$. Therefore, if manual initialization of the parameters is performed in the 3D image space, the registration will most likely converge when a vertebral parameter is 5 mm translated in a single direction or 10 degrees rotated around a single axis from the reference 3D location and rotation of the vertebra. However, the results show that the registration tends to converge to incorrect optima even when the starting position is less than 5 mm from the reference parameters, e.g. in case of vertebrae L2 and L4 in image 9 as shown in figure 5.5 (p. 108). The inspection of the resulting parameters showed that the registration error was caused by the same reason as in the initial registration experiment. Namely, the error occurred because the translation parameter z converged to the adjacent intervertebral discs, where a relatively high symmetry $S^{\text{[axial]}}$ was obtained, and not to the center of the vertebral body.

The results of the experiment that simulates manual determination of the vertebral parameters in the vertebral canal on the scoliotic vertebra L1 are presented in table 5.2 (p. 107). The registration results were compared to the mean $p_{\overline{12}[m]}$ of the manually determined vertebral parameters and show that the largest error occurs in the estimation of vertebral parameters z and γ, however, the mean distance $\bar{d} = 2.6$ mm in the normalized parameter space $\mathcal{I}_n$ indicates that the results are within the uncertainty of the manually determined parameters. The purpose of this experiment was to show that by using the proposed symmetry-based auto-registration, vertebral parameters can be obtained when the initialization is represented by pinpointing the approximate position of the vertebral center of rotation in the 3D image (figure 5.6, p. 108). Moreover, the results show that also relatively high vertebral rotation angles, which are in general present in scoliotic vertebrae, can be measured.

Table 5.1. Difference $d_{\Delta[m]}$ between the manually determined vertebral parameters, the median displacement $\tilde{d}_{[1]}$ after registration of $N_1 = 100$ displacements from the mean $p_{\overline{12}[m]}$ of the manually determined vertebral parameters and the median displacement $\tilde{d}_{[2]}$ after registration of $N_2 = 1000$ displacements from the reference vertebral parameters p[r], presented as distances in the normalized parameter space $\mathcal{I}_n$. The parameters that did not provide a good description of the center of rotation and/or rotation angles of the vertebrae are displayed in square brackets below the corresponding values. (Note*: The mean values are computed from the results that provided a good description.)

image	$d_{\Delta[m]}$ [mm]					$\tilde{d}_{[1]}$ [mm]					$\tilde{d}_{[2]}$ [mm]				
	L1	L2	L3	L4	L5	L1	L2	L3	L4	L5	L1	L2	L3	L4	L5
1	2.8	2.2	2.5	1.8	2.4	1.5	1.8	6.9 [y]	8.1 [y, z]	5.3	0.3	0.2	6.2 [y, z]	8.0 [y, z]	4.1
2	2.2	2.7	2.2	2.3	3.9	1.0	1.8	7.6 [y]	9.0 [y]	5.7	0.2	0.3	6.9 [y]	8.1 [y]	0.4
3	2.3	1.1	2.0	2.0	2.4	2.1	2.4	1.2	0.9	29.9 [y, z]	0.2	0.3	0.5	0.1	25.1 [y, z]
4	3.3	2.6	2.5	2.2	3.0	2.3	1.5	2.4	1.9	2.5	0.4	0.2	0.2	0.2	0.3
5	1.2	2.3	2.4	2.4	2.3	6.2 [z]	0.7	1.4	25.3 [y]	3.5	5.9 [z]	0.2	0.2	40.0 [y]	0.5
6	2.8	0.9	1.5	2.3	3.4	16.8 [z]	0.9	1.1	2.2	3.0	14.3 [z]	0.3	0.3	0.4	0.4
7	2.4	4.1	2.5	3.0	4.1	1.9	2.1	0.7	25.0 [y, z]	30.3 [y, z]	0.2	0.5	0.3	24.8 [y, z]	18.5 [y, z]
8	1.4	2.2	1.1	2.0	5.4	1.7	2.0	1.6	1.7	1.6	0.4	0.2	0.2	0.2	0.4
9	0.9	1.1	2.3	1.1	2.1	0.8	2.1	2.6	3.2	3.0	0.2	0.5	0.4	1.1	0.3
10	0.7	1.2	1.1	0.9	2.4	3.0	1.3	1.6	6.2	6.7	0.3	0.2	0.2	0.4	1.0
mean*	2.0	2.0	2.0	2.0	3.1	1.8	1.7	1.6	2.7	3.9	0.3	0.3	0.3	0.4	0.9

Table 5.2. Results of applying the symmetry-based auto-registration to the scoliotic vertebra L1. The vertebral parameters $p_{[i]}$ before registration, the vertebral parameters $p_{[r]}$ after registration and the corresponding distances d in the normalized parameter space $\mathcal{I}_n$ are relative to the the mean $p_{\overline{12}[m]}$ of the manually determined parameters.

parameters		x [mm]	y [mm]	z [mm]	α [deg]	β [deg]	γ [deg]	d [mm]
$p_{\overline{12}[m]}$		65.8	52.9	356.5	4.5	−22.5	−8.0	0.0
×	$\Delta p_{[i]}$	0.0	0.0	0.0	−4.5	+22.5	+8.0	12.2
	$\Delta p_{[r]}$	+0.2	−0.5	−0.5	−0.1	+2.0	−1.8	1.5
$+x$	$\Delta p_{[i]}$	+2.5	0.0	0.0	−4.5	+22.5	+8.0	12.4
	$\Delta p_{[r]}$	−1.2	−0.4	−3.7	+0.6	+2.7	−2.0	4.3
$-x$	$\Delta p_{[i]}$	−2.5	0.0	0.0	−4.5	+22.5	+8.0	12.4
	$\Delta p_{[r]}$	−0.5	−0.6	−2.7	+1.2	−0.9	−3.7	3.4
$+y$	$\Delta p_{[i]}$	0.0	+2.5	0.0	−4.5	+22.5	+8.0	12.4
	$\Delta p_{[r]}$	+0.8	−0.6	+0.4	+0.1	+0.6	−0.5	1.1
$-y$	$\Delta p_{[i]}$	0.0	−2.5	0.0	−4.5	+22.5	+8.0	12.4
	$\Delta p_{[r]}$	−0.5	−0.5	−2.8	0.0	+0.9	−1.0	3.0
$+z$	$\Delta p_{[i]}$	0.0	0.0	+2.5	−4.5	+22.5	+8.0	12.4
	$\Delta p_{[r]}$	+0.9	−0.9	−1.6	+0.7	+1.3	−1.4	2.3
$-z$	$\Delta p_{[i]}$	0.0	0.0	−2.5	−4.5	+22.5	+8.0	12.4
	$\Delta p_{[r]}$	0.0	−0.1	−2.1	−0.1	+1.6	−3.7	2.9
mean	$\overline{\Delta p_{[r]}}$	0.0	−0.5	−1.9	+0.4	1.2	−2.0	2.6
	$\overline{\lvert\Delta p_{[r]}\rvert}$	0.6	0.5	2.0	0.5	1.4	2.0	

5.4 Conclusions

A novel approach to the determination of the 3D location and rotation of vertebrae in CT images was presented. The proposed method does not require prior volume reformation, identification of the most appropriate axial cross-section or aid by high-level prior information, such as statistical shape and/or appearance models. Instead, the method benefits from the natural symmetry of the vertebral anatomy, namely from the symmetry of the vertebra as a whole structure and the symmetry of the vertebral body, vertebral column and vertebral canal. The flexibility in the determination of the 3D vertebral masks that encompass the vertebra or parts of the vertebra under investigation allows that an arbitrary number of masks of different shape, size and

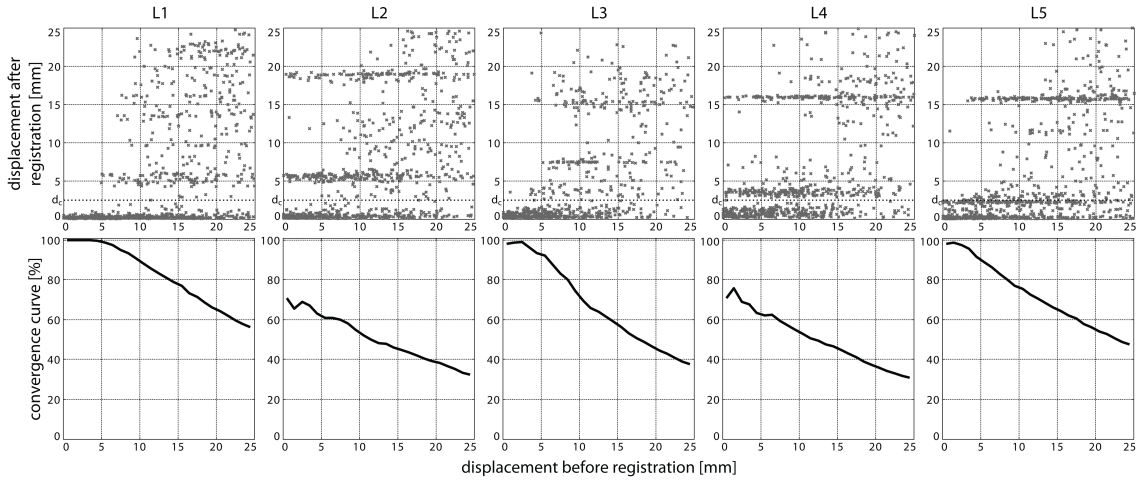

Figure 5.5. Scatter plots of the vertebral parameters before and after registration of $N_2 = 1000$ displacements from the reference vertebral parameters $p_{[r]}$, presented as distances in the normalized parameter space $\mathcal{I}_n$ for vertebrae in image 9 (top row). The corresponding convergence curves (bottom row) represent the ratio of the successful registration results, defined by the threshold distance $d_c = \sqrt{6} \approx 2.45$ mm.

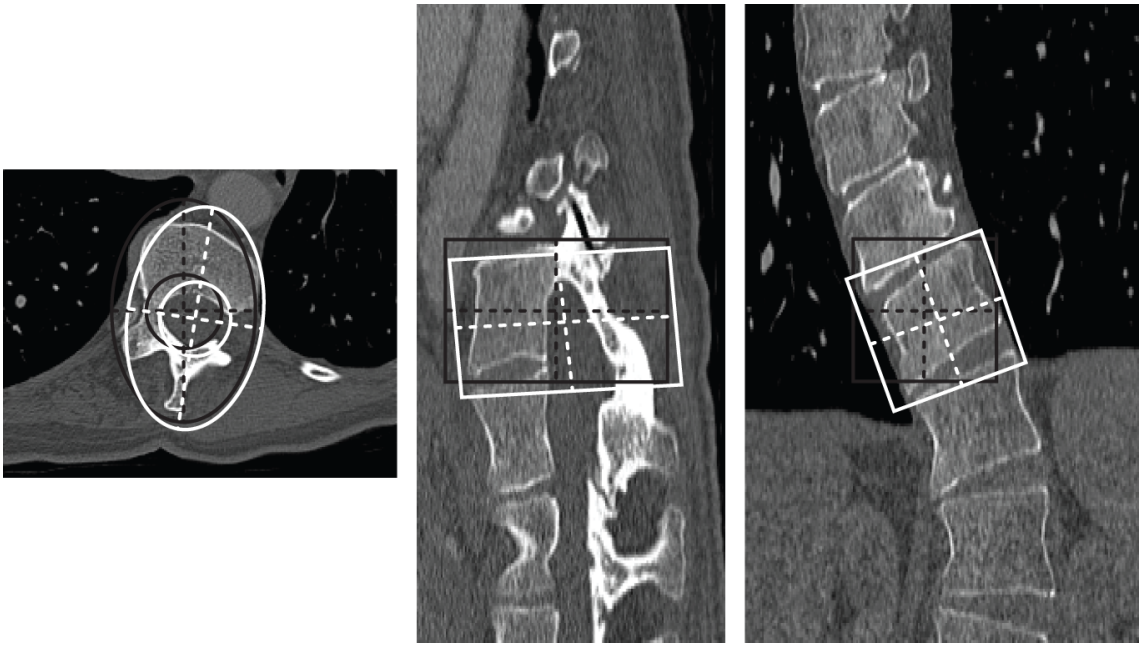

Figure 5.6. Example of the symmetry-based auto-registration of the scoliotic vertebra L1 in an axial (left), sagittal (middle) and coronal (right) cross-section. The vertebral parameters before (initialization with zero rotation angles) and after registration are shown with vertebral masks in black and white, respectively.

position according to the center of rotation and rotation angles of the vertebra can be determined for evaluation of symmetry. Although the size of the 3D vertebral masks was determined manually, reliable values can be obtained from a large set of vertebrae by statistical analysis of their size (the field of vertebral morphometry). However, it is important to note that a compromise between the number, size and sampling of the vertebral masks regulates the complexity of the computation, as a larger mask size or finer sampling increase the time needed for the computation of the corresponding symmetry.

The main drawback of the proposed method is that the reference vertebral parameters, i.e. the reference location and rotation of vertebrae in 3D, used to quantitatively evaluate the performance of the proposed method, can not uniquely defined and therefore may not be treated as a "gold standard". The same problem is present in existing methods for measuring vertebral rotation, where only local geometrical properties of the vertebral anatomy are usually taken into account, such as the posterior central aspect of the vertebral foramen (Aaro and Dahlborn, 1981), the junction of the inner surfaces of the two laminae (Ho et al., 1993), or the most posterior points of the pedicles (Göçen et al., 1999). Moreover, even if anatomical landmarks are identified on vertebrae before image acquisition (e.g. markers on cadaveric spines), the selection of landmarks can considerably influence the measured parameter values, as different landmarks result in different centers of rotation and rotation angles. The determination of the reference vertebral parameters therefore represents a difficult and poorly defined problem. On the other hand, we have approached this problem by exploiting global characteristics of the vertebrae, i.e. the natural symmetry that is present in vertebral anatomy.

The main purpose of this study was to verify if the natural symmetry of the vertebral anatomy is feasible for determining the 3D location and rotation of vertebrae. The results show that the vertebral parameters can be successfully determined in CT scans of both normal and scoliotic spines, however, determination of some of the parameters (e.g. translation parameters y and z) may need additional attention. The implementation of a more robust symmetry-based similarity measure may represent a solution to this problem and therefore improve the performance of the proposed method. Nevertheless, the possibility of deforming the 3D vertebral masks may be exploited to model more detailed properties of the vertebral anatomy, for example, mask shear and/or twist may provide a good description of mechanical vertebral torsion. Although the method is designed for 3D images of arbitrary modality and for vertebrae of arbitrary spinal sections, an estimation of the performance on other imaging modalities (e.g. MR spine images) and other spinal sections (e.g. on thoracic vertebrae) is needed to confirm such conclusions. The location of vertebrae and vertebral rotation angles are among the most important parameters for the evaluation of spinal deformities and may assist other image analysis methods. The proposed method may therefore aid the measurement of the dimensions of vertebral pedicles, foraminae and canal, and may be a valuable tool for clinical evaluation of the spinal deformities in 3D.

Acknowledgments

This work has been supported by the Ministry of Higher Education, Science and Technology, Slovenia, under grant P2-0232. The authors would like to thank P. Markelj from the University of Ljubljana, Faculty of Electrical Engineering, Slovenia, for the manual determination of vertebral rotation parameters.

"I think that one of these days," he said, "you're going to have to find out where you want to go. And then you've got to start going there. But immediately. You can't afford to lose a minute. Not you."

JEROME D. SALINGER, 1919 –
(The Catcher in the Rye, 1951)

CHAPTER 6

Modality-independent determination of vertebral position and rotation in 3D

TOMAŽ VRTOVEC, SÉBASTIEN OURSELIN, BOŠTJAN LIKAR AND FRANJO PERNUŠ

Submitted for conference presentation.

Abstract

The determination of position and rotation parameters of vertebrae is important for the understanding of normal and pathological spine anatomy. Existing techniques estimate the parameters from planar cross-sections, are relatively complex or require a lot of manual interaction. We have developed an automated and modality-independent method for the determination of position and rotation of vertebrae in three dimensions (3D) that is based on registration of image intensity gradients, extracted in 3D from symmetrical vertebral parts. The method was evaluated on 52 vertebrae; 26 were acquired by computed tomography (CT) and 26 by magnetic resonance (MR). The results show that by the proposed gradient-based registration of symmetrical vertebral parts, the position and rotation of vertebrae in 3D can be successfully determined in both CT and MR spine images.

6.1 Introduction

The determination of position and rotation of individual vertebrae is important for the understanding of the nature of normal and pathological spine anatomy. The Cobb technique (Cobb, 1948) is the most established method for measuring vertebral rotation from radiographic images of the spine in cases of scoliotic (Chockalingam et al., 2002, Shea et al., 1998) and kyphotic or lordotic deformities (Bernhardt and Bridwell, 1989, Pinel-Giroux et al., 2006). Techniques that exploit the information in three-dimensional (3D) imaging modalities, such as computed tomography (CT) and magnetic resonance (MR), were proposed in (Birchall et al., 1997, Hecquet et al., 1998, Krismer et al., 1996, Skalli et al., 1995) and further combined with low level image analysis methods (Chockalingam et al., 2002, Kouwenhoven et al., 2006, Pinel-Giroux et al., 2006, Shea et al., 1998). More sophisticated techniques were presented by Rogers et al. (2002), who measured axial vertebral rotation by registering circular areas in two MR axial cross-sections, Benameur et al. (2005b), who determined the vertebral pose by registering statistical shape models of vertebrae to pre-segmented vertebral bodies in stereoradiographic images, and Adam and Askin (2006), who defined axial vertebral rotation as the axis of maximum symmetry in axial CT cross-sections. The vertebral center of rotation, located in the mid-sagittal plane at the anterior wall of the vertebral canal (Molnár et al., 2006) and at the superior vertebral end-plate (Petit et al., 2004), was inherently included in the estimation of vertebral rotation. Although the aforementioned methods aim to exploit the information in 3D, the measurements are still performed in two-dimensional (2D) cross-sections and require a relatively high number of parameters or a lot of manual interaction. Besides manual determination of the center of rotation, the cross-sections are manually selected either from the original images or, in order to reduce the effect of virtual rotation (Hecquet et al., 1998, Skalli et al., 1995) and vertebral torsion (Kouwenhoven et al., 2006, Krismer et al., 1996), from manually reformatted images where cross-sections are perpendicular or tangent to the spine. Moreover,

the measurements are based on manually identified reference points (e.g. center of the vertebral body and the vertebral canal, extreme points of pedicles and processes), which reflect only local characteristics of vertebral anatomy.

The purpose of this study is to develop a method for the determination of position and rotation of vertebrae (i.e. vertebral parameters) that exploits the information available in 3D images, does not require manual interaction and takes into account the global characteristics of vertebral anatomy. We propose and test the performance of an automated, modality-independent method that is based on registration of image intensity gradients that are extracted in 3D from symmetrical vertebral parts. Automated determination of vertebral parameters in 3D may improve clinical diagnosis (e.g. diagnostics of spinal deformities) and support high-level image analysis techniques (e.g. segmentation of vertebrae).

6.2 Method

6.2.1 Vertebral parameters and natural vertebral symmetry

The position and rotation of a vertebra in a 3D image can be represented by vertebral parameters p, i.e. by translation parameters t (coordinates x, y and z represent the sagittal, coronal and axial position of the center of rotation, respectively) and rotation parameters φ (angles α, β and γ represent the rotation around coordinate axes x, y and z, respectively):

$$p = (t, \varphi) = (x, y, z, \alpha, \beta, \gamma) \ . \tag{6.1}$$

Symmetrical volume pairs of vertebral anatomy can be obtained by dividing the vertebral body by the following planes (figure 6.1, p. 114):

- The mid-sagittal plane of the vertebral body splits the whole vertebra into symmetrical left and right parts I_x and I'_x.
- The mid-coronal plane of the vertebral body splits the vertebral body into symmetrical anterior and posterior parts I_y and I'_y.
- The mid-axial plane of the vertebral body splits the vertebral body (and intervertebral discs) into symmetrical cranial and caudal parts I_z and I'_z.

The proposed method is based on the assumption that, if the translation parameters t are defined by the center of vertebral body and the rotation parameters φ are defined by the rotation of vertebra, the vertebral parameters p can be obtained by exploiting the natural symmetry of vertebral anatomy.

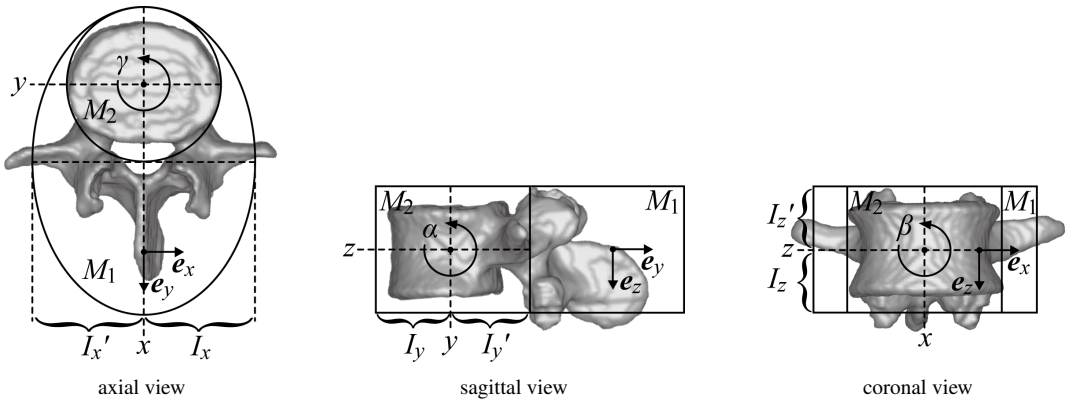

Figure 6.1. Division of the vertebral body by mid-sagittal, mid-coronal and mid-axial planes, yielding symmetrical volume pairs I_x - I'_x, I_y - I'_y and I_z - I'_z, respectively. The symmetry captured within two vertebral masks, M_1 and M_2, is used to determine the vertebral parameters $p = (x, y, z, \alpha, \beta, \gamma)$.

6.2.2 Registration of symmetrical vertebral parts

For each vertebra, two 3D vertebral masks, defined as elliptical cylinders, are created. The first mask M_1 roughly encompasses the whole vertebra and the second mask M_2 encompasses the vertebral body. The mid-axial, mid-sagittal and mid-coronal planes of the two masks determine mirror volume pairs that, when the vertebral masks are perfectly aligned with the vertebra (figure 6.1, p. 114), contain symmetrical parts of vertebral anatomy. Therefore, the vertebral masks most correctly estimate the parameters p (equation 6.1, p. 113) when the symmetry within the two masks is maximal.

The sagittal ($d = x$), coronal ($d = y$) and axial ($d = z$) symmetry S of the mirror volume pairs I_d and I'_d in the vertebral mask M is estimated by comparing the corresponding intensity gradients of I_d and I'_d (figure 6.2a, p. 115):

$$S\left(I_d, I'_d\right)\big|_M = -\frac{1}{K}\sum_{k=1}^{K}\left(v_k \cdot m_d\right)\left(\hat{v}'_k \cdot m_d\right) = \frac{1}{K}\sum_{k=1}^{K}|v_k|\left|v'_k\right|\cos\theta_k \cos\theta'_k\,, \tag{6.2}$$

where K is the number of voxels in each volume, and θ and θ' are the angles of the gradient vector v and its corresponding pair v' ($\hat{v}'$ denotes the mirrored vector), respectively, against the directional unit vector m_d; $d = \{x, y, z\}$ in the coordinate system of the mask M. The computed symmetry is a measure of similarity of gradient vectors v and $\hat{v}'$, projected in the selected direction d. The larger are the vectors and the more similar are their directions, the higher is the computed symmetry.

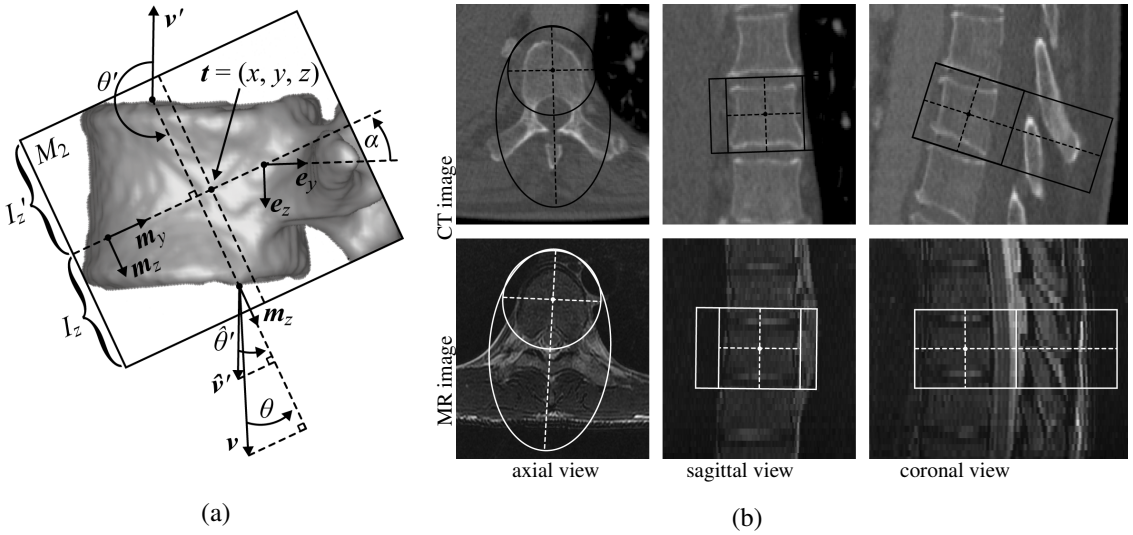

Figure 6.2. (a) An illustrative example of the computation of the axial symmetry $S_z\left(I_z, I'_z\right)$ for a single point inside the vertebral mask M_2. (b) Example of the initialization of vertebral masks for the T7 vertebra in their mid-plane cross-sections.

The sum of symmetries over the mid-sagittal ($d = x$) plane in mask M_1, and over the mid-coronal ($d = y$) and mid-axial ($d = z$) planes in mask M_2, represents the joint symmetry. The joint symmetry is therefore used as a criterion function $CF = CF(p)$ for the rigid registration of the corresponding mirror volume pairs:

$$CF = S\left(I_x, I'_x\right)\Big|_{M_1} + S\left(I_y, I'_y\right)\Big|_{M_2} + S\left(I_z, I'_z\right)\Big|_{M_2}. \tag{6.3}$$

The criterion function reaches its maximum (figure 6.3, p. 116) at vertebral parameters p^{opt} that maximize the joint symmetry of the mirror volume pairs, obtained from the 3D vertebral masks.

6.3 Experiments and results

6.3.1 Data and experiments

The proposed method was evaluated on 26 vertebrae from two CT (voxel size 0.7 × 0.7 × 1.0 mm) and 26 vertebrae from two T_2-weighted MR (voxel size 0.4 × 0.4 × 3.0 mm) spine images (table 6.1, p. 119). The images were filtered with a Gaussian kernel ($\sigma = 2$ mm) and the gradients were computed for each voxel. For the purpose of quantitative evaluation of the method, the position and rotation of each vertebra were determined manually (manually determined vertebral parameters p_{man}). The vertebral parameters were normalized, so that the

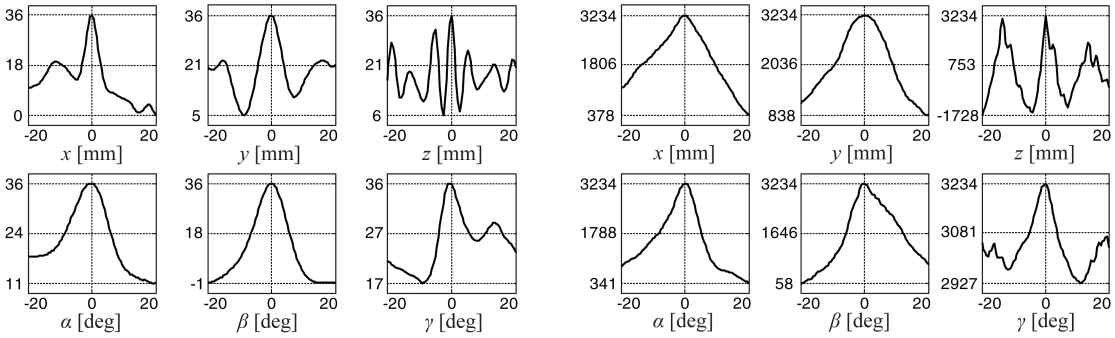

(a) (b)

Figure 6.3. Criterion function $CF = CF(p)$ (joint symmetry), evaluated by displacing each reference vertebral parameter independently, shown for the T7 vertebra from (a) a CT and (b) an MR spine image. The criterion function has rather large capture ranges and distinctive maxima.

translation of $t = (1, 1, 1)$ mm and rotation of $\varphi = (2, 2, 2)$ degrees were represented as a translation of $p_N = (1, 1, 1, 1, 1, 1)$ mm in the normalized parameter space (displacement $D = \sqrt{6}$ mm). The direction set (Powell's) method in multidimensions ($N_{iter} = 4$, $f_{tol} = 10^{-5}$) was used as the optimization technique in the registration procedure. The sizes of the 3D vertebral masks (figure 6.2b, p. 115) were $M_1 = (30, 50, 25)$ mm and $M_2 = (25, 25, 25)$ mm ($M = (a, b, c)$, where a and b are the ellipse half-axes and c is the cylinder half-height).

Manual determination of vertebral parameters is a difficult and error-prone task, affected by the subjective interpretation of the observer, low image resolution, vertebral torsion, imperfect symmetry of vertebral structures and interdependence of parameters (i.e. the center of rotation affects the rotation angles). An initial experiment of $N_1 = 50$ registrations was therefore performed on each vertebra to obtain the reference vertebral parameters. The registrations were initialized in the manually determined parameters p_{man}, and the starting positions were defined by randomly generated displacements ($D_{1,max} = 5$ mm), uniformly distributed in the normalized parameter space. The median of the obtained results represented the reference vertebral parameters p_{ref}, which were used for initialization in the main experiment of $N_2 = 500$ registrations on each vertebra ($D_{2,max} = 10$ mm). The results of the main experiment represented the basis for the quantitative evaluation of the proposed method.

6.3.2 Results

The results, presented in table 6.1 (p. 119) for all vertebrae, show that the method was successful on 23 out of 26 vertebrae from CT and on 20 out of 26 vertebrae from MR spine images. The cases of failure were detected by the large median displacement after the initial or main

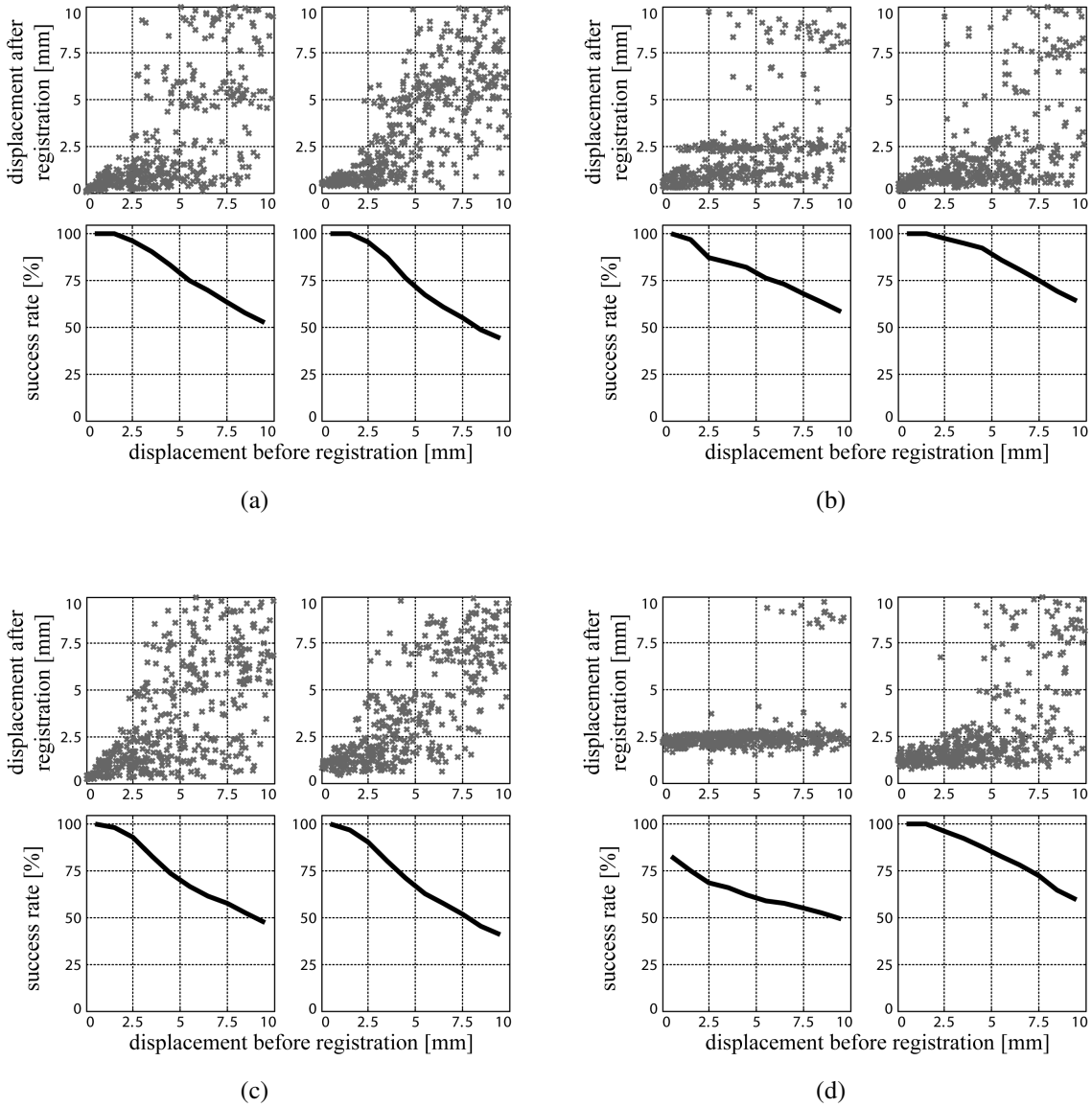

Figure 6.4. Scatter plots of the displacements of vertebral parameters from the reference vertebral parameters p_{ref} in the normalized parameter space before and after the main registration experiment ($N_2 = 500$), and the corresponding success rates ($D_{th} = \sqrt{6} \approx 2.45$ mm), shown for the T7 vertebrae in (a) CT and (b) MR spine images and for the T9 vertebrae in (c) CT and (d) MR spine images.

experiment ($\widetilde{D} > 10$ mm). Visual verification indicated that failures probably occurred due to non-vertebral anatomical structures such as ribs and arteries, which are less or non-symmetrical. Nevertheless, the method was successful for most vertebrae (43 out of 52; 83%), for which the mean of the median displacements after registration from the manually determined vertebral parameters p_{man} was 2.8 mm (initial experiment $N_1 = 50$) and from the reference vertebral parameters p_{ref} 1.3 mm (main experiment $N_2 = 500$). The results also show that the method is more accurate on CT spine images, which may be due to more distinctive intensity edges and higher image resolution in CT than in MR images used in the experiments.

Success rates, which are the cumulative ratios of successful registrations against all registrations, were obtained from the scatter plots of the main registration experiment results (figure 6.4, p. 117). A registration was considered successful when the displacement after registration was less than the threshold $D_{th} = \sqrt{6} \approx 2.45$ mm in the normalized parameter space, which corresponds to the translation of $t = (1, 1, 1)$ mm and rotation of $\varphi = (2, 2, 2)$ degrees. The obtained success rates indicated that an arbitrary registration converges if the displacement is lower than $D_{conv} \approx 2.5$ mm, which corresponds to a translation of 2.5 mm in a single direction or a rotation of 5.0 degrees around a single axis from the reference vertebral parameters.

6.4 Discussion

We proposed a method for the automated determination of position and rotation of vertebrae in 3D, which are among the most important parameters in the evaluation of spinal deformities. The method is applicable to both CT and MR spine images (i.e. modality-independent method) and exploits global characteristics of vertebral anatomy (i.e. natural symmetry of the vertebra). Moreover, image reformation, manual selection of cross-sections or a priori knowledge in the form of statistical shape models is not required. The size of the vertebral masks can be obtained by statistical analysis of the population.

The results show that the position and rotation of vertebrae in 3D can be successfully determined by the proposed gradient-based evaluation of vertebral symmetry. We have recently presented an intensity-based method for evaluation of symmetry on lumbar vertebrae in CT spine images (Vrtovec et al., 2007), where we reported low convergence of y and z translation parameters and, on the other hand, high precision of the method ($D_{conv} \approx 5.0$ mm). Although the proposed gradient-based method improves the distinctiveness of the maxima of the criterion function (figure 6.3, p. 116), a combination of the intensity and gradient-based approaches may result in a method of relatively high success rate and precision, which is the topic of ongoing research.

Table 6.1. Median displacements $\widetilde{D}_1$ and $\widetilde{D}_2$ after registration from the manually determined (p_{man}) and reference (p_{ref}) vertebral parameters, respectively, in the normalized parameter space for the vertebrae in CT and MR spine images (the mark × denotes the unsuccessful parameter estimations).

CT		**MR**		$\widetilde{D}_1$ **(**p_{man}**) [mm]**				$\widetilde{D}_2$ **(**p_{ref}**) [mm]**			
1	**2**	**1**	**2**	**(**N_1 **= 50)**				**(**N_2 **= 500)**			
T1	T1			3.1	3.3			0.8	0.9		
T2	T2			3.6	2.3			0.9	0.7		
T3	T3			2.5	5.0			1.0	1.6		
T4	T4			×	1.5			×	1.5		
T5	T5	T5	T5	3.5	2.5	3.2	3.0	0.7	×	×	1.3
T6	T6	T6	T6	4.6	2.0	4.4	×	0.7	1.1	×	×
T7	T7	T7	T7	2.0	3.0	3.0	1.9	0.9	1.0	1.2	0.9
T8	T8	T8	T8	2.2	3.7	1.9	1.9	1.0	2.5	1.1	0.7
T9	T9	T9	T9	2.2	1.9	3.0	2.7	1.2	1.6	2.3	1.4
T10	T10	T10	T10	1.7	2.6	2.7	4.2	1.0	2.4	1.7	×
T11	T11	T11	T11	2.3	3.9	2.4	3.3	0.7	×	1.2	×
T12	T12	T12	T12	1.1	1.1	1.4	3.9	0.7	0.8	0.8	×
	L1	L1	L1		2.4	4.9	3.3		0.4	0.7	2.5
	L2	L2	L2		1.6	1.9	2.4		0.7	2.3	2.4
		L3	L3			2.6	2.1			1.6	2.4
		L4	L4			3.8	2.8			0.9	1.9
		L5	L5			3.0	5.7			1.7	1.3
mean				**2.6**		**3.0**		**1.1**		**1.5**	

When shall we three meet again,
in thunder, lightning, or in rain?
When the hurly-burly's done,
when the battle's lost and won.

William Shakespeare, 1564 - 1616
(Macbeth, 1606)

CHAPTER 7

Conclusion

Automatic analysis of medical images is a wide area of scientific research that aims to develop new clinical tools for modern diagnostic radiology and medical health care. The focus of this thesis was on automatic analysis of three-dimensional (3D) spine images, a relatively specific field in medical image analysis with its own characteristics and requirements. The increasing number of scientific publications over the past years indicates that automatic analysis of spine images is becoming of particular interest. Although current methods for the treatment of spinal injuries and degenerative spinal disorders reach clinical expectations, the methods are still not widely accepted. However, present-day sedentary lifestyle reflects in spine and spine-related diseases affecting more and more people. This is why modern imaging techniques and automated image analysis methods play an important role in diagnosis and treatment planning for spinal disorders.

The methods for automated curved planar reformation (CPR) of computed tomography (CT) and magnetic resonance (MR) spine images were presented in chapter 2 and chapter 3, respectively. The main purpose of the proposed automated CPR methods is to reduce the structural complexity in favour of an improved feature perception of the spine, and to provide clinically relevant quantitative analysis of the 3D spine anatomy. Displaying the whole length of the spine within a single two-dimensional (2D) image makes the inspection of images quicker and more precise, while the probability of overlooking certain important features of the spine is reduced. The curvature of the spine and the rotation of vertebrae around the spine curve were obtained

automatically and used to transform the 3D spine images from the image-based to the spine-based coordinate system. The spinal curvature and vertebral rotation are inherent properties of the spine and therefore not affected by rigid body transformations. The generated CPR images are therefore independent of the position of the patient in the scanner and of the orientation of the image acquisition plane. Moreover, when visualizing and inspecting 3D images in the spine-based coordinate system, pathological anatomy is oriented comparable to healthy anatomy, thus facilitating image interpretation and allowing a more objective evaluation and diagnosis of the abnormalities, especially in the case of significant coronal (i.e. scoliosis) or sagittal (i.e. kyphosis or lordosis) spinal curvatures. CT is a standard orthopaedic modality that provides a good bone contrast but a relatively large radiation dose. On the other hand, MR is a non-invasive alternative that is especially adequate for frequent and whole-body scanning. The proposed spine-based coordinate system is modality-independent and therefore it may be used to join the advantages of both modalities by data fusion, i.e. by merging the CT and MR images of the same patient. Among the most significant parameters that may assist an orthopaedic surgeon in evaluating spinal deformities, is the length of the spinal axis, the Cobb angle, the locations of the centers of vertebral bodies, and vertebral rotation angles, i.e. axial rotation, sagittal and coronal inclination. Besides direct automated localization of the centers of vertebral bodies (i.e. the 3D spine curve) and measurement of axial vertebral rotation, the proposed methods implicitly allow automated measurement of the remaining parameters. The length of the spinal axis can be computed from the arc length, which is a geometrical property of the parameterized 3D spine curve. In case of a scoliotic spinal deformity, the location of the end vertebrae could be extracted from the course of curvature and axial vertebral rotation, allowing the measurement of the Cobb angle. The sagittal and coronal vertebral inclinations can be associated with the inclination of the planes, orthogonal to the 3D spine curve. Furthermore, the knowledge on the location and orientation of the spine in 3D can be exploited by other image analysis techniques and applied in a clinical environment. For example, for the identification and measurement of the dimensions of the spinal canal and the spinal cord, for segmentation methods that model the spinal curvature by taking into account spatial relationships between vertebrae, for statistical shape analysis of vertebrae and/or for the determination of inter- and intra-vertebral rotations. Automated measurement of the spine-specific parameters may therefore provide a complete quantitative representation of the spine in 3D.

A framework for quantitative analysis of spinal curvature in 3D was presented in chapter 4. The established methods for quantifying spinal deformities depend on various factors that induce high variability in the measurements (e.g. correct identification of the end vertebrae, determination of vertebral end-plate inclination). Besides, the methods are associated with a large number of clinically unintuitive parameters and/or require a relatively high degree of user interaction (e.g. precise outlining or drawing tangent lines to vertebral bodies). Moreover, although spinal curvatures can occur in an arbitrary plane, they are usually evaluated separately in either coronal or sagittal image plane, therefore in 2D. This requires the images to be uniform in orientation and size, which can be achieved by a standardized image acquisition process. On the

other hand, descriptors that measure the spinal curvature in 3D and are independent of the orientation and size of the spine may allow a more general (e.g. using images of different modality) and more objective (e.g. measuring the curvature in multiple image planes) evaluation of spinal deformities.

The main advantage of the presented 3D descriptors of geometric curvature (GC) and curvature angle (CA) is that the measurements are independent of the orientation and size of the spine. The acquisition of images is therefore not required to be standardized, thus allowing a comparison between images with different properties (e.g. different scanners, acquisition parameters, patient orientation, spinal deformities, clinical environments). The measures also do not depend on vertebral body or intervertebral disc shape, or vertebral end-plate inclination, but solely on the global properties of the 3D vertebral body lines, which were obtained by two different methods. The least squares fitting (LSF) method is based on spatial coordinates of vertebra centroids, which are clinically intuitive and can be unambiguously defined on images of different size, dimensionality (e.g. 2D or 3D images) and modality (e.g. radiographs, CT or MR images). However, the identification of vertebra centroids is a process that requires clinical experience and a relatively high amount of user interaction. The proposed automated edge distance optimization (EDO) method is an example of how computer-assisted image analysis techniques can be used to overcome these problems. The parametric description of the 3D vertebral body line may be useful in different applications and studies. Moreover, the analysis can be reduced to 2D without losing the independence of the orientation and size by observing the 3D vertebral body line separately in sagittal and coronal image planes. If the exact location of the thoracolumbar junction (TJ) was automatically identified, automated evaluation of total thoracic kyphosis (TK) and total lumbar lordosis (LL) may be possible. By comparing an arbitrary spine anatomy to the mean GC and CA values over a healthy population, the presence and exact location of hyperkyphosis and/or hyperlordosis may be easily identified and more objectively evaluated. The automated detection of all characteristic spine regions (i.e. flexion points of the 3D vertebral body line) may be further used to classify spinal deformities.

The methods for automated determination of position and rotation of vertebrae in 3D, which are among the most important parameters in the evaluation of spinal deformities, were proposed in chapters 5 and 6. The method in chapter 5 is intensity-based and applicable to CT spine images, while the method in chapter 6 is gradient-based an therefore modality-independent, i.e. applicable to both CT and MR spine images. In order do determine the vertebral position and rotation in 3D, the proposed methods do not require prior image reformation, identification of the most appropriate axial cross-section or aid by high-level a priori information, such as statistical shape and/or appearance models. Instead, the methods exploit global characteristics of the vertebral anatomy, i.e. the natural symmetry of the vertebra, the vertebral body, the vertebral column and the vertebral canal. The position and rotation of each vertebra (i.e. the vertebral parameters) were obtained by simultaneously matching mirror vertebra subvolumes by robust rigid autoregistration, where the natural symmetry of the vertebral anatomy was used as the similarity

measure. The results showed that the vertebral parameters can be successfully determined in CT and MR spine images, however, the determination of some of the parameters may need further improvement. When compared to the intensity-based method, the proposed modality-independent gradient-based method improved the distinctiveness of the similarity measure optima. Therefore, a combination of the intensity- and gradient-based approaches may result in a robust method with a relatively high success rate and precision. The natural symmetry of the vertebral anatomy may be exploited to model more detailed properties of the vertebral anatomy, for example, shear and/or twist of the subvolumes in the registration procedure may provide a good description of the mechanical vertebral torsion. The proposed method may also aid the measurement of the dimensions of vertebral pedicles, foraminae and canal, and may be a valuable tool for clinical evaluation of the spinal deformities in 3D.

In general, automated image analysis techniques highly depend on the resolution of images and time required to complete a series of computationally demanding tasks. Namely, the higher is the resolution of images, the better is the performance of the techniques and the more computationally demanding the tasks are. Modern CT and MR scanners already enable high resolution images that are acquired at a relatively high speed, yet the imaging technology is continuously advancing. Shorter acquisition times, greater numbers of cross-sections and increased power are the main characteristics of the next generation of CT and MR scanners, which will reflect in an even higher image resolution and reduction of the delivered ionizing radiation. The same holds true for the computational methods, as the next generation of computers will deliver computational speeds that will make present computationally demanding and therefore time-consuming tasks feasible for clinical practice.

Techniques for visualization and quantitative evaluation of medical images in general are extremely valuable in the development of image-assisted diagnosis, planning of surgical interventions and assessment of medical treatment outcomes. In the field of spine image analysis, quantitative assessment of spinal curvature and axial vertebral rotation is important not only for planning of orthopaedic surgical procedures and analysis of surgical results, but also for diagnosing and monitoring of the progression of spinal deformities. Computer-assisted visualization and quantitative evaluation of 3D spine images therefore remain challenging tasks in the field of medical image analysis.

I have always imagined that paradise will be
a kind of library.

JORGE LUIS BORGES, 1899 - 1986
(Dreamtigers, 1960)

Appendix

A Reprint permissions

Reprint permission in written form was obtained for the following material:

Figure 1.5a (p. 29): Roberts C, McDaniel N, Krupinski E, and Erly W. Oblique reformation in cervical spine computed tomography: A new look at an old friend. *Spine*, 28(2):167–170, 2003, © by Lippincott Williams & Wilkins.

Figure 1.5b (p. 29): Newton P, Hahn G, Fricka K, and Wenger D. Utility of three-dimensional and multiplanar reformatted computed tomography for evaluation of pediatric congenital spine abnormalities. *Spine*, 27(8):844–850, 2002, © by Lippincott Williams & Wilkins.

Figure 1.12a (p. 40): Rogers B, Wiese S, Blankenbaker D, Meyerand E, and Haughton V. Accuracy of an automated method to measure rotations of vertebrae from computerized tomography data. *Spine*, 30(6):694—696, 2005, © by Lippincott Williams & Wilkins.

Figure 1.12b (p. 40): Kouwenhoven J-WM, Vincken KL, Bartels LW, and Castelein RM. Analysis of preexistent vertebral rotation in the normal spine. *Spine*, 31(13):1467—1472, 2006, © by Lippincott Williams & Wilkins.

Figure 1.12c (p. 40): Adam CJ and Askin GN. Automatic measurement of vertebral rotation in idiopathic scoliosis. *Spine*, 31(3):E80—E83, 2006, © by Lippincott Williams & Wilkins.

Figure 1.13a (p. 41): Birchall D, Hughes D, Gregson V, and Williamson B. Demonstration of vertebral and disc mechanical torsion in adolescent idiopathic scoliosis using three-dimensional MR imaging. *European Spine Journal*, 14(2):123—129, 2005, © with kind permission from Springer Science and Business Media.

Figure 1.13b (p. 41): Haughton VM, Rogers B, Meyerand E, and Resnick DK. Measuring the axial rotation of lumbar vertebrae in vivo with MR imaging. *American Journal of Neuroradiology*, 23(7):1110—1116, 2002, © by American Society of Neuroradiology.

Figure 1.13c (p. 41): Rogers B, Haughton V, Arfanakis K, and Meyerand E. Application of image registration to measurement of intervertebral rotation in the lumbar spine. *Magnetic Resonance in Medicine*, 48(6):1072—1075, 2002, © reprinted with permission of Wiley-Liss, Inc., a subsidiary of John Wiley & Sons, Inc.

Always read stuff that will make you look good if you die in the middle of it.

PATRICK J. O'ROURKE, 1947 -

Bibliography

Aaro S and Dahlborn M. Estimation of vertebral rotation and the spinal and rib cage deformity in scoliosis by computer-tomography. *Spine*, 6(5):460–467, 1981. (cited on pages 13, 14, 37, 38, 39, 78, 96 and 109)

Adam C and Askin G. Automatic measurement of vertebral rotation in idiopathic scoliosis. *Spine*, 31(3):E80–E83, 2006. (cited on pages 9, 14, 31, 39, 40, 97 and 112)

Adam C, Izatt M, Harvey J, and Askin G. Variability in Cobb angle measurements using reformatted computerized tomography scans. *Spine*, 30(14):1664–1669, 2005. (cited on pages 11, 34 and 82)

Ajemba P, Ramirez L, Durdle N, Hill D, and Raso V. A support vectors classifier approach to predicting the risk of progression of adolescent idiopathic scoliosis. *IEEE Transactions on Information Technology in Biomedicine*, 9(2):276–282, 2005. (cited on pages 10 and 32)

Amendt L, Ause-Ellias K, Eybers J, Wadsworth C, Nielsen D, and Weinstein S. Validity and reliability testing of the Scoliometer. *Physical Therapy*, 70(2):108–117, 1990. (cited on pages 11 and 34)

Apicella P and Mirowitz S. Interactive multiplanar reformation of conventional two-dimensional MR images. *Clinical Imaging*, 19(4):279–282, 1995. (cited on pages 9, 30 and 66)

Arlet V, Odent T, and Aebi M. Congenital scoliosis. *European Spine Journal*, 12(5):456–463, 2003. (cited on pages 10 and 32)

Aronsson D, Stokes I, Ronchetti P, and Richards B. Surgical correction of vertebral axial rotation in adolescent idiopathic scoliosis: Prediction by lateral bending films. *Journal of Spinal Disorders & Techniques*, 9(3):214–219, 1996. (cited on pages 10, 31, 76 and 96)

Asamoah V, Mellerowicz H, Venus J, and Klöckner C. Measuring the surface of the back: Value in diagnosis of spinal diseases. *Orthopade*, 29(6):480–489, 2000. (cited on pages 11 and 33)

Asazuma T, Nakamura M, Matsumoto M, Chibo K, and Toyama Y. Postoperative changes of spinal curvature and range of motion in adult patients with cervical spinal cord tumors: Analysis of 51 cases and review of the literature. *Journal of Spinal Disorders & Techniques*, 17(3):178–182, 2004. (cited on pages 10, 32 and 82)

Aykroyd R and Mardia K. A wavelet approach to shape analysis for spinal curves. *Journal of Applied Statistics*, 30(6):605–623, 2003. (cited on pages 11 and 34)

Aylward S and Bullitt E. Initialization, noise, singularities, and scale in height ridge traversal for tubular object centerline extraction. *IEEE Transactions on Medical Imaging*, 21(2):61–75, 2002. (cited on pages 6, 25 and 49)

Bankman I, Spitz T, and Pavlopoulos S. Two-dimensional shape and texture quantification. In: *Handbook of Medical Imaging: Processing and Analysis* (I Bankman, ed.), chap. 14, pp. 215–230 (Academic Press, San Diego, CA, USA), 2000. (cited on pages 7 and 26)

Beekman C and Hall V. Variability of scoliosis measurement from spinal roentgenograms. *Physical Therapy*, 59(6):764–765, 1979. (cited on pages 11 and 32)

Benameur S, Mignotte M, De Guise J, Benameur S, Parent S, Labelle H, and Skalli W. 3D/2D registration and segmentation of scoliotic vertebrae using statistical models. *Computerized Medical Imaging and Graphics*, 27(5):321–337, 2003a. (cited on page 61)

Benameur S, Mignotte M, Parent S, Labelle H, Skalli W, and De Guise J. A hierarchical statistical modeling approach for the unsupervised 3D reconstruction of the scoliotic spine. In: *Proceedings of the 10th IEEE International Conference on Image Processing - ICIP 2003*, vol. 1, pp. 561–564 (IEEE, Barcelona, Spain), 2003b. (cited on pages 49 and 61)

Benameur S, Mignotte M, Destrempes F, and De Guise J. Three-dimensional biplanar reconstruction of scoliotic rib cage using the estimation of a mixture of probabilistic prior models. *IEEE Transactions on Biomedical Engineering*, 52(10):1713–1728, 2005a. (cited on pages 15 and 42)

Benameur S, Mignotte M, Labelle H, and De Guise J. A hierarchical statistical modeling approach for the unsupervised 3-D biplanar reconstruction of the scoliotic spine. *IEEE Transactions on Biomedical Engineering*, 52(12):2041–2057, 2005b. (cited on pages 15, 42, 97 and 112)

Bendels G, Klein R, Samimi M, and Schmitz A. Statistical shape analysis for computer aided spine deformity detection. In: *Journal of WSCG: Proceedings of the 13th International*

Conference in Central Europe on Computer Graphics, Visualization and Computer Vision (V Skala, ed.), vol. 13, pp. 57–64 (Plzen - Bory, Czech Republic), 2005. (cited on pages 11 and 34)

Benson D, Schultz A, and Dewald R. Roentgenographic evaluation of vertebral rotation. *Journal of Bone and Joint Surgery - American Volume*, 58(8):1125–1129, 1976. (cited on pages 12 and 34)

Bergeron C, Labelle H, Ronsky J, and Zernicke R. Robust prediction of three-dimensional spinal curve from back surface for non-invasive follow-up of scoliosis. In: *Proceedings of the SPIE Medical Imaging 2005: Visualization, Image-Guided Procedures, and Display Conference* (R Galloway and K Cleary, eds.), vol. 5744, pp. 772–780 (SPIE, San Diego, CA, USA), 2005. (cited on pages 11 and 34)

Bernhardt M and Bridwell K. Segmental analysis of the sagittal plane alignment of the normal thoracic and lumbar spines and thoracolumbar junction. *Spine*, 14(7):717–721, 1989. (cited on pages 12, 35, 82, 83, 87, 97 and 112)

Berthonnaud E, Dimnet J, Roussouly P, and Labelle H. Analysis of the sagittal balance of the spine and pelvis using shape and orientation parameters. *Journal of Spinal Disorders & Techniques*, 18(1):40–47, 2005a. (cited on pages 83, 92 and 98)

Berthonnaud E, Labelle H, Roussouly P, Grimard G, Vaz G, and Dimnet J. A variability study of computerized sagittal spinopelvic radiologic measurements of trunk balance. *Journal of Spinal Disorders & Techniques*, 18(1):66–71, 2005b. (cited on pages 14 and 40)

Bifulco P, Sansone M, Cesarelli M, Allen R, and Bracale M. Estimation of out-of-plane vertebra rotations on radiographic projections using CT data: A simulation study. *Medical Engineering and Physics*, 24(4):295–300, 2002. (cited on pages 15 and 42)

Birchall D, Hughes D, Hindle J, Robinson L, and Williamson J. Measurement of vertebral rotation in adolescent idiopathic scoliosis using three-dimensional magnetic resonance imaging. *Spine*, 22(20):2403–2407, 1997. (cited on pages 9, 14, 31, 39, 76, 78, 79, 97 and 112)

Birchall D, Hughes D, Gregson B, and Williamson B. Demonstration of vertebral and disc mechanical torsion in adolescent idiopathic scoliosis using three-dimensional MR imaging. *European Spine Journal*, 14(2):123–129, 2005. (cited on pages 14, 39 and 41)

Bitter I, Sato M, Bender M, McDonnell KT, Kaufman A, and Wan M. CEASAR: A smooth, accurate and robust centerline extraction algorithm. In: *Proceedings of the IEEE Visualization 2000 Conference - Vis 2000* (T Ertl, B Hamann, and A Varshney, eds.), pp. 45–52 (IEEE, Salt Lake City, UT, USA), 2000. (cited on pages 6, 25 and 49)

Bjõrck A. *Numerical methods for least squares problems* (SIAM: Society for Industrial and Applied Mathematics, Philadelphia, PA, USA), 1996. (cited on page 84)

Boisvert J, Pennec X, Ayache N, Labelle H, and Cheriet F. 3D anatomical variability assessment

of the scoliotic spine using statistics on Lie groups. In: *Proceedings of the 3rd IEEE International Symposium on Biomedical Imaging: From Nano to Macro - ISBI 2006*, pp. 750–753 (IEEE, Arlington, VA, USA), 2006. (cited on pages 11 and 34)

Booth S and Clausi D. Image segmentation using MRI vertebral cross-sections. In: *Proceedings of the IEEE 2001 Canadian Conference on Electrical and Computer Engineering* (S Dunne, ed.), vol. 2, pp. 1303–1307 (IEEE, Totonto, ON, Canada), 2001. (cited on pages 14 and 39)

Börnert P. 2D RF-pulse-encoded curved-slice imaging. *Magnetic Resonance Materials in Physics Biology and Medicine*, 16(2):86–92, 2003. (cited on pages 7, 25 and 66)

Börnert P and Schäffter T. Curved slice imaging. *Magnetic Resonance in Medicine*, 36(6):932–939, 1996. (cited on pages 7 and 25)

Brant-Zawadzki M. CT screening: Why I do it. *American Journal Of Roentgenology*, 179(2):319–326, 2002. (cited on pages 11 and 34)

Brown M and McNitt-Gray M. Medical image interpretation. In: *Handbook of Medical Imaging Vol 2. Medical Image Processing and Analysis* (M Sonka and J Fitzpatrick, eds.), chap. 7, pp. 399–445 (SPIE Press, Bellingham, WA, USA), 2000. (cited on pages 7 and 26)

Brown M and Semelka R. MR imaging abbreviations, definitions, and descriptions: A review. *Radiology*, 213(3):647–662, 1999. (cited on pages 9 and 30)

Campbell-Kyureghyan N, Jorgensen M, Burr D, and Marras W. The prediction of lumbar spine geometry: Method development and validation. *Clinical Biomechanics*, 20(5):455–464, 2005. (cited on pages 11 and 34)

Carballido-Gamio J, Belongie S, and Majumdar S. Normalized cuts in 3-D for spinal MRI segmentation. *IEEE Transactions on Medical Imaging*, 23(1):36–44, 2004. (cited on pages 15 and 42)

Carman D, Browne R, and Birch J. Measurement of scoliosis and kyphosis radiographs: Intraobserver and interobserver variation. *Journal of Bone and Joint Surgery - American Volume*, 72(3):328–333, 1990. (cited on pages 11 and 32)

Cassar-Pullicino V and Eisenstein S. Imaging in scoliosis: What, why and how? *Clinical Radiology*, 57(7):543–562, 2002. (cited on pages 10, 32, 61, 62 and 79)

Chen YT and Wang MS. Three-dimensional reconstruction and fusion for multi-modality spinal images. *Computerized Medical Imaging and Graphics*, 28(1–2):21–31, 2004. (cited on pages 14, 15 and 42)

Cheung J, Wever D, Veldhuizen A, Klein J, Verdonck B, Nijlunsing R, Cool J, and Van Horn J. The reliability of quantitative analysis on digital images of the scoliotic spine. *European Spine Journal*, 11(6):535–542, 2002. (cited on pages 11, 33, 62, 82 and 97)

Chi WM, Cheng CW, Yeh WC, Chuang SC, Chang TS, and Chen JH. Vertebral axial rotation

measurement method. *Computer Methods and Programs in Biomedicine*, 81(1):8–17, 2006. (cited on pages 12, 34 and 96)

Chockalingam N, Dangerfield P, Giakas G, Cochrane T, and Dorgan J. Computer-assisted Cobb measurement of scoliosis. *European Spine Journal*, 11(4):353–357, 2002. (cited on pages 11, 33, 82, 88, 97 and 112)

Cholewicki J, Crisco J, Oxland T, Yamamoto I, and Panjabi M. Effects of posture and structure on three-dimensional coupled rotations in the lumbar spine: A biomechanical analysis. *Spine*, 21(21):2421–2428, 1996. (cited on pages 14 and 40)

Cobb J. Outline for the study of scoliosis. *American Academy of Orthopaedic Surgeons Instructional Course Lectures*, 5:261–275, 1948. (cited on pages 10, 12, 32, 33, 34, 35, 36, 82, 88, 96, 97 and 112)

Coetsier M, Vercauteren M, and Moerman P. A new radiographic method for measuring vertebral rotation in scoliosis. *Acta Orthopaedica Belgica*, 43(5):598–605, 1977. (cited on pages 12 and 34)

Coonrad R, Murrell G, Motley G, Lytle E, and Hey L. A logical coronal pattern classification of 2,000 consecutive idiopathic scoliosis cases based on the Scoliosis Research Society-defined apical vertebra. *Spine*, 23(12):1380–1391, 1998. (cited on pages 10 and 32)

Côté P, Cassidy J, Yong-Hing K, Sibley J, and Loewy J. Apophysial joint degeneration, disc degeneration, and sagittal curve of the cervical spine: Can they be measured reliably on radiographs? *Spine*, 22(8):859–864, 1997. (cited on pages 12 and 35)

Cyteval C, Thomas E, Picot M, Derieffy P, Blotman F, and Taourel P. Normal vertebral body dimensions: A new measurement method using MRI. *Osteoporosis International*, 13(6):468–473, 2002. (cited on pages 10 and 32)

De Smet A, Tarlton M, Cook L, Fritz S, and Dwyer S. A radiographic method for three-dimensional analysis of spinal configuration. *Radiology*, 137(2):343–348, 1980. (cited on pages 12 and 35)

Deacon P, Flood B, and Dickson R. Idiopathic scoliosis in three dimensions: A radiographic and morphometric analysis. *Journal of Bone and Joint Surgery - British Volume*, 66(4):509–512, 1984. (cited on pages 11, 12, 32 and 34)

Diab K, Sevastik J, Hedlund R, and Suliman I. Accuracy and applicability of measurement of the scoliotic angle at the frontal plane by Cobb's method, by Ferguson's method and by a new method. *European Spine Journal*, 4(5):291–295, 1995. (cited on pages 11 and 32)

Do T, Fras C, Burke S, Widmann R, Rawlins B, and Boachie-Adjei O. Clinical value of routine preoperative magnetic resonance imaging in adolescent idiopathic scoliosis: A prospective study of three hundred and twenty-seven patients. *Journal of Bone and Joint Surgery - American Volume*, 83-A(4):577–579, 2001. (cited on pages 10 and 32)

Doi K, MacMahon H, Katsuragawa S, Nishikawa R, and Jiang Y. Computer-aided diagnosis in radiology: Potential and pitfalls. *European Journal of Radiology*, 31(2):97–109, 1997. (cited on pages 14, 15, 40 and 42)

Drerup B. Principles of measurement of vertebral rotation from frontal projections of the pedicles. *Journal of Biomechanics*, 17(12):923–935, 1984. (cited on pages 12 and 34)

Drerup B. Improvements in measuring vertebral rotation from the projections of the pedicles. *Journal of Biomechanics*, 18(5):369–378, 1985. (cited on pages 12 and 34)

Drerup B. Radiologic interpretation of lumbar vertebral rotation. *Spine*, 17(6):728–729, 1992. (cited on pages 12 and 34)

Drerup B and Hierholzer E. Evaluation of frontal radiographs of scoliotic spines - part I: Measurement of position and orientation of vertebrae and assessment of clinical shape parameters. *Journal of Biomechanics*, 25(11):1357–1362, 1992a. (cited on pages 12 and 35)

Drerup B and Hierholzer E. Evaluation of frontal radiographs of scoliotic spines - part II: Relations between lateral deviation, lateral tilt and axial rotation of vertebrae. *Journal of Biomechanics*, 25(12):1443–1450, 1992b. (cited on pages 12 and 35)

Drerup B and Hierholzer E. Back shape measurement using video rasterstereography and 3-dimensional reconstruction of spinal shape. *Clinical Biomechanics*, 9(1):28–36, 1994. (cited on pages 11 and 34)

Drerup B and Hierholzer E. Assessment of scoliotic deformity from back shape asymmetry using an improved mathematical model. *Clinical Biomechanics*, 11(7):376–383, 1996. (cited on pages 11, 32, 62 and 78)

Duke K, Aubin C, Dansereau J, and Labelle H. Biomechanical simulations of scoliotic spine correction due to prone position and anaesthesia prior to surgical instrumentation. *Clinical Biomechanics*, 20(9):923–931, 2005. (cited on pages 10, 31 and 82)

Dumas R, Le Bras A, Champain N, Savidan M, Mitton D, Kalifa G, Steip JP, De Guise J, and Skalli W. Validation of the relative 3D orientation of vertebrae reconstructed by bi-planar radiography. *Medical Engineering and Physics*, 26(5):415–422, 2004. (cited on pages 12 and 35)

Duong L, Cheriet F, and Labelle H. Three-dimensional classification of spinal deformities using fuzzy clustering. *Spine*, 31(8):923–930, 2006. (cited on page 83)

Edgar M. A new classification of adolescent idiopathic scoliosis. *Lancet*, 360(9329):270–271, 2002. (cited on pages 10 and 32)

Ferguson A. The study and treatment of scoliosis. *Southern Medical Journal*, 23:116–120, 1930. (cited on pages 10, 32 and 33)

Ge Y, Stelts D, Vining D, Wang J, and Ge Y. Computing the centerline of a colon: A ro-

bust and efficient method based on 3D skeletons. *Journal of Computer Assisted Tomography*, 23(5):786–794, 1999. (cited on pages 6, 25 and 49)

Ghebreab S and Smeulders A. Combining strings and necklaces for interactive three-dimensional segmentation of spinal images using an integral deformable spine model. *IEEE Transactions on Biomedical Engineering*, 51(10):1821–1829, 2004. (cited on pages 15, 42, 49 and 61)

Giger M. Computer-aided diagnosis in radiology. *Academic Radiology*, 9(1):1–3, 2002. (cited on pages 15 and 42)

Gille O, Champain N, Benchikh-El-Fegoun A, Vital JM, and Skalli W. Reliability of 3D reconstruction of the spine of mild scoliotic patients. *Spine*, 32(5):568–573, 2007. (cited on pages 11, 15, 34 and 42)

Glassman S, Berven S, Bridwell K, Horton W, and Dimar J. Correlation of radiographic parameters and clinical symptoms in adult scoliosis. *Spine*, 30(6):682–688, 2005a. (cited on pages 14 and 40)

Glassman S, Bridwell K, Dimar J, Horton W, Berven S, and Schwab F. The impact of positive sagittal balance in adult spinal deformity. *Spine*, 30(18):2024–2029, 2005b. (cited on pages 14 and 40)

Göçen S, Havitçioglu H, and Alici E. A new method to measure vertebral rotation from CT scans. *European Spine Journal*, 8(4):261–265, 1999. (cited on pages 13, 37, 38, 62, 78, 96 and 109)

Goh S, Price R, Leedman P, and Singer K. A comparison of three methods for measuring thoracic kyphosis: Implications for clinical studies. *Rheumatology*, 39(3):310–315, 2000a. (cited on pages 11, 12, 33, 36, 37, 82, 88 and 97)

Goh S, Tan C, Price R, Edmondston S, Song S, Davis S, and Singer K. Influence of age and gender on thoracic vertebral body shape and disc degeneration: An MR investigation of 169 cases. *Journal of Anatomy*, 197(4):647–657, 2000b. (cited on pages 14 and 42)

Gong JS and Xu JM. Role of curved planar reformations using multidetector spiral CT in diagnosis of pancreatic and peripancreatic diseases. *World Journal of Gastroenterology*, 10(13):1943–1947, 2004. (cited on pages 6, 25 and 49)

Greenspan A, Pugh J, Norman A, and Norman R. Scoliotic index: A comparative evaluation of methods for the measurement of scoliosis. *Bulletin of the Hospital for Joint Diseases*, 39(2):117–125, 1978. (cited on pages 10, 32 and 33)

Grenier JM, Scordilis P, and Wessely M. Lumbar MRI part 1: Normal imaging appearance of the lumbar spine. *Clinical Chiropractic*, 8(4):205–215, 2005. (cited on pages 9 and 30)

Grenier JM, Scordilis P, Seaman D, and Wessely M. Lumbar MRI part 2: Common pathological

conditions. *Clinical Chiropractic*, 9(1):39–47, 2006. (cited on pages 9 and 30)

Hajnal J, Hill D, and Hawkes D (Eds.). *Medical Image Registration*. The Biomedical Engineering Series (CRC Press LLC, Boca Raton, FL, USA), 2001. (cited on page 101)

Harrison D, Cailliet R, Janik T, Troyanovich S, Harrison D, and Holland B. Elliptical modeling of the sagittal lumbar lordosis and segmental rotation angles as a method to discriminate between normal and low back pain subjects. *Journal of Spinal Disorders & Techniques*, 11(5):430–439, 1998. (cited on pages 13, 36 and 37)

Harrison D, Harrison D, Cailliet R, Troyanovich S, Janik T, and Holland B. Cobb method or Harrison posterior tangent method: Which to choose for lateral cervical radiographic analysis. *Spine*, 25(16):2072–2078, 2000. (cited on pages 12, 35, 36, 82, 88 and 97)

Harrison D, Janik T, Harrison D, Cailliet R, and Harmon S. Can the thoracic kyphosis be modeled with a simple geometric shape? The results of circular and elliptical modeling in 80 asymptomatic patients. *Journal of Spinal Disorders & Techniques*, 15(3):213–220, 2002. (cited on pages 13, 37, 82, 83, 88 and 97)

Harrison D, Harrison D, Janik T, Cailliet R, Ferrantelli J, Haas J, and Holland B. Modeling of the sagittal cervical spine as a method to discriminate hypolordosis: Results of elliptical and circular modeling in 72 asymptomatic subjects, 52 acute neck pain subjects, and 70 chronic neck pain subjects. *Spine*, 29(22):2485–2492, 2004. (cited on pages 13 and 37)

Haughton V, Rogers B, Meyerand E, and Resnick D. Measuring the axial rotation of lumbar vertebrae in vivo with MR imaging. *American Journal of Neuroradiology*, 23(7):1110–1116, 2002. (cited on pages 14, 39 and 41)

He S, Dai R, Lu B, Cao C, Bai H, and Jing B. Medial axis reformation: A new visualization method for CT angiography. *Academic Radiology*, 8(8):726–733, 2001. (cited on pages 6, 25 and 49)

Hecquet J, Legaye J, and Duval-Beaupère G. Access to a three-dimensional measure of vertebral axial rotation. *European Spine Journal*, 7(3):206–211, 1998. (cited on pages 78, 96 and 112)

Heithoff K and Herzog R. Computed tomography (CT) and enhanced CT of the spine. In: *The Adult Spine* (J Frymoyer, ed.) (Raven Press, New York, NY, USA), 1991. (cited on pages 13 and 37)

Herring J and Dawant B. Automatic lumbar vertebral identification using surface-based registration. *Journal of Biomedical Informatics*, 34(2):74–84, 2001. (cited on pages 15 and 42)

Herring J, Dawant B, Maurer C, Muratore D, Galloway R, and Fitzpatrick J. Surface-based registration of CT images to physical space for image-guided surgery of the spine: A sensitivity study. *IEEE Transactions on Medical Imaging*, 17(5):743–752, 1998. (cited on pages 10 and 31)

Ho E, Upadhyay S, Chan F, Hsu L, and Leong J. New methods of measuring vertebral rotation from computed tomographic scans: An intraobserver and interobserver study on girls with scoliosis. *Spine*, 18(9):1173–1177, 1993. (cited on pages 12, 13, 14, 35, 37, 38, 39, 78, 96 and 109)

Hoad C and Martel A. Segmentation of MR images for computer-assisted surgery of the lumbar spine. *Physics in Medicine and Biology*, 47(19):3503–3517, 2002. (cited on pages 15 and 42)

Hoad C, Martel A, Kerslake R, and Grevitt M. A 3D MRI sequence for computer assisted surgery of the lumbar spine. *Physics in Medicine and Biology*, 46(8):N213–N220, 2001. (cited on pages 15 and 42)

Hu Y and Haynor D. Multirigid registration of MR and CT images of the cervical spine. In: *Proceedings of the SPIE Medical Imaging 2004: Image Processing Conference* (J Fitzpatrick and M Sonka, eds.), vol. 5370, pp. 1527–1538 (SPIE, San Diego, CA, USA), 2004. (cited on pages 14 and 42)

Hu Y, Mirza S, Jarvik J, Heagerty P, and Haynor D. MR and CT image fusion of the cervical spine: A noninvasive alternative to CT-myelography. In: *Proceedings of the SPIE Medical Imaging 2005: Visualization, Image-Guided Procedures, and Display Conference* (R Galloway and K Cleary, eds.), vol. 5744, pp. 481–491 (SPIE, San Diego, CA, USA), 2005. (cited on pages 14 and 42)

Huynh T, Dansereau J, and Maurais G. Development of a vertebral endplate 3-D reconstruction technique. *IEEE Transactions on Medical Imaging*, 16(5):689–696, 1997. (cited on pages 15 and 42)

Huysmans T, Haex B, Van Audekercke R, Vander Sloten J, and Van Der Perre G. Three-dimensional mathematical reconstruction of the spinal shape, based on active contours. *Journal of Biomechanics*, 37(11):1793–1798, 2004. (cited on pages 14 and 40)

Janik T, Harrison D, Cailliet R, Troyanovich S, and Harrison D. Can the sagittal lumbar curvature be closely approximated by an ellipse? *Journal of Orthopaedic Research*, 16(6):766–770, 1998. (cited on pages 13, 36 and 37)

Jaremko J, Poncet P, Ronsky J, Harder J, Dansereau J, Labelle H, and Zernicke R. Estimation of spinal deformity in scoliosis from torso surface cross sections. *Spine*, 26(14):1583–1591, 2001. (cited on pages 11 and 34)

Jochimsen T and Norris D. Single-shot curved slice imaging. *Magnetic Resonance Materials in Physics Biology and Medicine*, 14(1):50–55, 2002. (cited on pages 7, 25 and 66)

Kaminsky J, Klinge P, Rodt T, Bokemeyer M, Luedemann W, and Samii M. Specially adapted interactive tools for an improved 3D-segmentation of the spine. *Computerized Medical Imaging and Graphics*, 28(3):119–127, 2004. (cited on pages 9, 11, 29, 33, 50, 65 and 78)

Kanitsar A, Fleischmann D, Wegenkittl R, Felkel P, and Gröller M. CPR - curved planar refor-

mation. In: *Proceedings of the IEEE Visualization 2002 Conference - Vis 2002* (R Moorhead, M Gross, and K Joy, eds.), pp. 37–44 (IEEE, Boston, MA, USA), 2002. (cited on pages 6, 25 and 49)

Kanitsar A, Wegenkittl R, Fleischmann D, and Gröller M. Advanced curved planar reformation: Flattening of vascular structures. In: *Proceedings of the IEEE Visualization 2003 Conference - Vis 2003* (G Turk, J van Vijk, and R Moorehad, eds.), pp. 43–50 (IEEE, Seattle, WA, USA), 2003. (cited on pages 6, 25 and 49)

Kaus M, Pekar V, Lorenz C, Weese J, Truyen R, and Lobregt S. Automated 3-D PDM construction from segmented images using deformable models. *IEEE Transactions on Medical Imaging*, 22(8):1005–1013, 2003. (cited on page 61)

Kim H, Ishikawa S, Ohtsuka Y, Shimizu H, Shinomiya T, and Viergever M. Automatic scoliosis detection based on local centroids evaluation on moiré topographic images of human backs. *IEEE Transactions on Medical Imaging*, 20(12):1314–1320, 2001. (cited on pages 11 and 34)

King H, Moe J, Bradford D, and Winter R. The selection of fusion levels in thoracic idiopathic scoliosis. *Journal of Bone and Joint Surgery - American Volume*, 65(9):1302–1313, 1983. (cited on pages 10, 32 and 92)

Knott P, Mardjetko S, Nance D, and Dunn M. Electromagnetic topographical technique of curve evaluation for adolescent idiopathic scoliosis. *Spine*, 31(24):E911–E915, 2006. (cited on pages 11 and 34)

Korovessis P, Stamatakis M, and Baikousis A. Reciprocal angulation of vertebral bodies in the sagittal plane in an asymptomatic Greek population. *Spine*, 23(6):700–704, 1998. (cited on pages 12, 35, 82, 83 and 97)

Kouwenhoven JW, Vincken K, Bartels L, and Castelein R. Analysis of preexistent vertebral rotation in the normal spine. *Spine*, 31(13):1467–1472, 2006. (cited on pages 14, 39, 40, 83, 97 and 112)

Krismer M, Sterzinger W, Christian H, Frischhut B, and Bauer R. Axial rotation measurement of scoliotic vertebrae by means of computed tomography scans. *Spine*, 21(5):576–581, 1996. (cited on pages 13, 37, 38, 39, 78, 96, 97 and 112)

Kuklo T, Lenke L, O'Brien M, Lehman R, Polly D, and Schroeder T. Accuracy and efficacy of thoracic pedicle screws in curves more than 90 degrees. *Spine*, 30(2):222–226, 2005a. (cited on pages 9 and 31)

Kuklo T, Potter B, and Lenke L. Vertebral rotation and thoracic torsion in adolescent idiopathic scoliosis: What is the best radiographic correlate? *Journal of Spinal Disorders & Techniques*, 18(2):139–147, 2005b. (cited on pages 10, 13, 31, 37 and 78)

Law TY and Heng PA. Automatic centerline extraction for 3D virtual bronchoscopy. In: *Lecture*

Notes in Computer Science (LNCS): Proceedings of the 3rd International Conference on Medical Image Computing and Computer-Assisted Intervention - MICCAI 2000 (S Delp, A DiGioia, and B Jaramaz, eds.), vol. 1935, pp. 786–795 (Springer-Verlag, Pittsburgh, PA, USA), 2000. (cited on pages 6, 25 and 49)

Lee SM, Suk SI, and Chung ER. Direct vertebral rotation: A new technique of three-dimensional deformity correction with segmental pedicle screw fixation in adolescent idiopathic scoliosis. *Spine*, 29(3):343–349, 2004. (cited on pages 10, 31 and 96)

Lenke L, Betz R, Harms J, Bridwell K, Clements D, Lowe T, and Blanke K. Adolescent idiopathic scoliosis: A new classification to determine extent of spinal arthrodesis. *Journal of Bone and Joint Surgery - American Volume*, 83-A(8):1169–1181, 2001. (cited on pages 10, 32 and 92)

Leonardi M, Righini A, Agati R, Brayda G, and Zanotti B. Curved CT reformatted images of head scans. *Journal of Computer Assisted Tomography*, 15(6):1074–1076, 1991. (cited on pages 6 and 25)

Liljenqvist U, Halm H, Hierholzer E, Drerup B, and Weiland M. 3-dimensional surface measurement of spinal deformities with video rasterstereography. *Zeitschrift für Orthopädie und Ihre Grenzgebiete*, 136(1):57–64, 1998. (cited on pages 11 and 34)

Liljenqvist U, Link T, and Halm H. Morphometric analysis of thoracic and lumbar vertebrae in idiopathic scoliosis. *Spine*, 25(10):1247–1253, 2000. (cited on pages 14 and 42)

Liljenqvist U, Allkemper T, Hackenberg L, Link T, Steinbeck J, and Halm H. Analysis of vertebral morphology in idiopathic scoliosis with use of magnetic resonance imaging and multiplanar reconstruction. *Journal of Bone and Joint Surgery - American Volume*, 84(3):359–368, 2002. (cited on pages 9, 31 and 66)

Lorenz C and Krahnstover N. Generation of point-based 3D statistical shape models for anatomical objects. *Computer Vision and Image Understanding*, 77(2):175–191, 2000. (cited on page 61)

Mac-Thiong J, Labelle H, Vandal S, and Aubin C. Intra-operative tracking of the trunk during surgical correction of scoliosis: A feasibility study. *Computer Aided Surgery*, 5(5):333–342, 2000. (cited on page 82)

Mac-Thiong JM, Labelle H, Charlebois M, Huot MP, and de Guise J. Sagittal plane analysis of the spine and pelvis in adolescent idiopathic scoliosis according to the coronal curve type. *Spine*, 28(13):1404–1409, 2003. (cited on pages 14 and 40)

Maddah M, Soltanian-Zadeh H, Afzali-Kusha A, and Maddah M. Snake modeling and distance transform approach to vascular centerline extraction and quantification. *Computerized Medical Imaging and Graphics*, 27(6):503–512, 2003. (cited on pages 6, 25 and 49)

Masharawi Y, Rothschild B, Dar G, Peleg S, Robinson D, Been E, and I H. Facet orientation

in the thoracolumbar spine: Three-dimensional anatomic and biomechanical analysis. *Spine*, 29(16):1755–1763, 2004. (cited on pages 14 and 42)

Mehta M. Radiographic estimation of vertebral rotation in scoliosis. *Journal of Bone and Joint Surgery - British Volume*, 55(3):513–520, 1973. (cited on pages 12 and 34)

Menten R, Mousny M, Saint-Martin C, and Clapuyt P. Planispheric multiplanar reformatted CT: A new method for evaluation of paediatric congenital spine abnormalities. *Pediatric Radiology*, 35(6):627–629, 2005. (cited on pages 8, 29 and 65)

Molnár S, Manó S, Kiss L, and Csernátony Z. Ex vivo and in vitro determination of the axial rotational axis of the human thoracic spine. *Spine*, 31(26):E984–E991, 2006. (cited on pages 97 and 112)

Morrissy R, Goldsmith G, Hall E, Kehl D, and Cowie G. Measurement of the Cobb angle on radiographs of patients who have scoliosis: Evaluation of intrinsic error. *Journal of Bone and Joint Surgery - American Volume*, 72(3):320–327, 1990. (cited on pages 11, 32 and 82)

Muggleton J and Allen R. Automatic location of vertebrae in digitized videofluoroscopic images of the lumbar spine. *Medical Engineering and Physics*, 19(1):77–89, 1997. (cited on pages 15 and 42)

Nash C and Moe J. A study of vertebral rotation. *Journal of Bone and Joint Surgery - American Volume*, 51(2):223–229, 1969. (cited on pages 12, 34, 35, 96 and 97)

Newton P, Hahn G, Fricka K, and Wenger D. Utility of three-dimensional and multiplanar reformatted computed tomography for evaluation of pediatric congenital spine abnormalities. *Spine*, 27(8):844–850, 2002. (cited on pages 8, 28, 29, 50 and 65)

Nojiri K, Matsumoto M, Chiba K, and Toyama Y. Morphometric analysis of the thoracic and lumbar spine in Japanese on the use of pedicle screws. *Surgical and Radiologic Anatomy*, 27(2):123–128, 2005. (cited on pages 14 and 42)

Novosad J, Cheriet F, Petit Y, and Labelle H. Three-dimensional (3-D) reconstruction of the spine from a single X-ray image and prior vertebra models. *IEEE Transactions on Biomedical Engineering*, 51(9):1628–16?9, 2004. (cited on pages 15 and 42)

Ochi T, Shimizu K, Yasuhara Y, Shigesawa T, Mochizuki T, and Ikezoe J. Curved planar reformatted CT angiography: Usefulness for the evaluation of aneurysms at the carotid siphon. *American Journal of Neuroradiology*, 20(6):1025–1030, 1999. (cited on pages 6 and 25)

Oda I, Abumi K, Cunningham B, Kaneda K, and McAfee P. An in vitro human cadaveric study investigating the biomechanical properties of the thoracic spine. *Spine*, 27(3):E64–E70, 2002. (cited on pages 14 and 40)

Ogon M, Giesinger K, Behensky H, Wimmer C, Nogler M, Bach C, and Krismer M. Interobserver and intraobserver reliability of Lenke's new scoliosis classification system. *Spine*,

27(8):858–862, 2002. (cited on pages 10 and 32)

Omeroğlu H, Ozekin O, and Biçimoğlu A. Measurement of vertebral rotation in idiopathic scoliosis using the Perdriolle torsionmeter: A clinical study on intraobserver and interobserver error. *European Spine Journal*, 5(3):167–171, 1996. (cited on pages 12 and 35)

Orchowski J, Polly D, Klemme W, Oda I, and Cunningham B. The effect of kyphosis on the mechanical strength of a long-segment posterior construct using a synthetic model. *Spine*, 25(13):1644–1648, 2000. (cited on pages 14 and 40)

Panigrahy S, Caruthers S, Krejza J, and Barnes P. Registration of three-dimensional MR and CT studies of the cervical spine. *American Journal of Neuroradiology*, 21(2):282–289, 2000. (cited on pages 14 and 42)

Parent S, Labelle H, Skalli W, Latimer B, and de Guise J. Morphometric analysis of anatomic scoliotic specimens. *Spine*, 27(21):2305–2311, 2002. (cited on pages 14 and 42)

Patwardhan A, Rimkus A, Gavin T, Bueche M, Meade K, Bielski R, and Ibrahim K. Geometric analysis of coronal decompensation in idiopathic scoliosis. *Spine*, 21(10):1192–1200, 1996. (cited on pages 11 and 33)

Peng Z, Zhong J, Wee W, and Lee JH. Automated vertebra detection and segmentation from the whole spine MR images. In: *Proceedings of the 27th Annual International Conference of the Engineering in Medicine and Biology Society (EMBS) - EMBC 2005* (Y Zhang, L Xu, C Roux, T Zhuang, T Tamura, and H Galiana, eds.), pp. 2527–2530 (IEEE, Shanghai, China), 2005. (cited on pages 11, 15, 33, 42 and 78)

Perchet D, Fetita C, and Preteux F. Advanced navigation tools for virtual bronchoscopy. In: *Proceedings of the SPIE Medical Imaging 2004: Image Processing Conference* (E Dougherty, J Astola, and K Egiazarian, eds.), vol. 5298, pp. 147–158 (SPIE, San Jose, CA, USA), 2004. (cited on pages 6, 25 and 49)

Perdriolle R and Vidal J. Thoracic idiopathic scoliosis curve evolution and prognosis. *Spine*, 10(9):785–791, 1985. (cited on pages 12 and 34)

Perdriolle R, Le Borgne P, Dansereau J, De Guise J, and Labelle H. Idiopathic scoliosis in three dimensions: A succession of two-dimensional deformities? *Spine*, 26(24):2719–2726, 2001. (cited on pages 15 and 42)

Petit Y, Aubin CE, and Labelle H. Spinal shape changes resulting from scoliotic spine surgical instrumentation expressed as intervertebral rotations and centers of rotation. *Journal of Biomechanics*, 37(2):173–180, 2004. (cited on pages 10, 31, 96, 97 and 112)

Pinel-Giroux FM, Mac-Thiong JM, de Guise J, Berthonnaud E, and Labelle H. Computerized assessment of sagittal curvatures of the spine: Comparison between Cobb and tangent circles techniques. *Journal of Spinal Disorders & Techniques*, 19(7):507–512, 2006. (cited on pages 12, 36, 37, 82, 88, 97 and 112)

Polly D, Kilkelly F, McHale K, Asplund L, Mulligan M, and Chang A. Measurement of lumbar lordosis: Evaluation of intraobserver, interobserver, and technique variability. *Spine*, 21(13):1530–5, 1996. (cited on pages 82, 88 and 97)

Poncet P, Trochu F, and Dansereau J. Curvilinear three-dimensional modeling of spinal curves with dual kriging. *Computer Methods in Biomechanics and Biomedical Engineering*, 2(4):295–308, 1999. (cited on pages 11 and 33)

Poncet P, Dansereau J, and Labelle H. Geometric torsion in idiopathic scoliosis: Three-dimensional analysis and proposal for a new classification. *Spine*, 26(20):2235–2243, 2001. (cited on pages 10, 12, 32, 35, 88 and 92)

Porter R. Idiopathic scoliosis: The relation between the vertebral canal and the vertebral bodies. *Spine*, 25(11):1360–1366, 2000. (cited on pages 14 and 42)

Press W, Teukolsky S, Vetterling W, and Flannery B. *Numerical recipes in C++: The art of scientific computing* (Cambridge University Press, Cambridge, UK), 2nd ed., 2002. (cited on pages 57, 73 and 101)

Prince R, Devine A, and Dick I. The clinical utility of measured kyphosis as a predictor of the presence of vertebral deformities. *Osteoporosis International*, 18(5):621–627, 2007. (cited on pages 13 and 37)

Prokesch R, Chow L, Beaulieu C, Nino-Murcia M, Mindelzun R, Bammer R, Huang J, and Jeffrey R. Local staging of pancreatic carcinoma with multi-detector row CT: Use of curved planar reformations initial experience. *Radiology*, 225(3):759–765, 2002a. (cited on pages 6 and 25)

Prokesch R, Coulam C, Chow L, Bammer R, and Rubin G. CT angiography of the subclavian artery: Utility of curved planar reformations. *Journal of Computer Assisted Tomography*, 26(2):199–201, 2002b. (cited on pages 6 and 25)

Rabassa A, Guinto Jr F, Crow W, Chaljub G, Wright G, and Storey G. CT of the spine: Value of reformatted images. *American Journal Of Roentgenology*, 161(6):1223–1227, 1993. (cited on pages 8, 27 and 65)

Raman R, Napel S, Beaulieu C, Bain E, Jeffrey Jr R, and Rubin G. Automated generation of curved planar reformations from volume data: Method and evaluation. *Radiology*, 223(1):275–280, 2002. (cited on pages 6, 25 and 49)

Raman R, Napel S, and Rubin GD. Curved-slab maximum intensity projection: Method and evaluation. *Radiology*, 229(1):255–260, 2003. (cited on pages 6, 25, 49 and 61)

Ramirez L, Durdle N, Raso V, and Hill D. A support vector machines classifier to assess the severity of idiopathic scoliosis from surface topography. *IEEE Transactions on Information Technology in Biomedicine*, 10(1):84–91, 2006. (cited on pages 10 and 32)

Reisman J, Höppner J, Huang SH, Zhang L, Lai SH, and Odry B amd Novak C. Robust local intervertebral disc alignment for spinal MRI. In: *Proceedings of the SPIE Medical Imaging 2006: Image Processing Conference* (J Reinhardt and J Pluim, eds.), vol. 6144 (SPIE, San Diego, CA, USA), 2006. (cited on pages 14 and 40)

Richards B, Sucato D, Konigsberg D, and Ouellet J. Comparison of reliability between the Lenke and King classification systems for adolescent idiopathic scoliosis using radiographs that were not premeasured. *Spine*, 28(11):1148–1156, 2003. (cited on pages 10 and 32)

Robb R. Three-dimensional visualization in medicine and biology. In: *Handbook of Medical Imaging: Processing and Analysis* (I Bankman, ed.), chap. 42, pp. 685–712 (Academic Press, San Diego, CA, USA), 2000. (cited on pages 5 and 21)

Roberts C, McDaniel N, Krupinski E, and Erly W. Oblique reformation in cervical spine computed tomography: A new look at an old friend. *Spine*, 28(2):167–170, 2003a. (cited on pages 8, 28, 29, 50 and 65)

Roberts M, Cootes T, and Adams J. Linking sequences of appearance sub-models via constraints: An application in automated vertebral morphometry. In: *Proceedings of the British Machine Vision Conference - BMVC 2003* (T Cootes and C Taylor, eds.), pp. CD–ROM (BMVA, Norwich, UK), 2003b. (cited on pages 14 and 42)

Rogers B, Haughton V, Arfanakis K, and Meyerand E. Application of image registration to measurement of intervertebral rotation in the lumbar spine. *Magnetic Resonance in Medicine*, 48(6):1072–1075, 2002. (cited on pages 14, 39, 41, 78, 97 and 112)

Rogers B, Wiese S, Blankenbaker D, Meyerand E, and Haughton V. Accuracy of an automated method to measure rotations of vertebrae from computerized tomography data. *Spine*, 30(6):694–696, 2005. (cited on pages 14, 39 and 40)

Rothman S, Dobben G, Rhodes M, Glenn WJ, and Azzawi YM. Computed tomography of the spine: Curved coronal reformations from serial images. *Radiology*, 150(1):185–190, 1984. (cited on pages 8, 28 and 65)

Rousseeuw P and Leroy A. *Robust regression and outlier detection*. Wiley Series in Probability and Statistics (Wiley-Interscience, New York, NY, USA), 2003. (cited on pages 71 and 73)

Roussouly P, Gollogly S, Berthonnaud E, and Dimnet J. Classification of the normal variation in the sagittal alignment of the human lumbar spine and pelvis in the standing position. *Spine*, 30(3):346–353, 2005. (cited on pages 83 and 92)

Rubin G, Napel S, and Leung A. Volumetric analysis of volumetric data: A paradigm shift. *Radiology*, 200(2):312–317, 1996. (cited on pages 5 and 21)

Russell G, Raso V, Mclvor J, and Hill D. A comparison of four computerized methods for measuring vertebral rotation. *Spine*, 15(1):24–27, 1990. (cited on pages 12 and 35)

Sakas G. Trends in medical imaging: From 2D to 3D. *Computers and Graphics*, 26(4):577–587, 2002. (cited on pages 3 and 19)

Samara Y, Fiebich M, Dachman AH, Kuniyoshi JK, Doi K, and Hoffmann KR. Automated calculation of the centerline of the human colon on CT images. *Academic Radiology*, 6(6):352–359, 1999. (cited on pages 6, 25 and 49)

Saroul L, Gerlach S, and Hersch R. Exploring curved anatomic structures with surface sections. In: *Proceedings of the IEEE Visualization 2003 Conference - Vis 2003* (G Turk, J van Vijk, and R Moorehad, eds.), pp. 27–34 (IEEE, Seattle, WA, USA), 2003. (cited on pages 6, 25 and 49)

Schmitz A, Jaeger U, Koenig R, Kandyba J, Wagner U, Giesecke J, and Schmitt O. A new MRI technique for imaging scoliosis in the sagittal plane. *European Spine Journal*, 10(2):114–117, 2001. (cited on pages 10 and 32)

Sethian JA. *Level set methods and fast marching methods. Evolving interfaces in computational geometry, fluid mechanics, computer vision, and materials science*. Cambridge Monographs on Applied and Computational Mathematics (Cambridge University Press, Cambridge, UK), 2nd ed., 1999. (cited on page 57)

Sevastik B, Xiong B, Sevastik J, Hedlund R, and Suliman I. Vertebral rotation and pedicle length asymmetry in the normal adult spine. *European Spine Journal*, 4(2):95–97, 1995. (cited on pages 10 and 32)

Shea K, Stevens P, Nelson M, Smith J, Masters K, and Yandow S. A comparison of manual versus computer-assisted radiographic measurement: Intraobserver measurement variability for Cobb angles. *Spine*, 23(5):551–555, 1998. (cited on pages 11, 32, 82, 97 and 112)

Skalli W, Lavaste F, and Descrimes JL. Quantification of three-dimensional vertebral rotations in scoliosis: What are the true values? *Spine*, 20(5):546–553, 1995. (cited on pages 12, 13, 35, 37, 78, 96, 97 and 112)

Smyth P, Taylor C, and Adams J. Automatic measurement of vertebral shape using active shape models. *Image Vision and Computing*, 15(8):575–581, 1997. (cited on pages 14 and 42)

Stagnara P, De Mauroy J, Dran G, Gonon G, Costanzo G, Dimnet J, and Pasquet A. Reciprocal angulation of vertebral bodies in a sagittal plane: Approach to references for the evaluation of kyphosis and lordosis. *Spine*, 7(4):335–342, 1982. (cited on pages 12 and 35)

Stokes I. Axial rotation component of thoracic scoliosis. *Journal of Orthopaedic Research*, 7(5):702–708, 1989. (cited on pages 12 and 35)

Stokes I. Three-dimensional terminology of spinal deformity: A report presented to the Scoliosis Research Society by the Scoliosis Research Society Working Group on 3-D terminology of spinal deformity. *Spine*, 19(2):236–248, 1994. (cited on pages 10, 32, 79 and 83)

Stokes I. Analysis of symmetry of vertebral body loading consequent to lateral spinal curvature. *Spine*, 22(21):2495–2503, 1997. (cited on pages 14 and 40)

Stokes I and Aronsson D. Disc and vertebral wedging in patients with progressive scoliosis. *Journal of Spinal Disorders & Techniques*, 14(4):317–322, 2001. (cited on pages 10, 32 and 96)

Stokes I and Aronsson D. Computer-assisted algorithms improve reliability of King classification and Cobb angle measurement of scoliosis. *Spine*, 31(6):665–670, 2006. (cited on pages 11, 33, 82 and 97)

Stokes I, Bigalow L, and Moreland M. Measurement of axial rotation of vertebrae in scoliosis. *Spine*, 11(3):213–218, 1986. (cited on pages 12, 34 and 96)

Stokes I, Bigalow L, and Moreland M. Three-dimensional spinal curvature in idiopathic scoliosis. *Journal of Orthopaedic Research*, 5(1):102–113, 1987. (cited on pages 82, 83 and 88)

Stokes I, Armstrong J, and Moreland M. Spinal deformity and back surface assymetry in idiopathic scoliosis. *Journal of Orthopaedic Research*, 6(1):129–137, 1988. (cited on pages 11 and 34)

Stokes I, Aronson D, Ronchetti P, Labelle H, and Dansereau J. Reexamination of the Cobb and Ferguson angles: Bigger is not always better. *Journal of Spinal Disorders & Techniques*, 6(4):333–338, 1993. (cited on pages 11 and 32)

Tamura Y, Sugano N, Sasama T, Sato Y, Tamura S, Yonenobu K, Yoshikawa H, and T O. Surface-based registration accuracy of CT-based image-guided spine surgery. *European Spine Journal*, 14(3):291–297, 2005. (cited on pages 10 and 31)

Tan S, Teo E, and Chua H. Quantitative three-dimensional anatomy of lumbar vertebrae in Singaporean Asians. *European Spine Journal*, 11(2):152–158, 2002. (cited on pages 14 and 42)

Tan S, Teo E, and Chua H. Quantitative three-dimensional anatomy of cervical, thoracic and lumbar vertebrae of Chinese Singaporeans. *European Spine Journal*, 13(2):137–146, 2004. (cited on pages 14 and 42)

Teo J, Chui C, Wang Z, Ong S, Yan C, Wang S, Wong H, and Teoh S. Heterogeneous meshing and biomechanical modeling of human spine. *Medical Engineering and Physics*, 29(2):277–290, 2007. (cited on pages 14 and 40)

Toyone T, Tanaka T, Kato D, Kaneyama R, and Otsuka M. Patients' expectations and satisfaction in lumbar spine surgery. *Spine*, 30(23):2689–2694, 2005. (cited on pages 4 and 20)

Tredwell S, Sawatzky B, and Hughes B. Rotations of a helix as a model for correction of the scoliotic spine. *Spine*, 24(12):1223–1227, 1999. (cited on pages 11 and 34)

Udupa J. Three-dimensional visualization: Principles and approaches. In: *Handbook of Medical*

Imaging Vol 3. Display and PACS (Y Kim and S Horii, eds.), chap. 1, pp. 5–65 (SPIE Press, Bellingham, WA, USA), 2000. (cited on pages 5 and 21)

Vedantam R, Lenke L, Keeney J, and Bridwell K. Comparison of standing sagittal spinal alignment in asymptomatic adolescents and adults. *Spine*, 23(2):211–215, 1998. (cited on pages 92, 97 and 98)

Verdonck B, Nijlunsing R, Gerritsen F, Cheung J, Wever D, Veldhuizen A, Devillers S, and Makram-Ebeid S. Computer assisted quantitative analysis of deformities of the human spine. In: *Lecture Notes in Computer Science (LNCS): Proceedings of the 1st International Conference on Medical Image Computing and Computer-Assisted Intervention - MICCAI'98* (W Wells, A Colchester, and S Delp, eds.), vol. 1496, pp. 822–831 (Springer-Verlag, Cambridge, MA, USA), 1998. (cited on pages 11, 33, 34, 62 and 78)

Villemure I, Aubin C, Grimard G, Dansereau J, and Labelle H. Progression of vertebral and spinal three-dimensional deformities in adolescent idiopathic scoliosis: A longitudinal study. *Spine*, 26(20):2244–2250, 2001. (cited on page 83)

Vrtovec T, Likar B, Tomaževič D, and Pernuš F. Automated robust generation of compact 3D statistical shape models. In: *Proceedings of the SPIE Medical Imaging 2004: Image Processing Conference* (J Fitzpatrick and M Sonka, eds.), vol. 5370, pp. 1312–1323 (SPIE, San Diego, CA, USA), 2004a. (cited on page 61)

Vrtovec T, Tomaževič D, Likar B, Travnik L, and Pernuš F. Automated construction of 3D statistical shape models. *Image Analysis and Stereology*, 23(2):111–120, 2004b. (cited on page 61)

Vrtovec T, Likar B, and Pernuš F. Automated curved planar reformation of 3D spine images. *Physics in Medicine and Biology*, 50(19):4527–4540, 2005. (cited on pages 65, 66, 67, 76, 78, 84 and 92)

Vrtovec T, Likar B, and Pernuš F. Determination of 3D location and rotation of lumbar vertebrae in CT images by symmetry-based auto-registration. In: *Proceedings of the SPIE Medical Imaging 2007: Image Processing Conference* (J Pluim and J Reinhardt, eds.), vol. 6512, pp. 65121Q–1 (SPIE, San Diego, CA, USA), 2007. (cited on page 118)

Wan M, Liang Z, Ke Q, Hong L, Bitter I, and Kaufman A. Automatic centerline extraction for virtual colonoscopy. *IEEE Transactions on Medical Imaging*, 21(12):1450–1460, 2002. (cited on pages 6, 25 and 49)

Weiss HR. Measurement of vertebral rotation: Perdriolle versus Raimondi. *European Spine Journal*, 4(1):34–38, 1995. (cited on pages 12 and 35)

Weiss K, Storrs J, and Banto R. Automated spine survey iterative scan technique. *Radiology*, 239(1):255–262, 2006. (cited on pages 66 and 92)

Weisstein E. *The CRC concise encyclopedia of mathematics* (CRC Press LLC, Boca Raton, FL,

USA), 1999. (cited on pages 56, 61, 72 and 74)

Wessberg P, Danielson B, and Willén J. Comparison of Cobb angles in idiopathic scoliosis on standing radiographs and supine axially loaded MRI. *Spine*, 31(26):3039–3044, 2006. (cited on pages 11 and 34)

Wever D, Veldhuizen A, Klein J, Webb P, Nijenbanning G, Cool J, and Horn J. A biomechanical analysis of the vertebral and rib deformities in structural scoliosis. *European Spine Journal*, 8(4):252–260, 1999. (cited on pages 14 and 40)

Wills B, Auerbach J, Zhu X, Caird M, David Horn B, Flynn J, Drummond D, Dormans J, and Ecker M. Comparison of Cobb angle measurement of scoliosis radiographs with preselected end vertebrae: Traditional versus digital acquisition. *Spine*, 32(1):98–105, 2007. (cited on pages 11 and 32)

Wright N. Imaging in scoliosis. *Archives of Disease in Childhood*, 82(1):38–40, 2000. (cited on pages 10 and 32)

Yang B, Yang C, and Ondra S. A novel mathematical model of the sagittal spine. *Spine*, 32(4):466–470, 2007. (cited on pages 11 and 33)

Yao J, O'Connor S, and Summers R. Automated spinal column extraction and partitioning. In: *Proceedings of the 3rd IEEE International Symposium on Biomedical Imaging: From Nano to Macro - ISBI 2006*, pp. 390–393 (IEEE, Arlington, VA, USA), 2006. (cited on pages 15 and 42)

Yazici M, Acaroglu E, Alanay A, Deviren V, Cila A, and Surat A. Measurement of vertebral rotation in standing versus supine position in adolescent idiopathic scoliosis. *Journal of Pediatric Orthopaedics*, 21(2):252–256, 2001. (cited on pages 13 and 39)

Zamora G, Sari-Sarraf H, and Long R. Hierarchical segmentation of vertebrae from X-ray images. In: *Proceedings of the SPIE Medical Imaging 2003: Image Processing Conference* (M Sonka and J Fitzpatrick, eds.), vol. 5032, pp. 631–642 (SPIE, San Diego, CA, USA), 2003. (cited on pages 15 and 42)

Zheng Y, Nixon M, and Allen R. Automated segmentation of lumbar vertebrae in digital videofluoroscopic images. *IEEE Transactions on Medical Imaging*, 23(1):45–52, 2004. (cited on pages 15 and 42)

Zmurko M, Mooney J, Podeszwa D, Minster G, Mendelow M, and Guirgues A. Inter- and intraobserver variance of Cobb angle measurements with digital radiographs. *Journal of Surgical Orthopaedic Advances*, 12(4):208–213, 2003. (cited on pages 11 and 32)

Zubairi J. Applications of computer-aided rasterstereography in spinal deformity detection. *Image Vision and Computing*, 20(4):301–306, 2002. (cited on pages 11 and 34)

Reading maketh a full man, conference a ready man, and writing an exact man.

Francis Bacon, 1561 - 1626
(The Essays: Of Studies, 1625)

Publications

Papers in journals

1. Tomaž Vrtovec, Sébastien Ourselin, Lavier Gomes, Boštjan Likar, and Franjo Pernuš. Automated generation of curved planar reformations from MR images of the spine. *Physics in Medicine and Biology*, 52(10):2865–2878, 2007.

2. Tomaž Vrtovec, Boštjan Likar, and Franjo Pernuš. Automated curved planar reformation of 3D spine images. *Physics in Medicine and Biology*, 50(19):4527–4540, 2005.

3. Tomaž Vrtovec. Curved planar reformation of CT spine images. *Elektrotehniški vestnik (Electrotechnical Review)*, 72(5):285–290, 2005.

4. Tomaž Vrtovec, Dejan Tomaževič, Boštjan Likar, Ludvik Travnik, and Franjo Pernuš. Automated construction of 3D statistical shape models. *Image Analysis & Stereology*, 23(2):111–120, 2004.

- Tomaž Vrtovec, Boštjan Likar, and Franjo Pernuš. Quantitative analysis of spinal curvature in 3D: Application to CT images of normal spine. *Submitted for journal publication*.

source of bibliographic records: shared bibliographic/catalogue database COBISS.SI/COBIB.SI (http://www.cobiss.si)

Papers in conference proceedings

1. Tomaž Vrtovec, Boštjan Likar, and Franjo Pernuš. Determination of 3D location and rotation of lumbar vertebrae in CT images by symmetry-based auto-registration. In: *Proceedings of the SPIE Medical Imaging 2007: Image Processing Conference* (J. Pluim and J. Reinhardt, eds.), vol. 6512, pp. 65121Q–1 (SPIE, San Diego, CA, USA, Feb 17-22), 2007.

2. Tomaž Vrtovec, Sébastien Ourselin, Lavier Gomes, Boštjan Likar, and Franjo Pernuš. Generation of curved planar reformations from magnetic resonance images of the spine. In: *Lecture Notes in Computer Science (LNCS): Proceedings of the 9th International Conference on Medical Image Computing and Computer-Assisted Intervention - MICCAI 2006* (R. Larsen, M. Nielsen, and J. Sporring, eds.), vol. 4191, pp. 135–143 (Springer-Verlag, Copenhagen, Denmark, Oct 1-6), 2006.

3. Tomaž Vrtovec, Boštjan Likar, and Franjo Pernuš. Curved planar reformation of CT spine data. In: *Proceedings of the SPIE Medical Imaging 2005: Image Processing Conference* (J.M. Fitzpatrick and J.M. Reinhardt, eds.), vol. 5747, pp. 1446–1456 (SPIE, San Diego, CA, USA, Feb 12-17), 2005.

4. Tomaž Vrtovec, Boštjan Likar, and Franjo Pernuš. Spine-based coordinate system. In: *Proceedings of the 27th IEEE Annual International Conference of the Engineering in Medicine and Biology Society (EMBS) - EMBC 2005* (Y.T. Zhang, L.X. Xu, C. Roux, T.G. Zhuang, T. Tamura, and H. Galiana, eds.), pp. 5120–5123 (IEEE, Shanghai, China, Sep 1-4), 2005.

5. Tomaž Vrtovec, Boštjan Likar, Dejan Tomaževič, and Franjo Pernuš. Automated robust generation of compact 3D statistical shape models. In: *Proceedings of the SPIE Medical Imaging 2004: Image Processing Conference* (J.M. Fitzpatrick and M. Sonka, eds.), vol. 5370 pp. 1312–1323 (SPIE, San Diego, CA, USA, Feb 14-19), 2004.

6. Tomaž Vrtovec, Dejan Tomaževič, Boštjan Likar, and Franjo Pernuš. Statistical shape deformable model of a lumbar vertebra. In: *Proceedings of the 8th Computer Vision Winter Workshop - CVWW 2003* (O. Drbohlav, ed.), pp. 91–96 (Valtice, Czech Republic, Feb 3-6), 2003.

- Tomaž Vrtovec, Sébastien Ourselin, Boštjan Likar, and Franjo Pernuš. Modality-independent determination of vertebral parameters in 3D. *Submitted for conference presentation*.

Monographs and other completed works

1. Tomaž Vrtovec. Statistični deformabilni model oblike ledvenega vretenca (Translation of the title: Statistical shape deformable model of the lumbar vertebra). *BSc thesis* (F Pernuš, supervisor), University of Ljubljana, Faculty of Electrical Engineering (Ljubljana, Slovenia), 2002.

Nothing shocks me. I'm a scientist.

INDIANA JONES
(Indiana Jones and the Temple of Doom, 1984)

About the author

Tomaž Vrtovec was born on March 6th 1978 in Šempeter pri Novi Gorici, Slovenia. After spending a lively childhood in his home village of Bukovica and nearby Renče, he finished secondary school in Nova Gorica in 1997.

In the same year he began the undergraduate studies at the University of Ljubljana, Faculty of Electrical Engineering, Slovenia. After specializing in telecommunications, he successfully defended his BSc thesis in 2002. As a PhD student he joined the Laboratory of Imaging Technologies at the University of Ljubljana, Faculty of Electrical Engineering, Slovenia, where he has been employed as a researcher since 2003. In 2006, he spent six months in Australia with the CSIRO ICT Centre as a visiting researcher. His research interests are concentrated around biomedical image analysis and development of computer vision systems.

In his free time he cultivates various hobbies, among the most favorite are visiting new places home and around the world, when possible in the saddle of a bicycle, taking and developing black & white photographies, and examining his continuously growing collection of coins.

Nič me ne preseneti. Sem znanstvenik.

INDIANA JONES
(Indiana Jones in tempelj usode, 1984)

O avtorju

Tomaž Vrtovec se je rodil 6. 3. 1978 v Šempetru pri Novi Gorici. Po živahnem otroštvu v domači vasi Bukovica in sosednjih Renčah je leta 1997 opravil maturo na gimnazijskem programu Srednjega šolskega centra v Novi Gorici.

V istem letu se je vpisal na dodiplomski študijski program elektrotehnike na Fakulteti za elektrotehniko, Univerza v Ljubljani, ter po študiju na smeri telekomunikacije leta 2002 uspešno zagovarjal diplomsko nalogo. Kot podiplomski študent se je pridružil Laboratoriju za slikovne tehnologije na Fakulteti za elektrotehniko, Univerza v Ljubljani, kjer je od leta 2003 tudi zaposlen kot mladi raziskovalec. Leta 2006 je v sklopu doktorskega študija preživel šest mesecev v Avstraliji kot gostujoči raziskovalec na inštitutu CSIRO ICT Centre. Njegovo področje raziskovanja obsega obdelavo in analizo biomedicinskih slik ter razvoj sistemov z računalniškim vidom.

V prostem času se ukvarja z različnimi konjički, najljubši izmed njih so obiskovanje krajev doma in po svetu, če je mogoče v sedlu kolesa, razvijanje fotografij v črno-beli tehniki ter preučevanje njegove nenehno rastoče zbirke kovancev.

To see a World in a Grain of Sand
And a Heaven in a Wild Flower,
Hold Infinity in the palm of your hand
And Eternity in an hour.

William Blake, 1757 – 1827
(Auguries of Innocence, 1805)

Acknowledgments

During the past years I have been supported by many people, and it is a pleasure to use this opportunity and express my gratitude to them.

Prof. Dr. Franjo Pernuš introduced me to the field of medical imaging and provided the valuable guidance to reach the end of my studies. I consider it a privilege to have been working in his group. I have benefited immensely from Prof. Dr. Boštjan Likar, who supported my work with continuous interest, advice and discussion. Without him, my work would not be as it is. The present and former members of the Laboratory of Imaging Technologies – Dr. Darko Škerl, Dr. Uroš Vovk, Marko Bukovec, Mario Medved, Dejan Stojaković, Dr. Dejan Tomaževič, Miran Bürmen, Primož Markelj and Žiga Špiclin – created a relaxing atmosphere along very frequent coffee breaks, which sometimes went on until the early hours. Spending six months with the CSIRO ICT Centre in Australia was a wonderful and fruitful experience that was made possible by Prof. Dr. Sébastien Ourselin. I also appreciate the financial support provided by the Ministry of Higher Education, Science and Technology, Slovenia, according to the "Junior Researchers" program.

Last, but certainly far from least, I want to express my gratitude to my parents, Anka and Vojko, and my sister, Jana, for their continuous encouragement, support and especially patience. I can only but hope that some things will never change.

THANK YOU

Tomaž

V zrnu peska videti cel Svet
in Nebo v Roži na poljani,
Večni čas imeti v hip ujet
in Neskončnost obdržati v dlani.

William Blake, 1757 – 1827
(Slutnja nedolžnosti, 1805)

Zahvala

V veliko zadovoljstvo mi je, da lahko izrabim to priložnost za zahvalo vsem, ki so me v teh letih podpirali.

Prof. dr. Franjo Pernuš me je vpeljal v področje obdelave biomedicinskih slik ter mi priskrbel dragoceno vodstvo, ki me je pripeljalo do zaključka mojega študija. Delo v njegovi skupini je bilo zame privilegij. Ogromno znanja in izkušenj sem pridobil od prof. dr. Boštjana Likarja, ki je podpiral moje delo z neprestanim zanimanjem, nasveti ter razpravami. Brez njega moje delo ne bi bilo takšno, kot je. Sedanji ter bivši člani Laboratorija za slikovne tehnologije – dr. Darko Škerl, dr. Uroš Vovk, mag. Marko Bukovec, Mario Medved, mag. Dejan Stojaković, dr. Dejan Tomaževič, Miran Bürmen, Primož Markelj in Žiga Špiclin – so ustvarili sproščeno vzdušje ter zelo pogoste odmore za kavo, ki so se včasih zavlekli tudi v jutranje ure. Šestmesečno delo na inštitutu CSIRO ICT Centre v Avstraliji mi bo ostalo v spominu kot čudovita ter uspešna izkušnja, za kar ima zasluge predvsem prof. dr. Sébastien Ourselin. Zelo cenim tudi štiri in pol leta trajajočo finančno podporo Ministrstva za visoko šolstvo, znanost in tehnologijo v okviru programa "mladih raziskovalcev".

Posebne zahvale so deležni moji starši Anka in Vojko ter sestra Jana, ki so me v teh letih spremljali z neprestanim spodbujanjem, podporo in še posebej potrpežljivostjo. Ob tem lahko samo upam, da se nekatere stvari ne bodo nikoli spremenile.

HVALA

Tomaž

The most merciful thing in the world is the inability of the human mind to correlate all its contents.

HOWARD P. LOVECRAFT, 1890 – 1937
(The Call of Cthulhu, 1926)

Index

D

E

F

T

V

X